MONTANA STATE UNIVERSITY

Volcanism and associated sedimentation in a retroarc foreland basin : the Upper Cretaceous Two Medicine formation of west-central Montana
by Angela Elaine Smith

A thesis submitted in partial fulfillment of the requirements for the degree of Master of Science in Earth Sciences
Montana State University
© Copyright by Angela Elaine Smith (1998)

Abstract:
Deposits of the Campanian Two Medicine Formation near Wolf Creek, Montana, provide essential sedimentologic information necessary for interpretation of the response of alluvial systems to explosive and effusive intra-basinal volcanism. The Two Medicine Formation consists of approximately 1500 meters of interbedded sandstone, conglomerate, and mudstone, with lava flow and rhyolitic tuff. Lithofacies analysis implies deposition of the western facies was by sandy-gravelly braided systems within well-developed, fine-grained floodplains. In addition to normal fluid gravity flow processes, deposition also occurred via debris flow and hyperconcentrated flow. Channel response to volcaniclastic deposition was avulsion during high discharge events, reworking of choked braided systems, and incision into floodplain deposits.

Lithofacies analysis suggests deposition of the eastern facies was by braided distributary channels. Channels tunneled sediments to the marsh, tidal mudflat, and beach environments. Fluid gravity flow, hyperconcentrated flow, and debris flow processes influenced the depositional setting by overwhelming the coastal plain with sediment. Lacustrine deposits formed after high discharge events plugged channels, resulting in restricted ponded water. Syn-eruption events resulted in progradation of the braid-delta; inter-eruption periods were characterized by the reworking of volcanic debris, and the reestablishment of beach, tidal mudflat, and marsh settings.

Source areas for the primary volcanic rocks most likely were from the local Wolf Creek volcanic centers. The volcaniclastic sediments are compositionally similar to the primary volcanic rocks; thus, sedimentation in the Two Medicine basin was likely dependent on the erosion of local volcanic carapaces. In addition, the eastern facies was deposited by sediment transported by longshore currents, the westerly braid-plain, and from the Adel Mountain volcanic center.

Volcanism-produced detritus ultimately mantled topography sufficiently to disguise tectonic activity in the Wolf Creek area. Thrust faulting was likely active near the end of Two Medicine deposition, as thrust-belt-derived clasts of Cambrian Flathead Sandstone begin to appear in the youngest Two Medicine deposits.

VOLCANISM AND ASSOCIATED SEDIMENTATION IN A RETROARC FORELAND BASIN: THE UPPER CRETACEOUS TWO MEDICINE FORMATION OF WEST-CENTRAL MONTANA

by

Angela Elaine Smith

A thesis submitted in partial fulfillment
of the requirements for the degree

of

Master of Science

in

Earth Sciences

MONTANA STATE UNIVERSITY-BOZEMAN
Bozeman, Montana

December 1998

N378
Sm51

APPROVAL

of a thesis submitted by

Angela Elaine Smith

This thesis has been read by each member of the thesis committee and has been found to be satisfactory regarding content, English usage, format, citations, bibliographic style, and consistency, and is ready for submission to the College of Graduate Studies.

Dr. James Schmitt James Schmitt 12-11-98

Approved for the Department of Earth Sciences

Dr. Andrew Marcus Andrew Marcus Dec 10, 1998

Approved for the College of Graduate Studies

Dr. Joseph J. Fedock Joseph J. Fedock 12/17/98

STATEMENT OF PERMISSION TO USE

In presenting this thesis in partial fulfillment of the requirements for a master's degree at Montana State University-Bozeman, I agree that the Library shall make it available to borrowers under rules of the Library.

If I have indicated my intention to copyright this thesis by including a copyright notice page, copying is allowable only for scholarly purposes, consistent with "fair use" as prescribed in the U.S. Copyright Law. Requests for permission for extended quotation from or reproduction of this thesis in whole or in parts may be granted only by the copyright holder.

Signature 

Date November 25, 1998

ACKNOWLEDGMENTS

I would like to express my most sincere gratitude to Jim Schmitt. Without his assistance, advice, expertise, and encouragement, this work would be in dire straits. My other committee members were most helpful. Steve Custer provided insightful comments for improving this manuscript, and I thank him for his honesty and sensibility. Todd Feeley was invaluable for providing knowledge of volcanology and petrology that aided in my understanding of those fields, and I thank him for his patience in reading about dirt. Finally, Jack Horner brought years of experience from working in the Two Medicine Formation, and I thank him for showing me the multiple implications of this study. Thanks to all for the enthusiasm and patience you showed over the past few years.

Funding was provided by Robert and Jacque Smith, D. L. Smith Memorial Scholarship, Edwin Mckee Grant (SEPM), Love Award (WGA), federal loans, and a Department of Earth Sciences teaching assistantship.

Thanks also go to my friends and fellow graduate comrades who are so supportive and encouraging. It would have been more difficult if I didn't have you guys to lean on, in particular, Mike and Amy O'Connell, Becca Laws, Stewart Dixon, and Kate Chase.

My husband Jim deserves so many thanks for his emotional support throughout this endeavor. Ditto to my parents, Robert and Jacque Smith, who also provided faith that this would go well.

TABLE OF CONTENTS

Page

LIST OF TABLES....x

LIST OF FIGURES....xi

ABSTRACT....xv

INTRODUCTION....1

Objectives....3
Geologic Setting....4
Elkhorn Mountains Volcanics....4
Adel Mountain Volcanics....7
Wolf Creek Volcanic Center....8
Western Interior Cretaceous Seaway....9

TWO MEDICINE FORMATION....10

Description....10
Western Facies....13
Age and Correlation....15
Eastern Facies....15
Age and Correlation....16

METHODS....18

LITHOFACIES....23

Conglomerate Lithofacies....27
Matrix-Supported, Massive Conglomerate (Gmm, Gmmi, Gmin)....27
Interpretation....28
Clast-Supported, Massive Conglomerate (Gcm, Gcmi, Gcms, Gcin)....32
Interpretation....33
Trough Cross-Bedded Conglomerate (Gt)....35
Interpretation....35

TABLE OF CONTENTS---Continued

Page

Horizontally-Bedded Conglomerate (Gh).....37
Interpretation.....37
Sandstone Lithofacies.....39
Massive Sandstone (Sm).....39
Interpretation.....40
Horizontally-Stratified Sandstone (Sh).....41
Interpretation.....41
Low-Angle (<15°), Trough Cross-Stratified Sandstone (Sl).....43
Interpretation.....43
Trough Cross-Stratified Sandstone (St).....44
Interpretation.....44
Ripple Cross-Laminated Sandstone (Sr, Srs, Src).....44
Interpretation.....45
Mudrock Lithofacies.....47
Laminated Silt and Mud (Fl).....47
Interpretation.....47
Massive Silt and Mud (Fm).....47
Interpretation.....48
Rootbeds of Silt and Mud (Fp).....49
Interpretation.....50
Non-Clastic Lithofacies.....50
Organic Deposits (O).....50
Interpretation.....50
Carbonate (Cl, Cn).....50
Interpretation.....51
Pyroclastic Lithofacies.....52
Matrix-Supported, Massive Lapilli Tuff (Lmm).....55
Interpretation.....55
Matrix-Supported, Massive Tuff (Tmm, Tmmg).....55
Interpretation.....56
Massive Tuff (Tm).....57
Interpretation.....57
Antidunal Tuff (Ta).....58
Interpretation.....59
Climbing-Ripple Cross-Laminated Tuff (Trc).....59
Interpretation.....60
Horizontally-Stratified Tuff (Th).....60

TABLE OF CONTENTS---Continued

Page

Interpretation....60
Vitrophyric Tuff (Tv)....61
Interpretation....62

VOLCANIC ROCK DESCRIPTIONS....65

Unit B-Latite Lava Flows....65
Interpretation....69
Unit C-Rhyolitic Ash-Flow Tuffs....69
Unit E-Trachyte Lava Flows....73
Interpretation....78
Adel Mountain Volcanics....78

LITHOFACIES ASSOCIATIONS....80

Western Facies....80
Channel Association....80
Fluid Gravity Flow (FGF)....83
Debris Flow (DF)....84
Hyperconcentrated Flow (HF)....84
Interpretation....85
Floodplain Association....86
Fluid Gravity Flow (FGF)....86
Debris Flow (DF)....88
Hyperconcentrated Flow (HF)....88
Pyroclastic Flow/Surges....89
Lava Flow....91
Interpretation....92
Eastern Facies....93
Marsh Association....93
Interpretation....93
Beach Association....94
Interpretation....95
Lacustrine Association....97
Interpretation....97
Distributary Channel Association....97
Fluid Gravity Flow (FGF)....99

TABLE OF CONTENTS---Continued

Page

Debris/Hyperconcentrated Flow (DF/HF).....100
Interpretation.....101
Tidal Mudflat Association.....101
Fluid Gravity Flow (FGF).....103
Debris Flow (DF).....103
Hyperconcentrated Flow (HF).....104
Lava/Autobrecciated Flow.....104
Interpretation.....105

PROVENANCE.....108

Conglomerate Composition.....108
Description.....108
Clast Composition Modes.....109
Sandstone Composition-Western Facies.....110
Texture.....111
Framework Grains.....111
Quartz, Monocrystalline (Qm).....111
Feldspar (F).....112
Lithic Fragments (Lv, Lp, Ls).....112
Accessory Minerals.....112
Sandstone Composition Modes.....113
Sandstone Composition-Eastern Facies.....113
Texture.....115
Framework Grains.....115
Quartz, Monocrystalline (Qm).....115
Quartz, Polycrystalline (Qp).....116
Feldspar (F).....116
Lithic Fragments (Lv, Lp, Ls).....116
Accessory Minerals.....117
Sandstone Composition Modes.....117
Paleocurrents.....118
Potential Sediment Source Areas.....118
Conglomerate Sources.....118
Western Facies Sandstones Sources.....120
Eastern Facies Sandstones Sources.....121

TABLE OF CONTENTS---Continued

Page

VOLCANIC ROCK SOURCE AREAS....124

Latite Lava Flows....124
Rhyolite Ash-Flow Tuffs....124
Trachyte Lava Flows....125
Trachybasalt Coherent and Autobrecciated Lava Flows....126

DEPOSITIONAL SYSTEMS....127

Western Facies....127
Braid-Plain Deposits....127
Depositional Model....128
Eastern Facies....129
Braid-Delta Deposits....130
Depositional Model....131

DISCUSSION....135

Volcanic Influences on Sedimentation....135
Tectonic Implications....139

CONCLUSIONS....142

REFERENCES CITED....144

APPENDICES....157

Appendix A....158
Locations of Measured Sections....159
Appendix B....161
Clast-Count Data....162
Appendix C....163
Histogram Plots of Clast-Count Data....164
Appendix D....165
Point-Count Data....166
Appendix E....167
Histogram Plots of Point-Count Data....168

LIST OF TABLES

Table Page

1. Table of lithofacies types and flow characteristics.....24

2. Table of conglomerate clast-count data.....162

3. Table of sandstone point-count data.....166

LIST OF FIGURES

Figure Page

1. Schematic diagram of Cretaceous Sevier foreland basin and associated depozones with explosive volcanism occurring in the magmatic arc....2

2. Schematic diagram illustrating volcanic setting within terrestrial and paralic environments....3

3. Timing of tectonic, depositional, intrusive transgressive/regressive, and volcanic events that occurred during the Late Cretaceous....5

4. Regional tectonic map for north-western Montana....6

5. Geologic map of area north of Wolf Creek, Montana....11

6. Photo of western facies field area. View to the west-northwest....12

7. Photo of eastern facies field area. View to the east-northeast....12

8. Schematic stratigraphic section of the western facies....14

9. Schematic stratigraphic section of the eastern facies....16

10. Location map of field area. See Appendix A for stratigraphic section locations....19

11. Location map of detailed stratigraphic sections for the western and eastern facies....20

12. Matrix-supported, massive conglomerate (Gmm)....28

13. Matrix-supported, massive conglomerate (Gmm) with clast-supported zones within the deposit....29

LIST OF FIGURES---Continued

Figure Page

14. Stacked clast-supported, massive conglomerates (Gcm) evidencing crude horizontal bedding....33

15. Close-up of trough cross-bedded conglomerate (Gt), upper half of photo....36

16. "Couplets" of horizontally-bedded conglomerate (Gh) and horizontally-stratified sandstone (Sh)....38

17. Spreiten in massive, bioturbated sandstone (Sm), eastern facies....40

18. Thick deposit of horizontally-stratified sandstone (Sh)....42

19. Wave ripple bedform, eastern facies....45

20. Climbing-ripple cross-lamination (Src) with low-angle cross-stratification (Sl) above....46

21. Ripple cross-laminated sandstones (wavy-flaser bedding) interbedded with muddy stringers....48

22. Rootbeds (Fp) in massive, blocky mudstone (Fm)....49

23. Deposit of poorly-consolidated nodular carbonate (Cn)....51

24. Modified pyroclastic flow model and associated deposits....53

25. Pyroclastic flow model incorporating debris flow transportation mechanisms....54

26. Vitrophyre or vitrophyric tuff (Tv) with abundant feldspar phenocrysts....61

27. Outcrop of unit C illustrating interfingering of vitrophyric tuff (Tv) with ashy, massive tuff (Tm) and horizontally-stratified tuff (Th)....63

28. Schematic diagram illustrating zones of welding and devitrification and vapor phase crystallization for ignimbrites or tuffs....64

LIST OF FIGURES---Continued

Figure Page

29. Common appearance of latite lava flow. Abundant feldspar phenocrysts.....66

30. Outcrop exposure of unit B (latite lava flows), central section, western facies.....67

31. Schematic stratigraphic section of latite lava flows and associated textures.....68

32. Schematic stratigraphic section of unit C and associated lithofacies.....70

33. Example of outcrop exposure for unit C, northern section. Two sheets visible.....71

34. Example of flow banding in welded tuff.....72

35. Outcrop exposure for unit E (trachyte lava flow), central section.....74

36. Schematic stratigraphic section for unit E and associated textures.....76

37. Outcrop exposure of Adel Mountain Volcanics, uppermost part of section RE-Kte.....79

38. Schematic stratigraphic section of channel association deposits, unit D, western facies.....81

39. Schematic stratigraphic section of channel and floodplain deposits, unit F, western facies.....82

40. Example of channel-fill deposits above floodplain mudstones.....85

41. Schematic stratigraphic section of floodplain deposits, unit D.....87

42. Pyroclastic flow (Tmm) deposited above poorly visible massive mudstone (Fm), floodplain association, western facies.....90

43. Accidental lithic clast of laminated, resilicified mudstone (Fl) within latite lava flow, floodplain association, western facies.....92

LIST OF FIGURES---Continued

Figure Page

44. Schematic stratigraphic section of marsh and beach associations, eastern facies....94

45. Interbedded low-angle cross-stratified (Sl), horizontally-stratified (Sh) and ripple cross-stratified (Sr) sandstones in beach association....96

46. Schematic stratigraphic section of lacustrine and channel associations, eastern facies....98

47. Outcrop of channel-fill within the coastal plain deposits of the eastern facies....99

48. Outcrop exposure of crevasse splay deposits....100

49. Schematic stratigraphic section of tidal mudflat association....102

50. Example of lava flow/autobrecciated flow with incorporated mudstone (squeeze-ups) from tidal mudflat....105

51. Schematic stratigraphic section of eastern facies lithofacies associations....106

52. Ternary diagram of modal compositional data....114

53. Schematic diagram of braid-plain depositional system....128

54. Schematic diagram of braid-delta, tidal mudflat, and beach depositional systems....130

55. Schematic block diagram illustrating interaction of eastern facies lithofacies after eruptions from Adel Mountian volcanic center....132

56. Schematic stratigraphic cross-section of Upper Cretaceous rocks in western Montana and southern Alberta....134

ABSTRACT

Deposits of the Campanian Two Medicine Formation near Wolf Creek, Montana, provide essential sedimentologic information necessary for interpretation of the response of alluvial systems to explosive and effusive intra-basinal volcanism. The Two Medicine Formation consists of approximately 1500 meters of interbedded sandstone, conglomerate, and mudstone, with lava flow and rhyolitic tuff. Lithofacies analysis implies deposition of the western facies was by sandy-gravelly braided systems within well-developed, fine-grained floodplains. In addition to normal fluid gravity flow processes, deposition also occurred via debris flow and hyperconcentrated flow. Channel response to volcaniclastic deposition was avulsion during high discharge events, reworking of choked braided systems, and incision into floodplain deposits.

Lithofacies analysis suggests deposition of the eastern facies was by braided distributary channels. Channels funneled sediments to the marsh, tidal mudflat, and beach environments. Fluid gravity flow, hyperconcentrated flow, and debris flow processes influenced the depositional setting by overwhelming the coastal plain with sediment. Lacustrine deposits formed after high discharge events plugged channels, resulting in restricted ponded water. Syn-eruption events resulted in progradation of the braid-delta; inter-eruption periods were characterized by the reworking of volcanic debris, and the reestablishment of beach, tidal mudflat, and marsh settings.

Source areas for the primary volcanic rocks most likely were from the local Wolf Creek volcanic centers. The volcaniclastic sediments are compositionally similar to the primary volcanic rocks; thus, sedimentation in the Two Medicine basin was likely dependent on the erosion of local volcanic carapaces. In addition, the eastern facies was deposited by sediment transported by longshore currents, the westerly braid-plain, and from the Adel Mountain volcanic center.

Volcanism-produced detritus ultimately mantled topography sufficiently to disguise tectonic activity in the Wolf Creek area. Thrust faulting was likely active near the end of Two Medicine deposition, as thrust-belt-derived clasts of Cambrian Flathead Sandstone begin to appear in the youngest Two Medicine deposits.

INTRODUCTION

Retroarc foreland basins typically develop adjacent to fold-thrust belts, far removed from their coeval magmatic arc (Dickinson, 1974; Jordan, 1995; DeCelles and Giles, 1996). Basin-fill originates primarily from erosion of sedimentary rocks in the fold-thrust belt with volcaniclastic sediment input typically limited to infrequent and distally-derived ash-fall deposits (Elder, 1988; Christiansen et al., 1994). Active eruptive centers are rarely present within the foreland basin, therefore, the influence of volcanism on retroarc foreland basin sedimentation has not been thoroughly investigated. Models for foreland basin sediment dispersal generally propose a Sevier-style thrust belt that sheds detritus from uplifted thrust sheets into particular basin depozones (wedge-top, foredeep, forebulge, and back-bulge) via alluvial fans and fluvial systems (DeCelles and Giles, 1996) (Figure 1). As seen in Figure 1, volcaniclastic sedimentation may be an important component of the retroarc foreland basin. Thus, these models and examples do not account for instances in which episodic and catastrophic eruptive activity alters foreland basin depositional environments and transportation mechanisms.

Late Cretaceous time in western Montana was characterized by explosive volcanism. Volcaniclastic sediment derived from magmatic centers associated with the Cordilleran magmatic arc was delivered to the Sevier foreland basin by way of extensive fluvial systems. This study focuses on the influence of Late Cretaceous intra-basin volcanism on foreland basin sedimentation in west-central Montana; specifically, the influence of volcanic processes

and detritus on the fluvial systems that flowed into the Cretaceous Western Interior Seaway. The Upper Cretaceous Two Medicine Formation near Wolf Creek, Montana, was deposited in a volcanically-influenced, non-marine to paralic setting and provides an excellent opportunity to study the record of interaction between volcanism and sedimentation (Figure2).

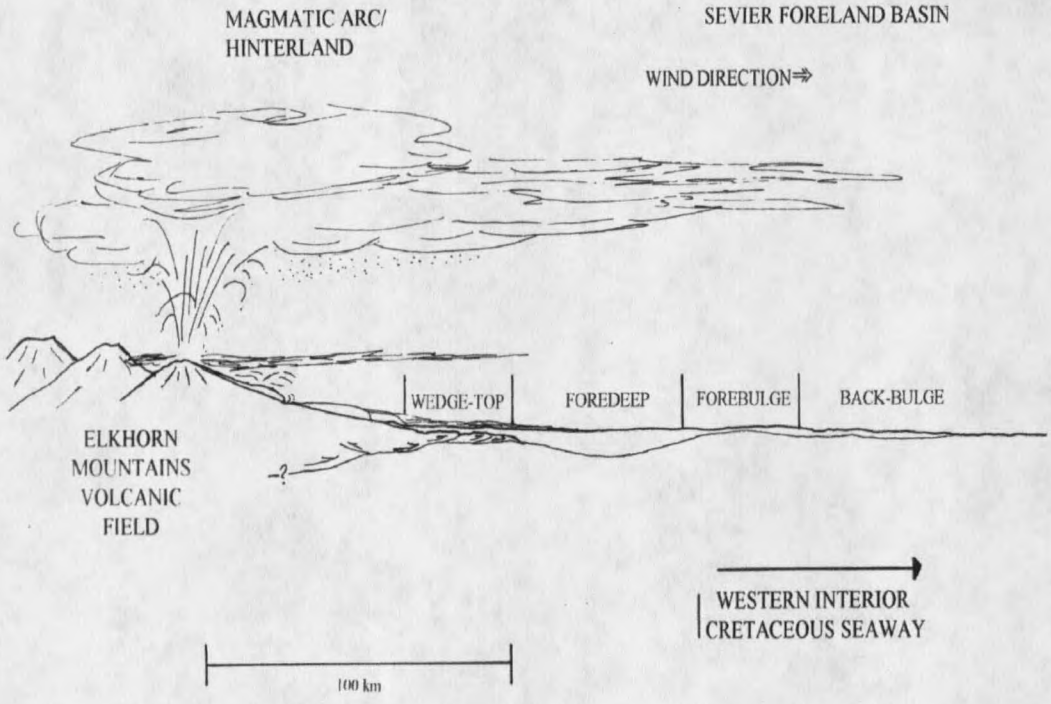


Figure 1: Schematic diagram depicting foreland basin depozones, and associated volcanic and tectonic features. Eruptions within the Elkhorn Mountains volcanic field sent volcaniclastic debris into the wedge-top depozone as proximal deposits. Medial deposits are found in the foredeep depozone, and are represented by the Two Medicine Formation. Air-fall comprises distal deposits in the back-bulge depozone, represented by bentonitic shales of the Western Interior Cretaceous Seaway. Modified from DeCelles and Giles (1996).

Objectives

The objectives of this analysis are to: 1) document the abundance and occurrence of coherent and autoclastic lava flow, pyroclastic flow, pyroclastic surge, and debris flow deposits that comprise the alluvial basin-fill of the Upper Cretaceous Two Medicine Formation, and 2) identify changes in processes of alluvial sediment transport due to sporadic addition of large volumes of volcanic detritus by volcanically-derived debris flow, hyperconcentrated flow, pyroclastic flow, and coherent lava flow. Fulfilling these objectives will allow interpretation of the nature and influence of eruptive activity on the foreland basin fluvial systems. Production of volcaniclastic sediment from intra-basinal volcanic centers is hypothesized to have altered the Sevier foreland basin depositional systems, especially in the Wolf Creek, Montana, study area. Ultimately, the implications of volcanism for evolution of the Sevier foreland basin need to be addressed, but that is beyond the scope of this study.

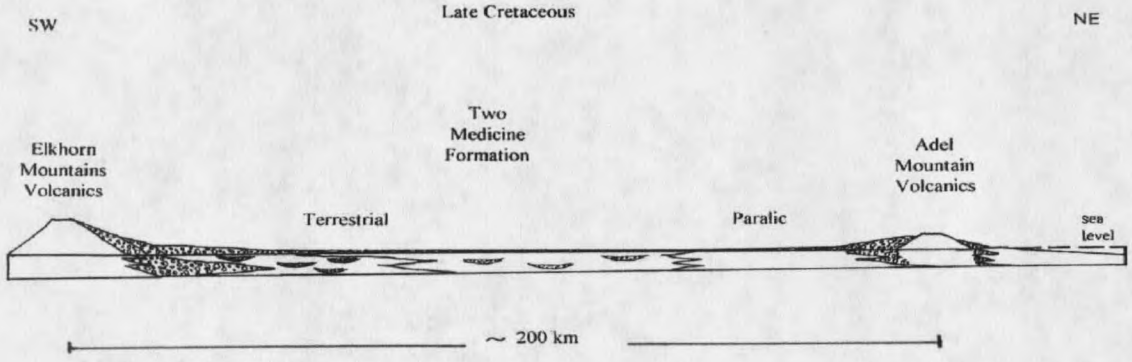


Figure 2: Schematic diagram depicting the interaction of volcanism from the Elkhorn Mountains and Adel Mountain volcanic centers in the Two Medicine depositional basin, during the Campanian.

Geologic Setting

During Late Cretaceous time in western Montana, the Cordilleran magmatic arc swept into the foreland basin. Overlapping spatially and temporally with subduction of the Farallon plate and accretion of exotic terranes along the western continental margin, the Idaho and Boulder batholiths developed synchronous with Sevier thrust belt deformation. Associated with Cordilleran magmatism, large, compositionally distinct volcanic centers (Elkhorn Mountains and Adel Mountain volcanic fields) developed between 80-70 Ma within the Sevier foreland basin (Lyons, 1944; Gwinn and Mutch, 1965; Viele and Harris, 1965; Klepper et al., 1971; Tilling, 1974; Chadwick, 1981; Gunderson and Sheriff, 1991) (Figure 3). Effusive and explosive eruptions in these volcanic centers produced lava flows, pyroclastic flows, and tephra clouds that contributed to the foreland basin-fill of the Upper Cretaceous Two Medicine Formation. Synchronous with volcanism, the adjacent Sevier thrust belt propagated basinward, as depicted in Figure 3 (Robinson and Marvin, 1967; Mudge and Sheppard, 1968; Peterson, 1981; Harlan et al., 1988; Harlan et al., 1991a; Harlan et al, 1991b). The fold-thrust belt advanced eastward resulting in deformation of the Elkhorn Mountains volcanic carapace and westernmost edges of the Adel Mountain volcanic field. How this thin-skinned deformation affected the fluvial systems is unknown.

Elkhorn Mountains Volcanics

The intrusion of the Boulder batholith at ~78-68 Ma (K/Ar) resulted in explosive eruptions producing voluminous (6000 km^3) volcanic deposits of the Elkhorn Mountains volcanic field (Tilling, 1974). The Elkhorn Mountains Volcanics consist of rhyolitic ash-flow

tuff, welded tuff, basaltic and andesitic lava flows, and volcanically-derived sandstone, mudstone, and conglomerate (Smedes, 1966). The Elkhorn Mountains Volcanics has been hypothesized to have once covered an area of 26,000 km^2, based on the areal distribution of rocks believed to be derived from the Elkhorn Mountains volcanic center (Smedes, 1966; Klepper et al., 1971; Tilling, 1974).

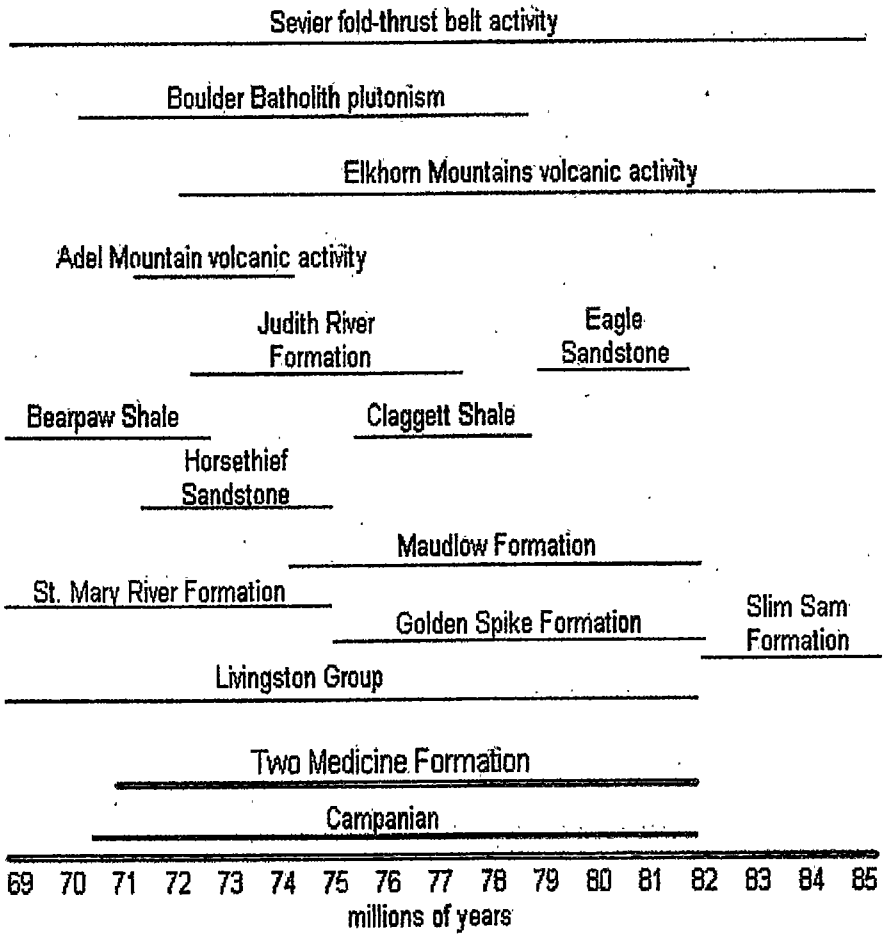


Figure 3: Timing of geologic and tectonic events associated with the Two Medicine Formation. From Lorenz (1981).

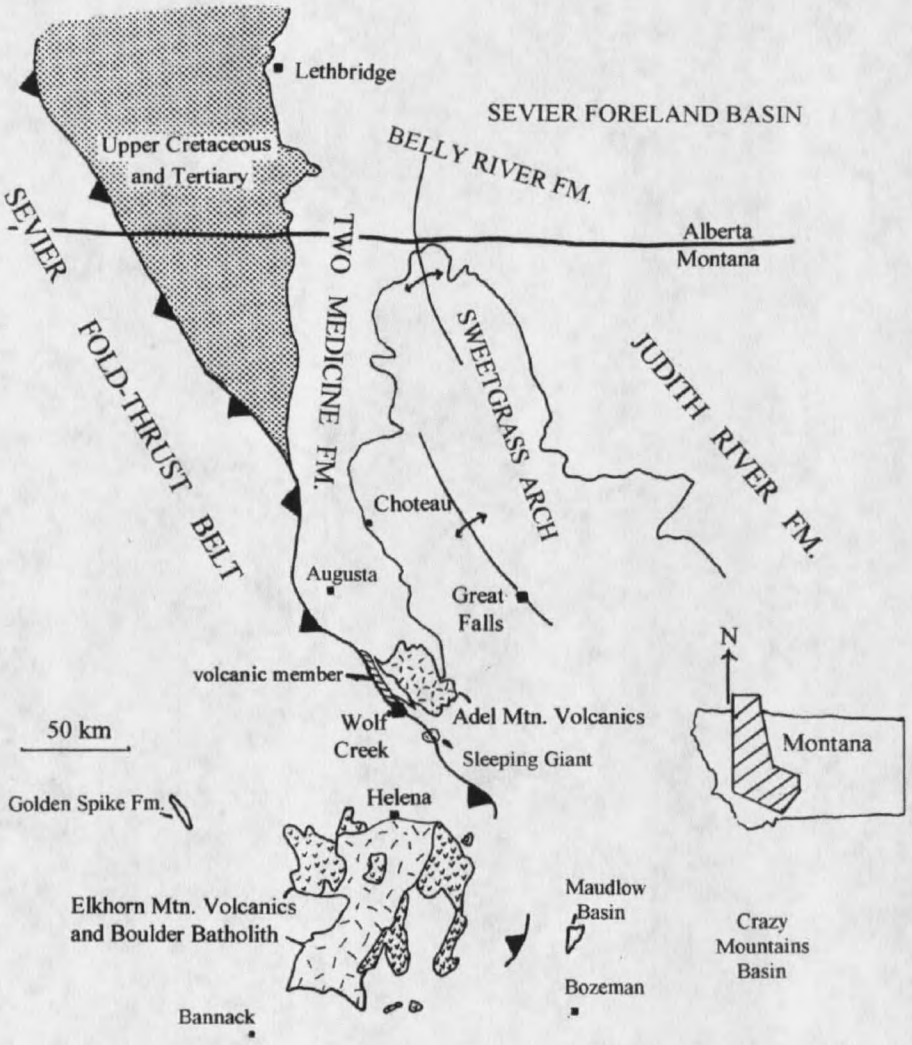


Figure 4: Regional map of the Two Medicine Formation, and tectonic and volcanic features associated with Two Medicine deposition. Modified from Lorenz (1981).

The Elkhorn Mountains volcanic field is believed to be the source for many of the Upper Cretaceous volcaniclastic sedimentary rocks of western Montana, including the volcanic units of the Upper Cretaceous Golden Spike Formation east of the Boulder batholith

(Gwinn and Mutch, 1965; Mackie, 1986) (Figure 4). The Golden Spike Formation contains dominantly non-volcaniclastic deposits; however, the uppermost units consist of ash-flow tuffs that have been stratigraphically correlated with ash-flow tuff sheets found in the middle unit of the Elkhorn Mountains Volcanics (Gwinn and Mutch, 1965; Viele and Harris, 1968; Mackie, 1986). The volcaniclastic Upper Cretaceous Maudlow Formation lies within the Helena salient north of Bozeman, Montana, and is also considered to be derived from the Elkhorn Mountains volcanic field based on similarities in tuff sheet ages (79-75 Ma, K/Ar) (Skipp and McGrew, 1977) (See Figures 3 and 4). The Crazy Mountains basin contains voluminous volcaniclastic rocks assigned to the Livingston Group that are associated with eruptions from the Elkhorn Mountains volcanic center (Roberts, 1963) (See Figures 3 and 4). South of the Boulder batholith, volcanic rocks have been found in the Upper Cretaceous Beaverhead Group at Grasshopper Creek near Bannack, Montana, though not in similar quantities as other localities, and are attributed to Elkhorn Mountains volcanic activity (Ivy, 1989) (See Figure 4). Elkhorn Mountains Volcanics ash-flow tuffs are stratigraphically correlated with ash-fall tuffs found in the Upper Cretaceous Two Medicine Formation (82-70 Ma, K/Ar) near Wolf Creek in west-central Montana (Schmidt, 1978) (See Figures 3 and 4).

Adel Mountain Volcanics

The Adel Mountain volcanic field erupted effusively northeast of the Elkhorn Mountains volcanic field (See Figure 4). The Adel Mountain Volcanics are characterized by trachybasalt and trachyandesite lava flows and sills; syenogabbro dikes; latite and quartz latite stocks and lava flows; and voluminous amounts of volcaniclastic debris in the form of

mudstone, sandstone, conglomerate, breccia, and rare ash-fall tuff layers (Lyons, 1944). K/Ar dating of dikes that cross-cut the Adel Mountain Volcanics has produced late Paleocene (58 Ma) (Schmidt, 1978), and Late Cretaceous (71.2 ± 2.7 Ma) (K/Ar-biotite) minimum ages (Gunderson and Sherriff, 1991). Dating of Adel Mountain Volcanics lavas and breccias from the base of the volcanic pile returned ages of 74 Ma (Harlan et al., 1991) and 81.1± 3.5 Ma (K/Ar - whole rock) (Gunderson and Sherriff, 1991), correlative with Elkhorn Mountains Volcanics and Two Medicine Formation ages (See Figure 3). The Adel Mountain Volcanics were mapped as Paleocene, and thus were considered to be lying on St. Mary River Formation rocks (Schmidt, 1978). As the dates for the Adel Mountain Volcanics imply deposition in the Campanian, rather than Maastrichtian or Paleocene, it is unlikely that the units that interfinger with the Adel Mountain Volcanics are St. Mary River Formation, but are instead Two Medicine Formation deposits.

Wolf Creek Volcanic Center

The Wolf Creek Volcanic Center may represent the locus of volcanic activity that produced the coherent lava flows in the volcanic member of the Two Medicine Formation (See Figure 4). Two intrusions are less than two miles from Wolf Creek. The compositions of the intrusions are latite and trachyte. Neither of these intrusive bodies have been dated, but due to the similarities in composition of the lava flows and the related intrusions, Schmidt (1972a, 1978) mapped and described them as Cretaceous. Both intrusions are mapped as sills (Schmidt, 1978), and similar intrusions have been hypothesized to be the remnants of laccoliths. Approximately 17 kilometers to the south, observed in the footwall of the

Eldorado thrust, is Sleeping Giant, a Cretaceous rhyodacite intrusion that has not been fully described and interpreted (Cannon et al., 1996) (See Figure 4).

Western Interior Cretaceous Seaway

Transgressive and regressive events in the Western Interior Cretaceous Seaway are recorded as the Santonian Telegraph Creek-Eagle regression (85 Ma), Campanian Claggett transgression (79 Ma), Judith River regression (77.5 Ma), Bearpaw transgression (75 Ma), and the Maastrichtian Fox Hills regression (73 Ma) (Gill and Cobban, 1973). Ammonite zones have been correlated into the Two Medicine Formation near the Dearborn River, and the assemblages parallel K/Ar dates from bentonites, Elkhorn Mountains Volcanics ash-flow tuffs, and Elkhorn Mountains Volcanics correlative volcaniclastic rocks (Gill and Cobban, 1973; Schmidt, 1978).

The Elkhorn Mountains volcanic center erupted within the Sevier foreland basin (wedge-top and foredeep depozones) and was later incorporated into the fold-thrust belt. The Adel Mountain volcanic field erupted along the western margin of the Western Interior Cretaceous Seaway during late stages of Elkhorn Mountains volcanism. The Two Medicine Formation, therefore, records the interplay of volcanism in the Elkhorn Mountains and Adel Mountain volcanic centers with terrestrial and paralic environments of the western margin of the seaway (See Figure 2).

TWO MEDICINE FORMATION

Description

Regionally, the Upper Cretaceous (Campanian)Two Medicine Formation is exposed in outcrops from Wolf Creek, Montana, northwards into Canada. The Two Medicine Formation is equivalent to the Judith River Formation east of the Sweetgrass Arch, and the Belly River Group in Canada (See Figure 4). The Two Medicine Formation overlies the Upper Cretaceous Virgelle Sandstone with a slight disconformity, and is conformably overlain by the Upper Cretaceous St. Mary River Formation at the type section near the Two Medicine River, Montana (Schmidt, 1978; Lorenz, 1981). South of Choteau, the St. Mary River Formation pinches out, resulting in deposition of the Horsethief Sandstone conformably on the Two Medicine Formation (Bibler and Schmitt, 1986). Fluvial deposits of sandstone, mudstone, and conglomerate compose most of the Two Medicine Formation near Choteau, Montana (Viele and Harris, 1965; Lorenz, 1981). However, to the south, the Two Medicine Formation rocks are dominantly volcaniclastic, and in fact, contain lava flows and ash-flow tuffs.

At the Wolf Creek, Montana locality, the Two Medicine Formation is divided by the Craig anticlinorium into two lithologically distinct and geographically separate facies belts (Figure 5) (Schmidt, 1978). The western facies is characterized by volcanically-derived sandstone, mudstone, conglomerate, and coherent lava flows (trachyte and latite), as well as

ash-flow and ash-fall tuffs of rhyolite-rhyodacite composition (the Big Skunk Formation of Viele and Harris (1965)) (Schmidt, 1978) (Figure 6). In contrast, the eastern facies is characterized principally by an abundance of mudstone, sandstone, and rare conglomerate with lava flows and autobreccias found only at the top of the formation (Figure 7) (Schmidt, 1978).

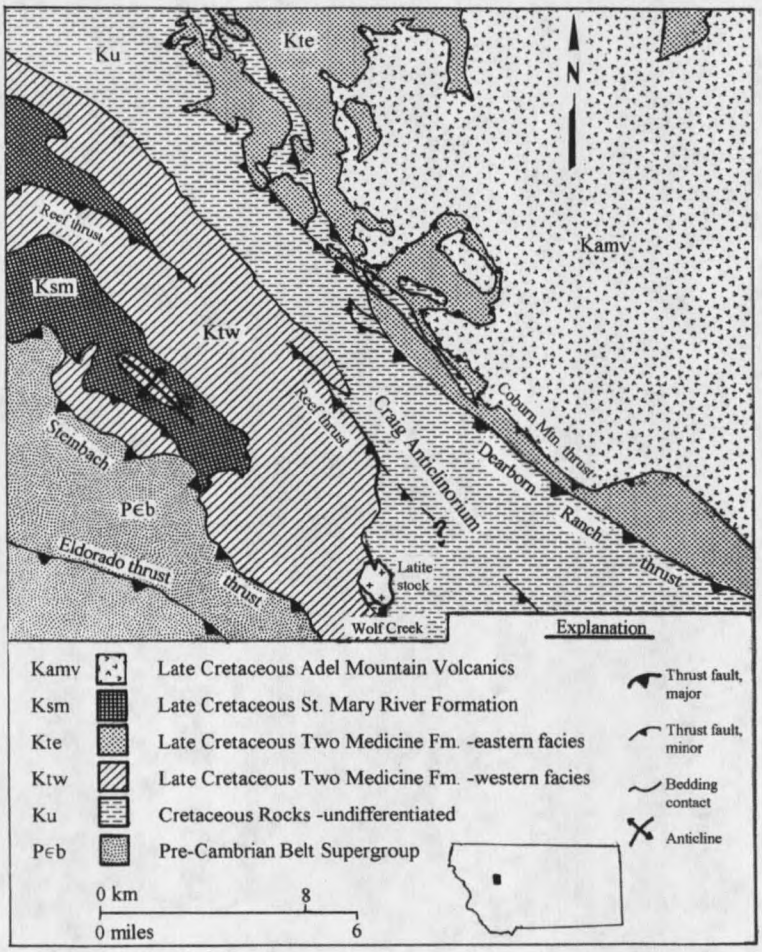


Figure 5: Geologic map of Wolf Creek and Coburn Mountain quadrangles. Modified from Schmidt (1972 a, b).



Figure 6: Western facies deposits exposed in thrust sheets associated with deformation in the Sevier fold-thrust belt. Lateral ridges delineate lava flows and ash-flow tuffs. View to the northwest. Prominent peak is Electric Mountain.



Figure7: Eastern facies deposits exposed on the eastern side of the Dearborn River. Dark deposits at the top of the exposure are Adel Mountain Volcanics. View of Elephant Mountain from Highway 287 to the east-northeast.

Western Facies

The western facies has been divided lithologically into two members: the sedimentary and volcanic members (Schmidt, 1978) (Figure 8). The sedimentary member (Kts) consists of interbedded sandstone, mudstone, and conglomerate, and lies conformably on the Virgelle Sandstone. The sedimentary member was not investigated in this study. The volcanic member was further subdivided by Schmidt (1978) based on lithology, texture, and rock type, and is comprised of units A through H. Unit A consists of interbedded sandstone and mudstone, and rare conglomerate (Schmidt, 1978). Clast composition records a distinct volcanic influence in the uppermost portion of unit A. In addition, unit A consists of a subunit (Unit AA) found only in the northwestern part of the Wolf Creek area, north of the Dearborn River (Schmidt, 1978). This unit is composed of volcanic breccia, sandstone, siltstone, and mudstone, and interfingers with the ash-flow tuff sheets of unit C (Schmidt, 1978). Stratigraphically, unit AA is equivalent to unit B, which is absent from the area where unit AA is found (Schmidt, 1978). Unit AA is not in the field areas of this study. Unit B is comprised of multiple tabular sheets of aphanitic-porphyritic latite. Unit C is characterized by multiple sheets of rhyolitic to rhyolitic welded and nonwelded tuff. Unit D consists of interbedded epiclastic sandstone, mudstone, and conglomerate. This unit coarsens upward, and is characterized by sheet-like deposits and rare channel-scour fill. Unit E is a tabular, aphanitic-porphyritic trachyte with well-developed trachytic texture. Unit F is comprised of interbedded epiclastic sandstone, mudstone, and conglomerate. This unit is distinctly more

coarse-grained than unit D, and has lenticular, channel-fill conglomerates. Unit F also has a subunit (Fa) of volcanic breccia that pinches out to the southeast along strike. Schmidt (1978) describes the unit as being monolithologic (trachytic clasts); however, the mapped unit becomes heterolithologic to the southeast. Unit G is a volcanic conglomerate that is poorly exposed. Finally, unit H consists of interbedded sandstone, mudstone, and conglomerate, but also has a component of ash that permits easy erosion, and therefore, poor exposure. For this study, only units A through F were examined, due to poor exposure of Kts and units G and H. Total thickness for the western facies is approximately 1500 m in the study area (Schmidt, 1978).

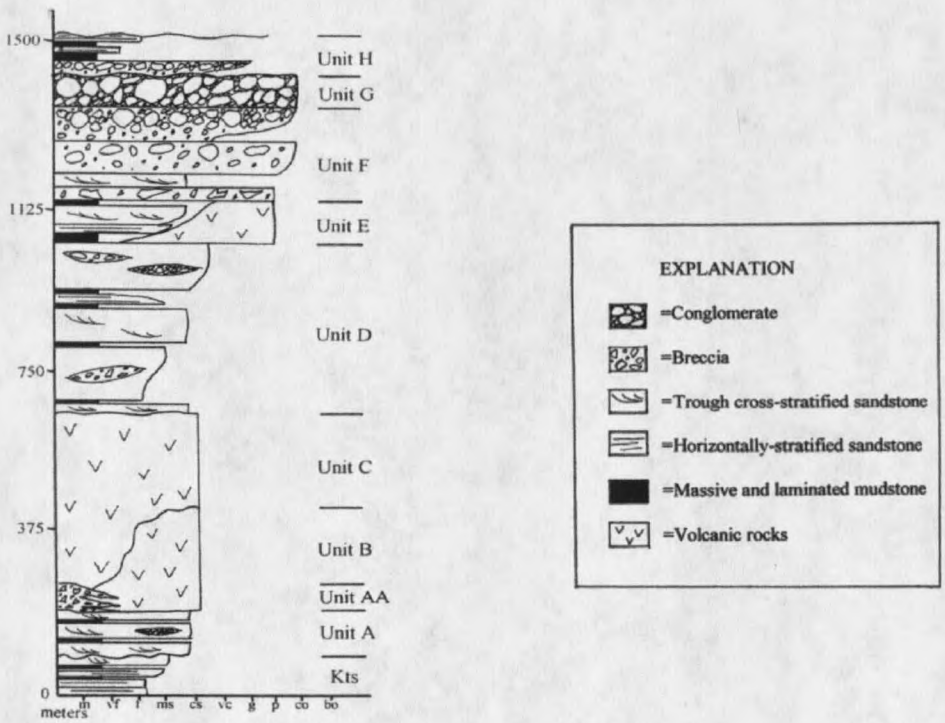


Figure 8: Schematic stratigraphic section of the Two Medicine Formation western facies. Units described in text. Thicknesses approximate. Modified from Schmidt (1978).

Ages and Correlations

The volcanic member of the Two Medicine Formation has been biostratigraphically dated by tracing lower and upper Campanian ammonite zones into the lowermost volcanic member (Gill and Cobban, 1973). Fossil assemblages give an estimated age range of 80-72 Ma (Gill and Cobban, 1973; Schmidt, 1978). K/Ar dating of plagioclase feldspar (72 ± 7 Ma) and biotite (73 ± 2 Ma) from the glassy welded tuff of unit C indicate that volcanic member ages correlate with the fossil assemblages (Robinson and Marvin, 1967). The aforementioned dates also coincide with a K/Ar age of 78 Ma from a lower unit of the Elkhorn Mountains Volcanics (Schmidt, 1978).

Eastern Facies

The eastern facies differs from the western facies by the minor occurrence of primary volcanic rocks. Additionally, it is finer-grain sized, is more mud-rich, and only the upper portion contains very coarse (boulder) volcanic conglomerates and breccias (Figure 9). The volcanic breccias are interfingered with the uppermost units of the eastern facies, and are likely derived from the Adel Mountain volcanic center (Lyons, 1944). The eastern facies is approximately 590 meters thick (Schmidt, 1978). Southeast of the study area, the Adel Mountain Volcanics overlie the Two Medicine Formation eastern facies with an angular unconformity that cuts the Upper Cretaceous Virgelle Sandstone as well (Schmidt, 1978). A northerly field area was chosen for the eastern facies due to the interfingering of the Adel Mountain Volcanics and uppermost Two Medicine Formation eastern facies and lack of major structural deformation.

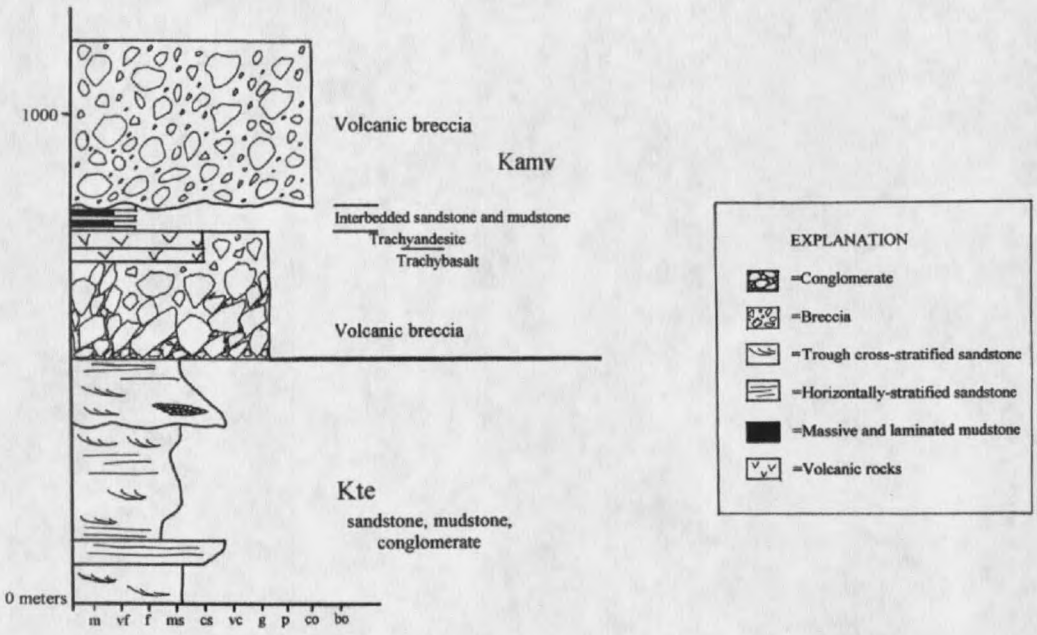


Figure 9: Schematic stratigraphic section of the Two Medicine Formation, eastern facies, and the Adel Mountain Volcanics. Thicknesses approximate, and interfingering of units not depicted. Modified from Schmidt (1978).

Ages and Correlations

The lowermost portion of the eastern facies has been determined to be correlative with the basal sedimentary member of the Two Medicine western facies since both rest conformably on the Virgelle Sandstone (Schmidt, 1978). In the study area, only the upper half of the eastern facies was measured (268 m) due to poor exposure of lower units. The uppermost 40 meters were assigned to the St. Mary River Formation by Schmidt (1978). However, these units are indistinguishable from Two Medicine Formation deposits, and recent dating of the Adel Mountain Volcanics has produced Late Cretaceous ages (Viele and Harris 1965; Schmidt, 1978; Sherrif and Gunderson, 1990). Therefore, the uppermost

volcaniclastic units are Two Medicine Formation deposits. In addition, Gill and Cobban (1973) placed these deposits at the top of the Two Medicine Formation, based on their littoral depositional environment. The eastern facies also has a nearshore component that could be equivalent to the Upper Cretaceous Horsethief Formation. This interpreted correlation is based on the occurrence of *Ostrea glabra*, a Late Cretaceous oyster found typically in Horsethief Formation sandstones (Schmidt and Zubovic, 1961)

Schmidt (1965) and Lyons (1944) included the Adel Mountain Volcanics rocks of this study in the volcanic breccia unit of the Adel Mountain Volcanics. Mapping of the deposits suggests that the volcanic rocks are conformable with underlying and interfingering sedimentary rocks. This permits conformable, yet discontinuous, contact between the volcanic and sedimentary rocks, and indicates the occurrence of a transition zone between the eastern facies of the Two Medicine Formation and the Adel Mountain Volcanics.

METHODS

Initial field reconnaissance was done to find well-exposed units for measurement and data collection using the Coburn Mountain and Wolf Creek geologic quadrangle maps (Schmidt, 1972a, 1972b). Three partial stratigraphic sections were measured (north, central, and south) in the western facies of the Two Medicine Formation, and two partial stratigraphic sections were measured through the eastern facies (RE and E2) (Figure 10). The stratigraphic sections were selected for accessibility, continuity of vertical exposure, and possible lateral correlativity along strike. Data were collected from both facies in order to identify transportation mechanism differences (and therefore, changes in depositional environment) between the western and eastern facies, and to compare the occurrence of primary volcanic rocks within the study area. Locations of stratigraphic sections are presented in Appendix A and Figure 11. The actual detailed stratigraphic sections are on file with the Department of Earth Sciences.

In order to document the relative abundance of lava flows, pyroclastic rocks, and epiclastic conglomerates found in the Upper Cretaceous Two Medicine Formation, information derived from detailed stratigraphic sections was analyzed. Information collected includes unit thickness, lateral extent of units between stratigraphic sections, rock type, geometry, shape and nature of the basal surfaces of units, and sedimentary structures. Additionally, stratigraphic sections measured in primary volcanic rocks provided information on vesicle content, lithophysae distribution, flow thickness, geometry, and lateral continuity

of units. Stratigraphic sections measured through pyroclastic rocks allowed observation of pyroclastic sedimentary structures, unit thickness, lateral continuity, occurrences of vesicles, pumice and accidental lithic clasts, and degree of welding.

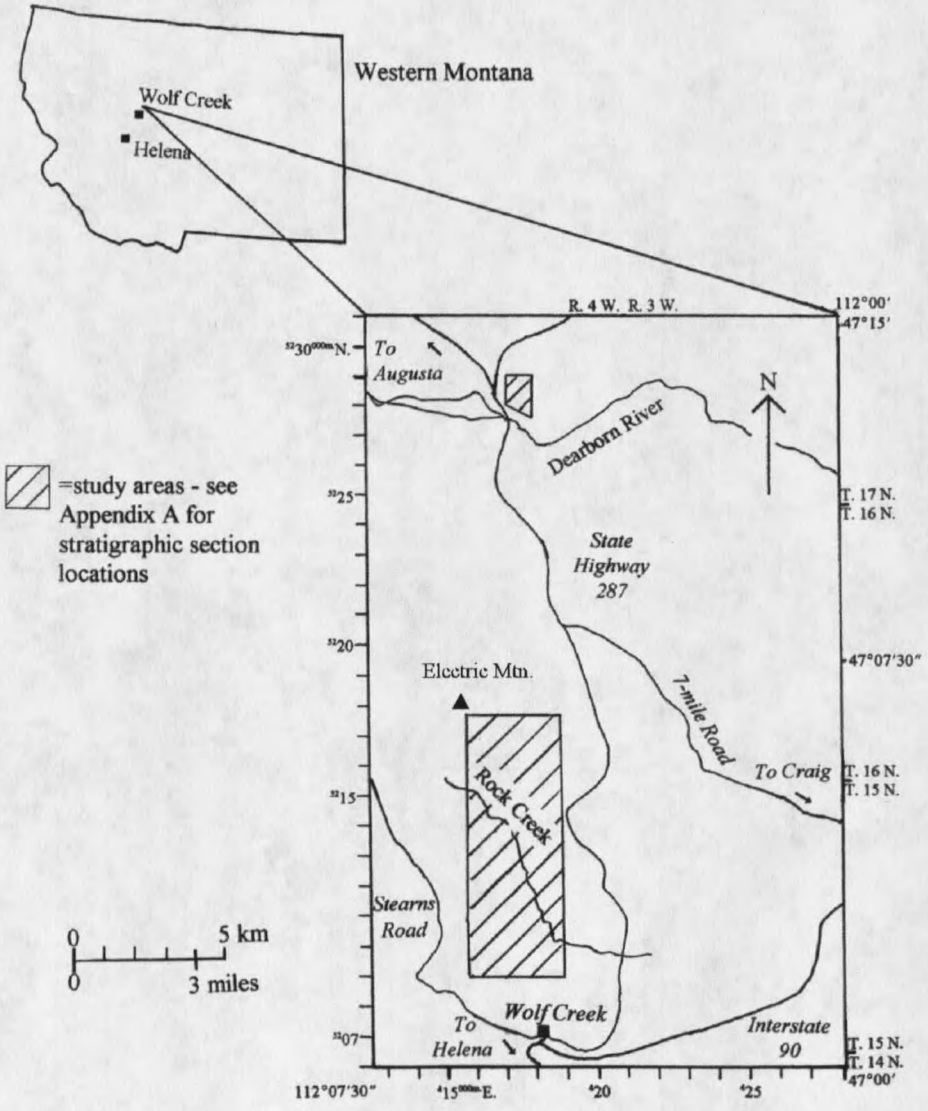


Figure 10: Location map of study areas. See Figure 11 for detailed maps of western and eastern study areas and locations of measured sections. See Appendix A for precise stratigraphic section locations. Modified from Schmidt (1972 a, b).

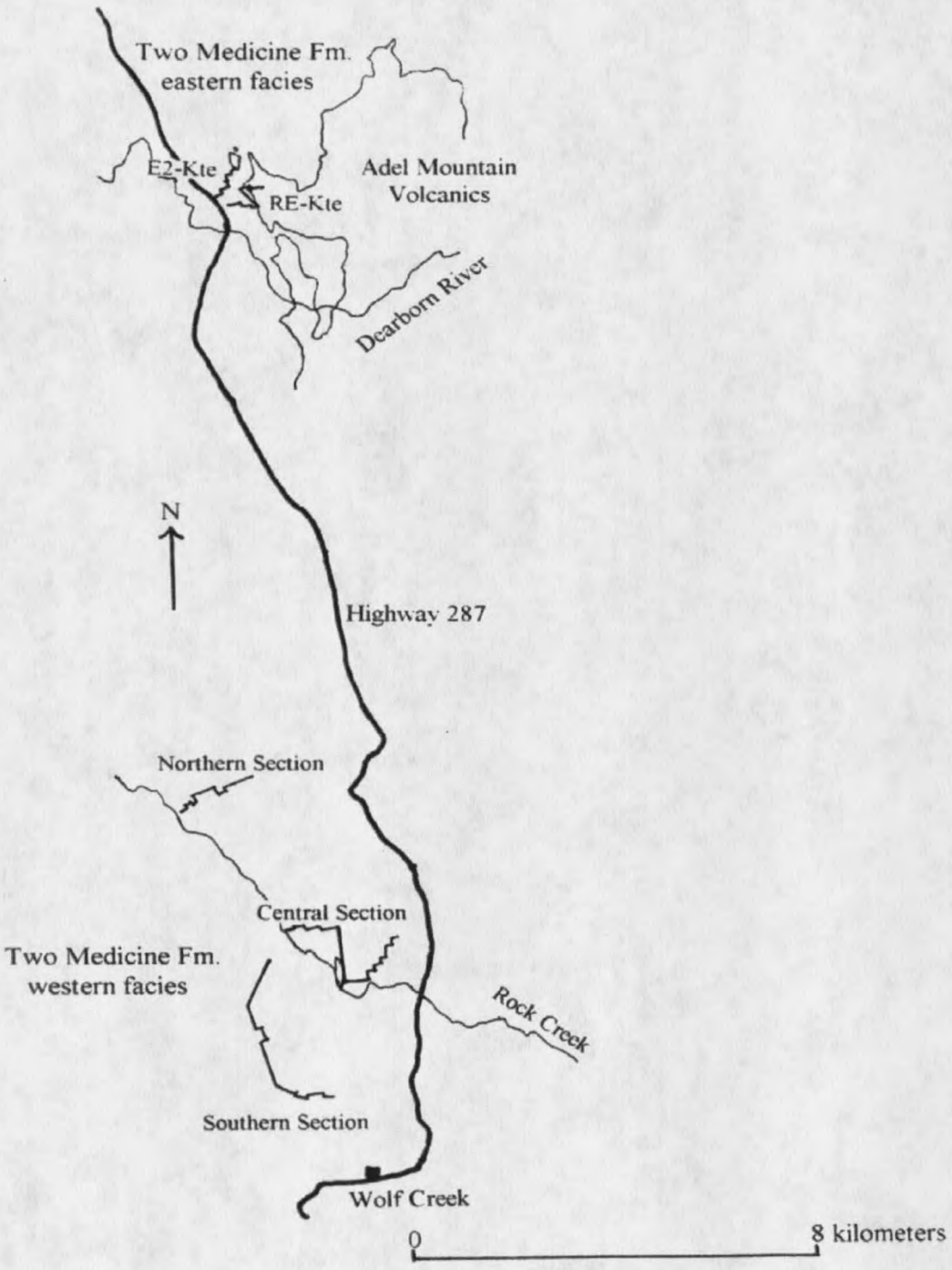


Figure 11: Detailed location map of study areas from Figure 10. See Appendix A for precise stratigraphic section locations. Modified from Schmidt (1972 a, b).

Stratigraphic analysis also led to delineation of lithofacies. Lithofacies were subdivided based on sedimentary structures and dominant (>50%) grain size, as well as basal surfaces, bed geometries, sorting, and grading characteristics (Miall, 1996). Lithofacies associations were then identified, based on repeated occurrences of groups of certain lithofacies. The associations permit interpretation of the depositional systems and ultimately, paleogeographic reconstructions.

Twenty-five volcanic rocks were thin sectioned to identify composition, flow banding, and mode of emplacement. Petrographic identification of major and minor mineral constituents and volcanic textures assisted in determining individual episodes of volcanism, and allowed comparisons between the dominant mineral assemblages known for the Adel Mountain Volcanics and Elkhorn Mountains Volcanics fields.

To aid in determining the effect volcanism had on sedimentation processes, twenty-eight thin sections of sedimentary rocks were analyzed. The thin sections were used to identify sandstone mineral composition, which assists interpretation of depositional environment and provenance. In order to determine the composition of sediment (volcaniclastic versus non-volcaniclastic) deposited in the Sevier foreland basin, point counts were taken of very fine, fine, medium, coarse, and very coarse sand-sized sandstones. Point counts of sandstone grains provide quantitative data on the amount of quartz, feldspar, volcanic lithic fragments, mafic minerals, and accessory minerals present in the deposits. This is necessary for understanding intereruptive influences on the fluvial system. Additionally, grain size comparisons may provide information on distance and duration of transport, and therefore, may assist in depositional environment interpretation. Provenance comparisons

between the western and eastern facies were determined using ternary diagrams that plot modal sandstone framework grain compositions.

Clast counts of conglomerate units identified in the western facies stratigraphic sections were used to evaluate relative abundance of volcanic versus nonvolcanic sediment sources. This was necessary for determining volcanic (syn-eruption and inter-eruption) mass wasting versus dispersal of thrust-belt derived sediment in the area around Wolf Creek, Montana, during Late Cretaceous time.

LITHOFACIES

The Upper Cretaceous Two Medicine Formation consists of conglomerate, sandstone, mudstone, and minor carbonate deposits interbedded with volcanic lava flows and pyroclastic ash-flow tuffs. Lithofacies types are based on predominant (>50%) grain size, bedding, stratification, bed geometry, texture, fabric, sorting of grains, and sedimentary structures found within sedimentary units D and F of the western facies, and the eastern facies (Miall, 1996) (Table 1). Pyroclastic lithofacies (unit C) are defined by clast size, lithology, bed geometry, stratification, and sedimentary structures (See Table 1). As the clastic rocks in the study area are predominantly volcaniclastic, interpretation of lithofacies is reliant upon comparisons with observations from known volcaniclastic settings and processes. Therefore, lithofacies interpretations are based on modern and ancient examples of volcaniclastic sedimentation, and the effects of volcanism on sedimentation processes. Using multiple sources results in multiple interpretations for each lithofacies; in some instances, it is difficult to identify the most preferred interpretation, based upon the uncertainty as to what precisely occurred. Lithofacies in this section, therefore are presented with interpretations that may or may not have occurred. In some instances, the choice is made based on whether the lithofacies conforms to prerequisite characteristics for certain processes, such as grain size.

Table 1. Summary of lithofacies types and flow characteristics for the Upper Cretaceous Two Medicine Formation.

	Code	Rock Description	Sedimentary Structures	Type of Process	Other Characteristics
Conglomerate Lithofacies	*Gmm*	matrix-supported, massive poorly sorted, mud to cobble, rounded to very angular clasts	ungraded	debris flow autobrecciated lava flow	laminar flow, high matrix strength, deposition *en masse* friction-induced breakage as flow travels
	Gmmi	matrix-supported, poorly sorted, massive, mud to cobbles, rounded to very angular clasts	inverse coarse-tail grading	debris flow	fully sheared flow, high dispersive pressures, increase in yield strength
	Gmin	matrix-supported, massive, poorly sorted, mud to cobbles, rounded to very angular clasts	inverse to normal coarse-tail grading	debris flow	high basal dispersive pressure that decreases upward within the flow, decreasing matrix strength
	Gcm	clast-supported, massive, pebble to boulders, very poorly sorted, rounded to angular clasts	ungraded bimodal	debris flow hyperconcentrated flow fluid gravity flow	high buoyancy, low turbulence, high yield strength, deposition *en masse* sheet flood, turbulent flow turbulent flow, traction current transport
	Gcmi	clast-supported, massive, pebble to boulders, very poorly sorted, rounded to angular clasts	coarse-tail inverse grading	debris flow hyperconcentrated flow autobrecciated lava flow	high yield strength, high dispersive pressures sheet flood, turbulent flow friction-induced breakage as flow travels
	Gcms	clast-supported, massive, pebble to boulders, very poorly sorted, rounded to angular clasts	coarse-tail normal grading	debris flow hyperconcentrated flow	high turbulence, low dispersive pressures, low yield strength, increased fluidity sheet flood, turbulent flow, low yield strength
	Gcin	clast-supported, massive, pebble to boulders, very poorly sorted, rounded to angular clasts	inverse to normal coarse-tail grading	debris flow	fluid-rich, basal tractive layer, normal to turbulent suspension of grains
	Gt	granule to cobble, moderate to poorly sorted	trough cross-bedding	fluid gravity flow	high turbulence, mixed bedload, channel-fill, diffuse gravel sheets
	Gh	granule to small cobble, moderate to poorly sorted	horizontal bedding	fluid gravity flow hyperconcentrated flow	traction current, turbulent grain support diffuse gravel sheets low turbulence, buoyancy, dispersive pressure, sheet flood

Table 1: Continued

	Code	Rock Description	Sedimentary Structures	Type of Process	Other Characteristics
	Sm	very fine to coarse sand, massive moderately to poorly sorted	ungraded	bioturbation hyperconcentrated flow debris flow	unknown flow characteristics high sediment concentrations, low turbulence bank-collapse, highly turbulent, deposits *en masse*
	Smi	very fine to coarse sand, massive, poorly sorted	inversely graded	debris flow	high dispersive pressures, laminar flow, increased yield strength
	Sh	very fine to coarse sand, moderate to poorly sorted, some outsized granules, small cobbles	horizontal lamination	fluid gravity flow hyperconcentrated flow	transition from subcritical to supercritical flow, no turbulence, plane bed transport laminar flow, upper flow regime, low turbulence
Sandstone Lithofacies	*Sl*	fine to very coarse sand, rare outsized pebbles, moderately to very poorly sorted	low-angle (<15°) trough cross-stratification coarsening and fining upwards sequences	fluid gravity flow	upper flow regime transformation low turbulence
	St	medium to very coarse sand, moderately to very poorly sorted, outsized pebbles common	trough cross-stratified coarsening and fining upwards sequences	fluid gravity flow	traction current transport, low flow regime turbulent
	Sr	very fine to fine sand, moderately to well sorted, outsized clasts very rare	ripple-cross-lamination asymmetric	fluid gravity flow	low flow regime, traction current transport
	Srs	very fine to fine sand, well to very well sorted	ripple cross-lamination symmetric	fluid gravity flow	low flow regime, bi-directional traction transport
	Src	very fine to fine sand, moderately to well sorted, few outsized clast	climbing ripple cross-lamination	fluid gravity flow	low flow regime, aggradation from influx of sediment, traction current transport
	Fl	mud and silt, well to moderately sorted	horizontally-laminated	fluid gravity flow	lower flow regime, suspension settling of grains, waning flow
	Fm	mud and silt, well to poorly sorted	massive	fluid gravity flow debris flow	suspension settling, lower flow regime dilute flow
Mudrock Lithofacies	*Fp*	mud and silt, root beds	massive	pedogenic	unknown characteristics, bioturbated

Table 1: Continued

	Code	Rock Description	Sedimentary Structures	Type of Process	Other Characteristics
Non-Clastic Lithofacies	*O*	coal, clay, iron oxide nodules	horizontally-stratified	diagenesis	abundant plant debris, standing water
	Cl	carbonate, laminated	horizontally-laminated	fluid gravity flow	waning flow, shallow water, low sediment influx
	Cn	carbonate, massive	nodular	chemical, pedogenic	pedosol development
Pyroclastic Lithofacies	*Lmm*	matrix-supported, pumice and accidental lithic lapilli, poorly sorted	massive lithics normally graded pumice ungraded	pyroclastic flow	extremely high fluidization some turbulence, high particle concentration
	Tmm	fine ash-sized pumice, glass shards, pumice and lithic lapilli, poorly sorted, matrix-supported	massive ungraded	pyroclastic flow	nonturbulent, high particle concentrations, laminar flow, deposition *en masse*
	Tmmg	fine ash-sized pumice, glass shards, pumice and lithic lapilli, poorly sorted, matrix-supported	massive density graded	pyroclastic flow	increased fluidity of the flow, dispersive pressure at top of flow, turbulent at flow base, density contrasts between clasts and matrix
	Tm	coarse ash, glass shards, medium to very coarse crystals and lithics poorly sorted	massive ungraded	pyroclastic flow	waning flow, nonturbulent, laminar flow
	Th	fine ash, accretionary lapilli	horizontally stratified	pyroclastic surge	turbulent, upper flow regime, planar bedding
	Ta	fine to coarse ash of glass and crystals, pumice and lithic lapilli, poorly sorted	antidunes	pyroclastic surge	upper flow regime, turbulent, high particle concentration, fluidized
	Trc	ash-sized glass shards; sub-angular lithics, poorly sorted	climbing ripple cross-lamination	pyroclastic surge	turbulent, high particle concentration, fluidized
	Tv	dense glass, aligned feldspar microlites, pumice and lithic lapilli	massive welded and nonwelded zones	pyroclastic flow	laminar flow, high yield strength, extreme temperatures

Conglomerate Lithofacies

Matrix-Supported, Massive Conglomerate (Gmm), (Gmmi), (Gmin)

This conglomerate lithofacies is dominantly ungraded, massive, and matrix-supported (Gmm), although two examples show evidence of grading. Clasts range in size from granule to cobble, with uncommon boulders and blocks present in some outcrops. Clasts are very angular to rounded, and poorly to very poorly sorted (Figure 12). Matrix is mud to very coarse sand size, moderately to poorly sorted, and may exhibit normal grading. Basal surfaces are sharp or follow pre-existing channel scours. Geometries include wedge-shaped, tabular, trough, and lenticular beds, and dimensions vary from 0.4 to 7 meters thick and 2 to tens of meters in length. Weak horizontal bedding may be visible in some outcrops, defined by grain size changes. Flame structures may be present at the base if mudstone is the underlying unit. Some beds also have vertical zones of concentrated pebbles, where the matrix seems to be disrupted, interpreted to be fluid-escape pipes or segregation pipes. In some instances, radially-jointed 0.3 to 0.6 meter diameter clasts are preserved in a red-orange matrix. Decreases in the percentage of matrix-support may lead to clast-supported zones or clusters (Figure 13). Some units possess inverse coarse-tail grading (Gmmi). Inverse coarse-tail grading may lead to clast-supported deposits at the top of the units, which is indicated as a clast-supported, massive conglomerate (Gcm), described below. Some conglomerates have inverse to normal coarse-tail grading (Gmin), described below.

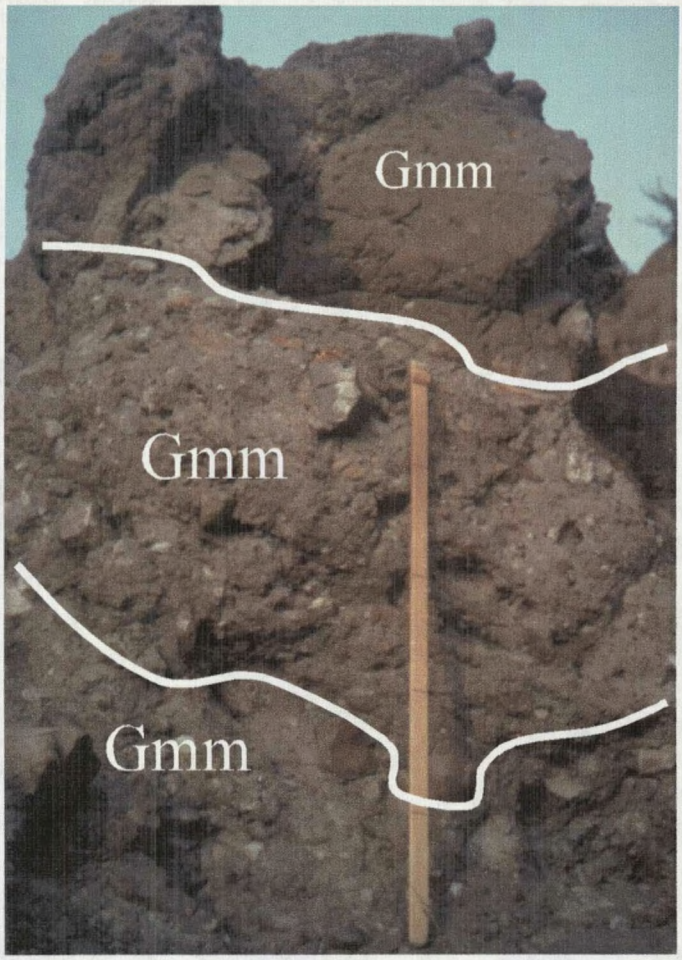


Figure 12: Matrix-supported, massive, conglomerate (Gmm) in eastern facies deposit approximately 320 meters from the base of section RE-Kte. View to the north. Jacob's staff is 1.5 meters tall.

Interpretation: Matrix-supported conglomerates (Gmm) are interpreted to have been deposited by debris flows which are dispersions of sediment in water (Fisher, 1971). Driven by gravity, debris flows typically follow topographic depressions or channels. Deposition usually occurs *en masse* due to the loss of transporting fluid and decrease in slope; therefore, the deposit "freezes" in place (Fisher, 1971; Runkel, 1990). In order to transport large

particles, these laminar flows must have a high matrix strength (Fisher, 1971; Vessel and Davies, 1981; Smith, 1987a). Additionally, the high density of the transporting fluid results in high buoyancy, which also allows large particles to be transported (Fisher, 1971). Typically, the support mechanism for ungraded debris flows is a combination of dispersive pressure, high matrix strength, and buoyancy (Vessel and Davies, 1981; Smith, 1986; Valentine et al., 1998).

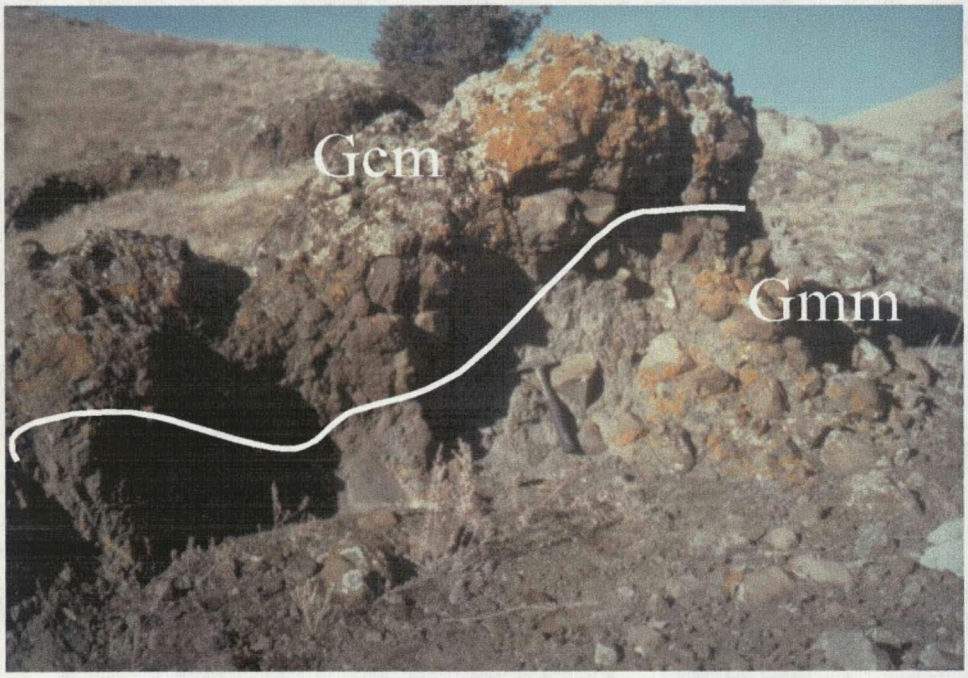


Figure 13: Clast-supported, massive, conglomerate (Gcm) above a matrix-supported, massive conglomerate (Gmm) in the eastern facies, approximately 260 meters above the base of stratigraphic section E2-Kte. Hammer for scale. View to the north.

Volcanic debris flows are characteristically cohesionless, due to the lack of clay minerals in the matrix (Smith and Lowe, 1991). The matrix is typically dominated by ash, glass shards, and crystal fragments. The strength of the flow is derived therefore, from grain

interactions (friction), and cohesion of silt-sized ash (Smith and Lowe, 1991). This results in volcanic debris flows that are thinner than the typical debris flow of Fisher (1971), and farther traveled. The flow also, therefore, does not necessarily deposit *en masse*, but by loss of competency during waning flow (Smith and Lowe, 1991).

Another influence on the behavior of volcanic debris flows is temperature. Viscosity decreases with increased temperature (Arguden and Rodolfo, 1990). Hot water and vapor decrease the internal friction of the flow, and therefore, increase the distance the flow can travel (Arguden and Rodolfo, 1990). In a hot flow, large clasts are supported by a combination of dispersive pressure and turbulence, due to the low internal strength (Arguden and Rodolfo, 1990). The upward movement of hot water vapor through the flow produces high internal pressures that also assist in supporting clasts (Arguden and Rodolfo, 1990). Temperature indicators in the field may be obscure. Red coloration of the deposits, clasts possessing radial cooling joints, and charred wood are inferred to be the result of heat during emplacement. Most deposits of Gmm that contain these high temperature indicators are interpreted to have been deposited by hot, volcanic debris flows; however, autobrecciated or autoclastic lava flow deposits may resemble hot debris flow deposits (Riggs et al., 1997).

Autobrecciated deposits are the result of mechanical breakdown of lava flows as they move downslope. Unfortunately, it is difficult to determine whether a poorly sorted conglomerate or breccia is a debris flow deposit or an autobrecciated lava flow. An interpretation based on matrix content, temperature of emplacement, and clast lithology may be possible, but it has been documented that these criteria are not always conclusive (Riggs et al., 1997).

Autobrecciation occurs through multiple processes. Brittle deformation at the base and front of a lava flow is a result of friction generated as the lava flow moves over a consolidated surface, producing a "flow breccia" (Fisher and Schmincke, 1984). Deposits of Gmm are interpreted to be autobrecciated lava flows when associated with an overlying lava flow (Ricketts, 1985); this is observed in one example, found in the eastern facies (measured section Kamv), and is the only interpreted "flow breccia" deposit.

Autobrecciation also results from quench-shattering of the lava flow as it enters water (Cas and Wright, 1988). Autobrecciated deposits formed from interaction with water may be called hyaloclastites or hydroclastics (Fisher and Schmincke, 1984; Cas and Wright, 1988). Deposits of Gmm lack evidence of quench-shattering, such as pillow-rinds. However, phreatic or phreatomagmatic eruptions may also produce hydroclastic deposits (Fisher and Schmincke, 1984). Explosions produced by either gases or the rapid transformation of water to steam result in fragmentation of lava flows (Fisher and Schmincke, 1984; Cas and Wright, 1988). As a lava flow encounters surface water, a phreatic explosion occurs, locally brecciating the lava flow (Furnes and Sturt, 1976; Ricketts, 1985). Deposits from phreatic or phreatomagmatic processes are typically fine-grained, although coarser lapilli do exist (Fisher and Schmincke, 1984). The larger clasts and bombs are characterized by cauliflower texture (Fisher and Schmincke, 1984). Textures indicating lava flow interaction with water are not found in deposits of Gmm.

Inverse coarse-tail grading (Gmmi) is due to either an increase in flow yield strength or high dispersive pressure forcing the larger clasts to the top of the flow during transport (Smith, 1987a). Dispersive pressures, or forces, also increase as the concentration of sediment

increases (Fisher, 1971). In a fully sheared flow, this would allow inverse coarse-tail grading, as larger particles tend to move toward the areas of lower shear (Fisher, 1971). Walton and Palmer (1988) also attribute inverse grading in volcanic debris flows to flow that is fully sheared at all times. As discussed above for ungraded debris flows, the lack of clay minerals in a flow reduces the strength, and this also decreases the resistance of the flow to shear (Smith and Lowe, 1991).

Inverse to normal coarse-tail grading (Gmin) is due to decreasing matrix strength in the debris flow, and high basal dispersive pressures that decrease upward within the flow (Fisher, 1971; Walton and Palmer, 1988; Arguden and Rodolfo, 1990). Additionally, particle settling within the flow produces an upper portion of the flow that is normally graded (Arguden and Rodolfo, 1990).

Clast-Supported, Massive Conglomerate
(Gcm), (Gcmi), (Gcms), (Gcin)

Deposits of this lithofacies are clast-supported, massive, and are commonly ungraded (Gcm), although grading is evident in some examples (Gcmi, Gcms, Gcin). Clasts are pebble to boulder size, rounded to angular, and very poorly sorted (Figure 14). Matrix is typically mud to very coarse sand-sized and very poorly sorted; however, in some instances, matrix is medium to fine sand and well sorted. Beds are 1 to 20 meters thick and laterally continuous for up to 10 meters. Bed geometries are tabular and lenticular. Basal surfaces are erosive, or sharp with mudstone flame structures and fluid escape pipes uncommon. Deposits may contain clasts that are weathered red-orange and possess radial cooling joints. In some instances, units are coarse-tail inverse graded (Gcmi), while other units are coarse-tail normal

graded (Gcms) and may become matrix-supported at the top of the deposit (Gmm). Some units show inverse to normal coarse-tail grading (Gcin). These examples of graded clast-supported, massive conglomerate are discussed below.

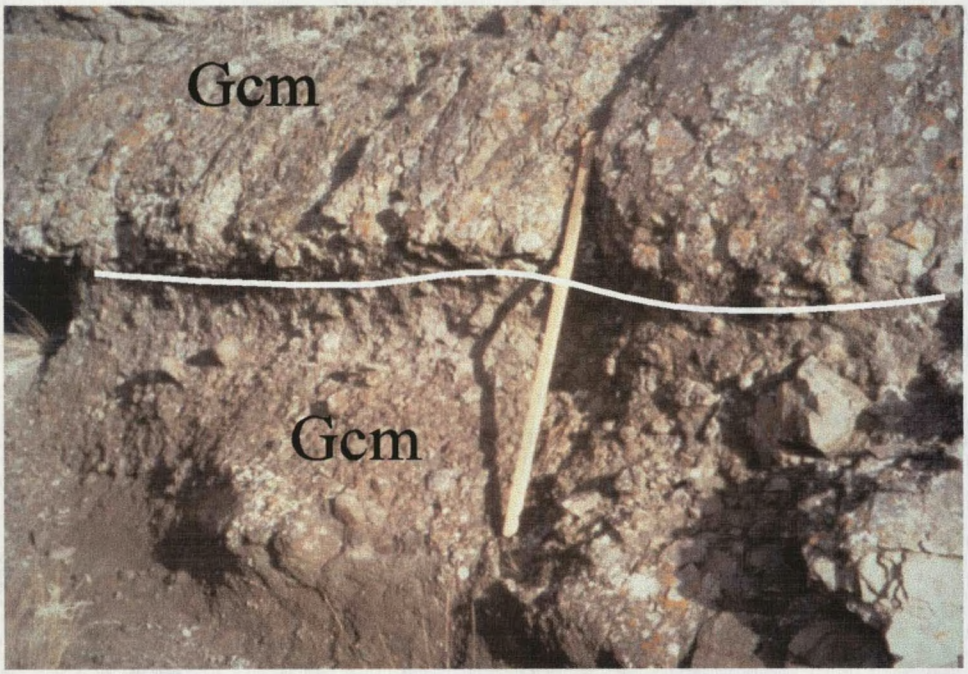


Figure 14: Two tabular bodies of clast-supported, massive conglomerate (Gcm) in eastern facies, approximately located 300 meters above the base of stratigraphic section RE-Kte. Jacob's staff for scale is 1.5 meters tall.

Interpretation: Clast-supported, massive, ungraded conglomerate (Gcm) may be the result of a clast-rich debris flow that supports clasts through high buoyancy, low turbulence, and high yield strength (Shultz, 1984; Walton and Palmer, 1988). Friction, in the form of dispersive pressure, determines the yield strength, and dispersive pressure is more influential in clast-rich flows (Shultz, 1984). Deposits are transported by laminar flow, and thus characteristically lack an erosive base. However, in some instances, Gcm was found with a

scoured basal surface, and this may indicate deposition in a pre-existing channel. Based on the lack of grading and sorting, it is likely that deposition was *en masse* (Fisher, 1971; Runkel, 1990).

Deposition by fluid-gravity flow is another interpretation for Gcm deposits that display bimodal grain-size distributions and erosive basal contacts; these are due to turbulent flow and traction current transport of large clasts, and infiltration of finer-grained sand during waning flow (Shultz, 1984; Smith, 1986). If the Gcm deposit is thin, and lacks bimodal grain-size distribution, it is most likely due to hyperconcentrated flow (Smith, 1986). In this instance, grain support would be through turbulence and increased dispersive pressures. As described for deposits of Gmm with evidence of high temperature emplacement, Gcm deposits not associated with a lava flow are interpreted as being transported by a hot, volcanic debris flow, or as the result of small, phreatic explosions that occurred when the extruding lava flow encountered surface water (Ricketts, 1985).

Coarse-tail inversely graded conglomerate (Gcmi) is deposited by a fully sheared debris flow with high strength and/or high dispersive pressure (Smith, 1987; Walton and Palmer, 1988). The high clast abundance permits higher dispersive pressures, and in a poorly sorted flow, the larger clasts are "pushed" to the top of the flow where shearing is less (Fisher, 1971; Shultz, 1984).

Coarse-tail normal graded conglomerate (Gcms) may be the result of a more turbulent debris flow, or a hyperconcentrated flow (Smith, 1987a). Turbulence causes the larger, denser clasts to be concentrated at the bottom of the flow; turbulent flows have low yield strength (Shultz, 1984). Normal grading may also be due to increased fluidity within the

flow, which results in a lower yield strength, permitting the "dropping" of larger clasts to the base of the flow once the flow has stopped (Shultz, 1984).

Inverse to normal coarse-tail grading in a clast-supported massive conglomerate (Gcin) is due to a debris flow that is fluid-rich or cohesionless, with a basal tractive layer, and normal to turbulent suspension of grains (Walton and Palmer, 1988). The deposit may form as the flow encounters a change in topography that leads to a change in flow behavior, such as thinning of the flow on a low slope, or restriction in a channel prevents flow, and produces a thicker deposit (Walton and Palmer, 1988).

Trough Cross-Bedded Conglomerate (Gt)

Trough cross-bedded conglomerate beds are characterized by clasts that range in size from granule to cobble, and are sub-rounded to rounded (Figure 15). The deposits of Gt are moderately to poorly sorted, and show trough cross-stratification. Basal surfaces are erosive, and bed geometries include lensoid and tabular sets. Individual sets are 0.2 to 0.5 meters thick and 0.6 to 1.2 meters long. Beds comprising cosets of Gt can be 0.5 to 1.5 meters thick and 1 to tens of meters long. Typical angle of inclined foresets is greater than 20°.

Interpretation: Trough cross-bedding in conglomerates can be the result of channel-fill (Waresback and Turbeville, 1990; Miall, 1996), diffuse gravel sheets (Hein and Walker, 1977), or gravel dune migration (Collinson, 1986; Miall, 1996).

Channel-fill deposits are typically thick (heights in excess of a few meters), and are produced as distal channel gravel bars migrate (Mathisen and Vondra, 1983; Blair and McPherson, 1994). Sediment is transported by turbulent flow and traction currents.



Figure 15: Trough cross-bedded conglomerate (Gt) above low-angle trough cross-stratified sandstone (Sl) in eastern facies, approximately 139 meters above the base of stratigraphic section RE-Kte. Pencil for scale is 10 centimeters long.

Diffuse gravel sheets are the result of pulses of high discharge within a channel (Todd, 1989). The gravel sheets are described as being one clast thick, turbulent, and in some instances, laminar (Hein and Walker, 1977). The flows resemble hyperconcentrated flows in this aspect and in the descriptions of flow behavior. The resulting deposits of gravel conform to the underlying bed geometry, and may appear to be low-angle (<15°) trough-cross-bedded (Todd, 1989). Multiple pulses of increased discharge result in diffuse gravel sheets that form packages greater than a meter thick (Todd, 1989). Diffuse gravel sheets are typically poorly sorted; this indicates a mixed bedload was rapidly transported and deposited (Smith, 1987a).

For normal streamflow dune migration, traction currents roll and slide large clasts downstream in the form of bars, especially during high discharge (Williams and Rust, 1969). Larger clasts are transported by turbulence. Sinuous crested three-dimensional dunes migrate into scours of the gravel bedform to produce trough cross-bedding (Collinson, 1986; Miall, 1996). Most examples of Gt exhibit cross-bedding that fines upward from gravel or cobble sized lags to pebble up to medium sand. This is a result of waning flow, and the inability of the flow to carry larger clasts (Collinson, 1986). Moderate sorting is characteristic of normal stream flow with the gravel framework infiltrated by medium to coarse sand (Smith, 1987a). For Two Medicine Formation trough cross-bedded conglomerate (Gt), gravel dune migration is the preferred transportation mechanism, due to the deposits being greater than one clast thick, and less than 3 meters thick.

Horizontally-Bedded Conglomerate (Gh)

Clasts found in horizontally-bedded conglomerate (Gh) range in size from granule to small cobble, and are sub-angular to sub-rounded. The deposits are moderately to poorly sorted, and horizontally-bedded. Basal surfaces are sharp and bed geometries are tabular or wedge-shaped. This lithofacies is also found interbedded with horizontally-stratified sandstone beds (Sh) less than 3 cm thick (Figure 16). Bed dimensions range from 0.2 to 0.4 meters thick and laterally for tens of meters.

Interpretation: The horizontal bedding in conglomerates is a result of grain-to-grain processes driven by traction current mechanisms during normal fluid flow (Smith, 1987; Waresback and Turbeville, 1990). Fully turbulent flow provides the support mechanism for

grains (Smith, 1986). When found interbedded with horizontally-stratified sandstones, the deposits most likely reflect waning flow or migration of longitudinal bars (Waresback and Turbeville, 1990).

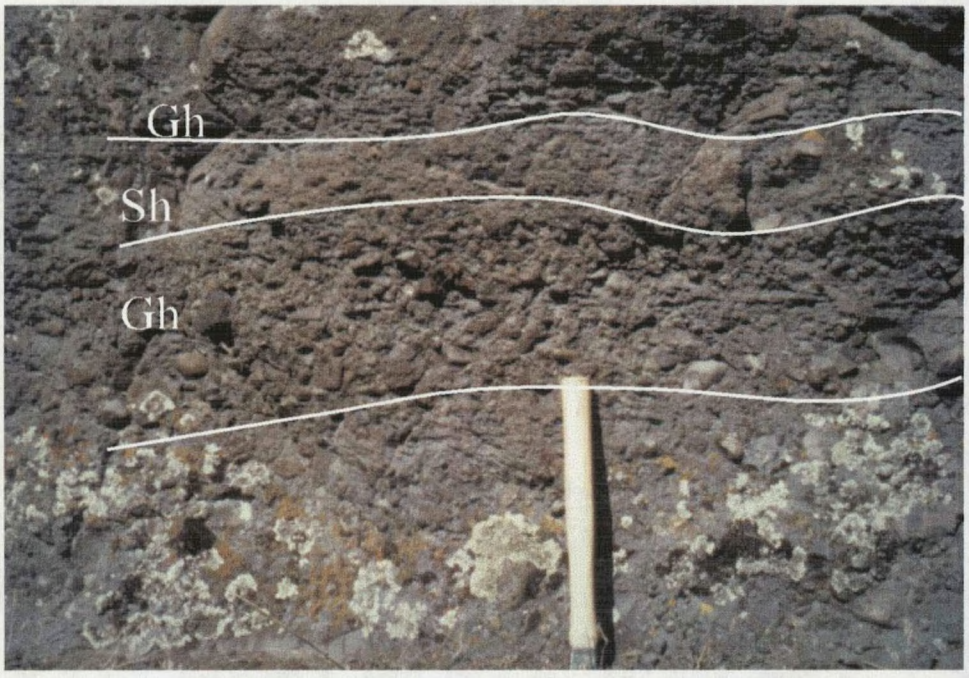


Figure 16: Horizontally-stratified sandstone (Sh) interbedded with horizontally-bedded conglomerate (Gh) "couplets" in western facies, approximately 95 meters from the base of southern stratigraphic section, unit F (S-F). Sledge hammer for scale.

Another mechanism for producing horizontal stratification is hyperconcentrated flow (Smith, 1987a), or sheetflood (Waresback and Turbeville, 1990; Blair and McPherson, 1994). Hyperconcentrated flows are high-energy flows with high sediment concentrations (Waresback and Turbeville, 1990). Turbulence is lessened (Pierson and Costa, 1987), and so grain support is from a combination of buoyancy, grain dispersive pressure, and turbulence

(Costa, 1988). Normal grading is the result of larger particles depositing as flow wanes (Costa, 1988). Deposition is by traction and suspension, and results in horizontal stratification of sediment (Smith, 1986). Polymodality also indicates hyperconcentrated flow; thus, the poorly sorted examples of Gh noted herein indicate transport by hyperconcentrated flow (Smith, 1986). However, with waning flow, clasts transported by traction are deposited, and as flow ceases, suspended sediments infiltrate between the larger clasts (Smith, 1986). This would result in bimodal distribution (Smith, 1986).

Another possible interpretation, but not the preferred interpretation, for the development of horizontally-bedded conglomerate (Gh) is successive deposition of gravel layers by multiple episodes of diffuse gravel sheets, which are more typically horizontally-bedded (Mathisen and Vondra, 1983). Horizontally-bedded conglomerates would have been deposited as longitudinal bars of low relief in a braided stream (Mathisen and Vondra, 1983).

Sandstone Lithofacies

Massive Sandstone (Sm), (Smi)

Moderate to poor sorting, very fine to coarse sand-sized, and sub-angular to sub-rounded grains characterize the massive sandstone lithofacies (Sm). Sharp basal contacts may also show soft sediment deformation when Sm is interbedded with massive mudstone (Fm) and laminated mudstone (Fl). Bed geometry is tabular or lensoid, and dimensions are 0.1 to 1 meter thick and 1 to tens of meters long. The upper surface of some beds has evidence of biogenic reworking, such as vertical and horizontal burrows, spreiten, wasp burrows, and root casts (Figure 17). Most units are ungraded; however some are inversely graded (Smi).

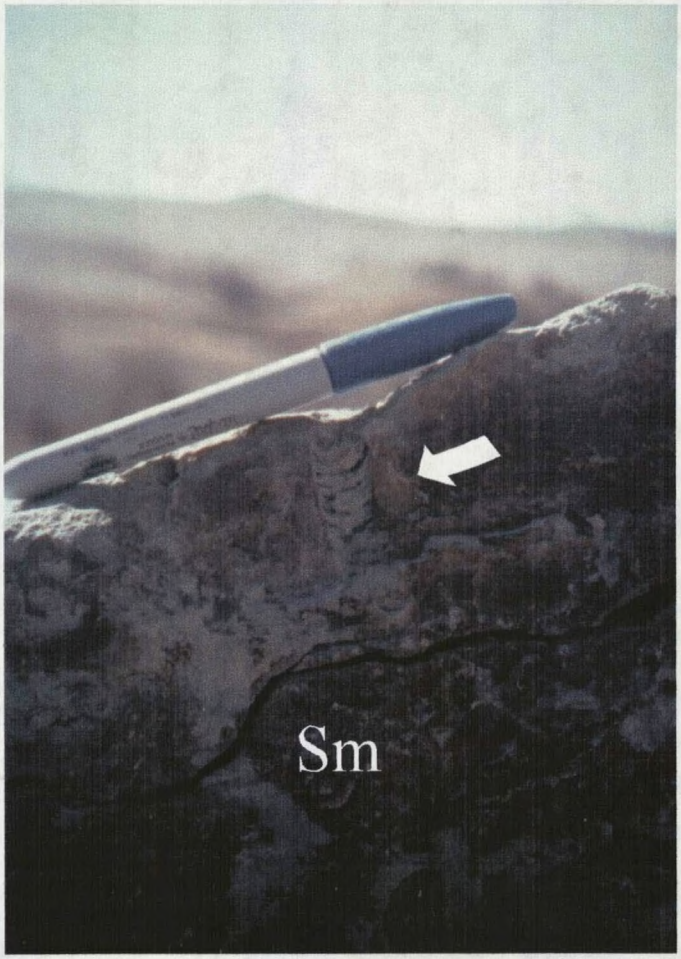


Figure 17: Spreiten in u-shaped vertical burrows in massive, bioturbated sandstone (Sm) of the eastern facies, approximately 24 meters above the base of stratigraphic section RE-Kte. Sharpie marker for scale.

Interpretation: Massive sandstone may be formed by rapid deposition of a well-sorted sand from a fluid gravity flow (Costa, 1988). Another mechanism for Sm formation would be a hyperconcentrated flow (Costa, 1988). Such Sm deposits are poorly sorted, and may posses horizontally stratified upper portions (Smith, 1987; Costa, 1988). Highly concentrated

sandy debris flows may be another possible mechanism for Sm deposits. Debris flows have a high yield strength for sediment support (Waresback and Turbeville, 1990). Inversely graded massive sandstone (Smi) could result from a sediment gravity flow, but one with high dispersive pressures (Costa, 1988) or an increase in yield strength (Waresback and Turbeville, 1990). One of the most common processes for forming massive sandstones is bioturbation by organisms or plant roots. For poorly-sorted massive sandstones, debris and hyperconcentrated flow processes were dominant; this was best observed in the western facies. In contrast, evidence of biogenic reworking was most dominant in the eastern facies.

Horizontally-Stratified Sandstone (Sh)

This lithofacies is represented by moderately to very poorly sorted grains, and very fine to coarse sand that is sub-angular to sub-rounded. Horizontally-stratified deposits exhibit fining and coarsening upward trends. Beds are 0.05 to 0.6 meters thick and 5 to tens of meters long with a tabular geometry (Figure 18). Basal surfaces are sharp or gradational. Some units contain rare "outsized" clasts of gravel to cobble size. Upper surfaces may exhibit soft-sediment deformation.

Interpretation: Horizontally-stratified sandstone forms in lower regime fluid flow, upper regime fluid flow, and hyperconcentrated flow. Lower flow regime flat beds are produced by traction transport of coarse sand grains (Harms et al., 1982). Upper regime fluid flow results in flat beds created by traction transport of all sand sizes (Harms et al., 1982; Miall, 1996). The deposits are well-sorted as stream flow capacity determines grain size (Harms et al., 1982). Deposition occurs as flow wanes, resulting in fining-upward sequences.

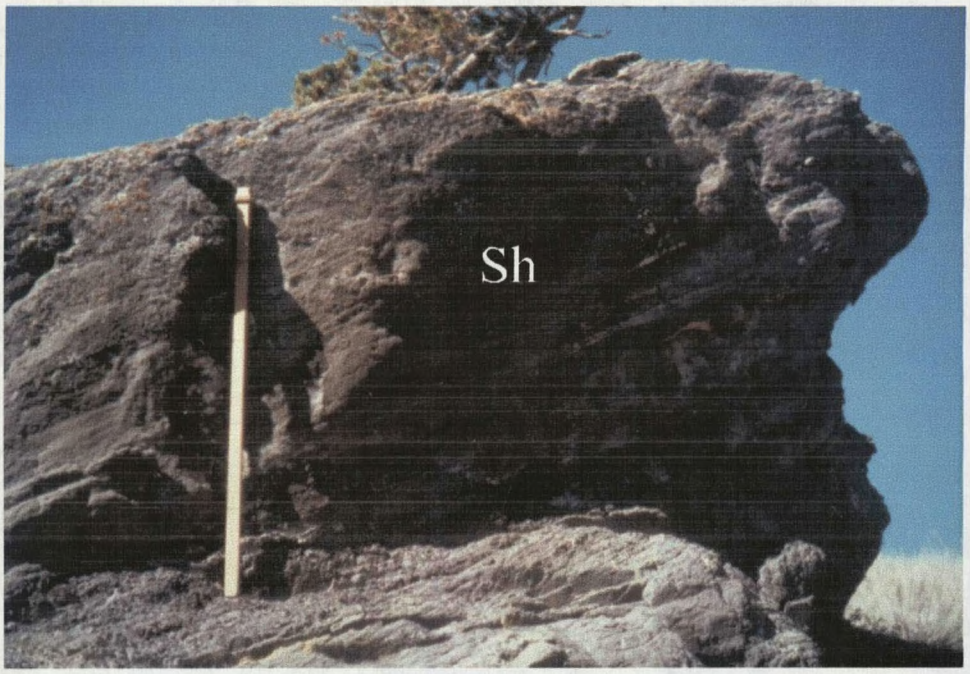


Figure 18: Horizontal-stratification in sandstone (Sh) of western facies, approximately 25 meters above the base of the northern stratigraphic section in unit F (N-F). Jacob's staff for scale is 1.5 meters tall.

Hyperconcentrated flow is an intermediate flow between fluid gravity flow and sediment gravity flow (Costa, 1988). Hyperconcentrated flow occurs during high sediment concentrations (40-70% by weight, 20-47% by volume) in normal streamflow (Costa, 1988), and is therefore different from typical flood events (Smith, 1986). Hyperconcentrated flow is characterized by dampened turbulent flow, and support mechanisms of buoyancy, dispersive pressures, and turbulence (Smith, 1986; Costa, 1988). Horizontally-bedded deposits produced by hyperconcentrated flow are typically poorly sorted with outsized pebble to cobble clasts common (Smith, 1987a). In some instances, Sh occurs in "couplets" that indicate multiple surges during flood events (Blair and McPherson, 1994) on a low-gradient, broad surface (See Figure 16) (Waresback and Turbeville, 1990).

Low-Angle (<15°), Trough Cross-Stratified Sandstone (Sl)

This lithofacies is moderately to very poorly sorted, with rare outsized pebbles common for most beds. In addition, it is comprised of fine to very coarse, sub-angular to sub-rounded sand grains, and low-angle (<15°) trough cross-stratification (See Figure 15). Bed geometries are tabular and lenticular, with bedding dimensions of 0.4 to 0.6 meters thick, and 1.2 to tens of meters in length. Coarsening and fining upwards sequences were observed within individual sets. Basal surfaces may be slightly erosive or sharp with rare gradational changes between lithofacies. In addition, herringbone sets were observed within the eastern facies.

Interpretation: Low-angle trough cross-stratification (Sl) is produced by fluid gravity flow under upper flow regime parameters, and may be formed as scour-fill, plane beds deposited on inclined surfaces, or by migration of antidunes (Smith, 1987b; R.C.M.Smith, 1991; Miall, 1996). Plane beds form during low turbulent flow by rolling and sliding of grains on the channel bed, and grains are deposited as flow wanes (Harms and Fahnestock, 1965). Low-angle trough cross-stratification formed by scour-fill is the result of grains filling a flood-generated scour, and implies rapid aggradation during and after high discharge in a shallow channel (Smith, 1987b, 1988; Orton, 1995; Palmer, 1997). Sl may also form when upper flow regime transformation occurs as horizontally-stratified sandstone (Sh) becomes Sl, or as Sl transforms to Sh (Miall, 1996). Low-angle trough cross-stratification in herringbone sets indicates tidal or oscillatory-driven flow (McCubbin, 1982).

Trough Cross-Stratified Sandstone (St)

This lithofacies is characterized by trough cross-stratification of medium to very coarse sand, and moderately to very poorly sorted sub-angular to sub-rounded grains with outsized clasts common. The basal contacts are erosive, with gradational grain size variations between sets common. Bed geometries are lenticular, and bedding dimensions range from thicknesses of 0.5 to 4 meters, and lengths of 3 to tens of meters. Individual sets range in size from 0.1 to 0.5 meters thick and 0.2 to 1.2 meters long. Both fining and coarsening upward sequences were observed within individual sets and entire units. Troughs are 0.1 to 0.45 meters thick and are 0.5 to 3 meters in length.

Interpretation: Trough cross-stratification is formed by fluid gravity flow during the migration of three-dimensional dunes (Mathisen and Vondra, 1983; Miall, 1996). Grains migrate down sinuous-crested or lingoid dune slip faces by traction current transport, in the form of bed load and saltation (Smith, 1987b; Bentham et al., 1993; Orton, 1995; Miall, 1996). Turbulent flow and traction provide grain transport, while turbulence and suspension are the grain support mechanisms (Smith, 1986; Valentine et al., 1998). Dunes form in the lower flow regime (Harms et al., 1982; Waresback and Turbeville, 1990), but transport of coarser grains usually indicates a higher flow velocity (Miall, 1996).

Ripple Cross-Laminated Sandstone
(Sr), (Srs), (Src)

The ripple cross-laminated sandstone lithofacies is predominately moderately to well-sorted, and very fine to fine sand that is sub-angular to sub-rounded. The bed geometry is

tabular. Individual ripples are 0.02 to 0.1 meters high, and 0.05 to 0.15 meters long. Sets are 0.05 to 1.5 meters thick and 1 to 5 meters long. Basal surfaces are sharp or gradational. Additionally, other units are characterized by climbing ripple cross-lamination (Src) (Figure 19). Some units possess sets of symmetric ripple cross-lamination (Srs) (Figure 20).

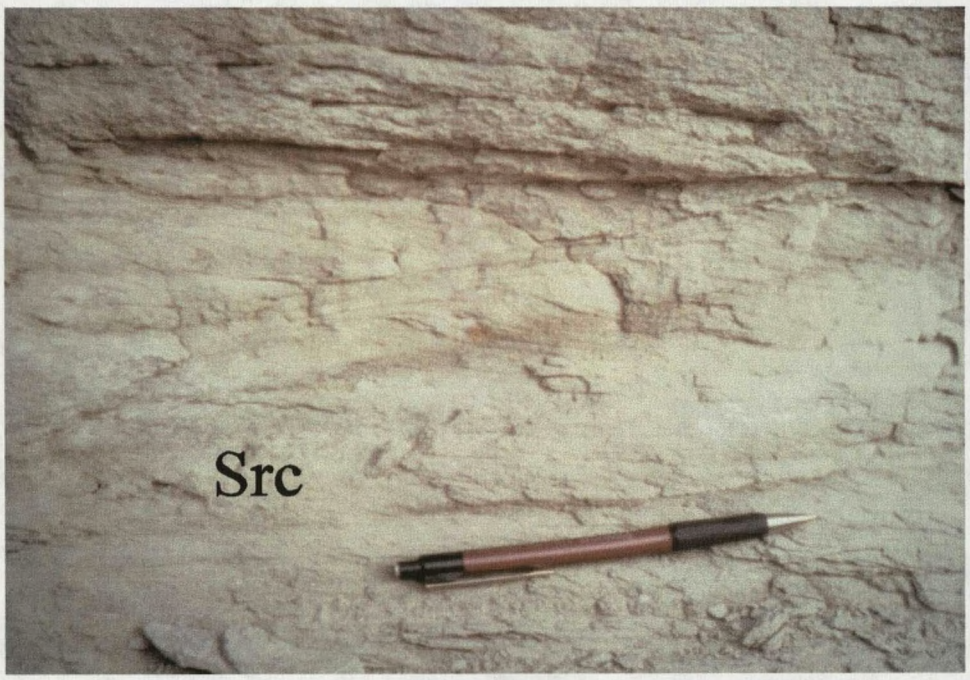


Figure 19: Climbing-ripple cross-lamination in sandstone (Src) of eastern facies, approximately 14 meters above the base of stratigraphic section E2-Kte. Pencil for scale.

Interpretation: Ripple cross-lamination is produced by fluid gravity flow. Ripples are formed within lower flow regime parameters, and by traction current transport of fine grains (Harms and Fahnestock, 1965). Current ripples (Sr) are unidirectional and have the lee-side preserved. Climbing ripples (Src) are produced as ripples migrate with a positive angle of climb (Harms et al., 1982). This is generally the result of abundant sediment added to the

fluvial system, and thus record deposition from suspension (Harms et al., 1982). Symmetric ripples (Srs) are produced by tidally-driven traction currents. Ebb and flow tides cause the stoss and lee sides of the migrating ripple to exchange depending on the tidal direction; therefore, if the ebb and flow tidal currents are of equal magnitude, ripple geometry is symmetric.



Figure 20: Wave ripple form sets in sandstone (Srs) of eastern facies, approximately 25 meters above the base of stratigraphic section RE-Kte. Pencil for scale (8 cm).

Mudrock Lithofacies

Laminated Silt and Mud (Fl)

This lithofacies is defined by laminated mudstone and siltstone, with well- to moderately sorted grains. Tabular geometry and sharp basal surfaces are common. The units typically fine upwards. Beds are 0.01 to 0.7 meters thick and 1 to tens of meters long. In some instances, Fl is interbedded with lenses of Sm or Sh, and Srs or Src; these are interpreted to be wavy and wavy-flaser bedding (Figure 21). Soft-sediment deformation is characteristic, especially in the eastern facies.

Interpretation: Mud laminae are produced during suspension settling by vertical accretion. Weak traction currents initially transport grains until flow wanes and deposition occurs (Miall, 1996). Wavy and wavy-flaser bedding form as tidally-driven flow transports sand during higher velocity flow, and mud during waning flow (Weimer et al., 1982).

Massive Silt and Mud (Fm)

Massive mudstone and siltstone consists of well- to poorly-sorted grains, with outsized sand grains common. The bed geometries are tabular, lenticular, and wedge-shaped. Fm also occurs as mud stringers separating stratified sets of St, Sl, Sr, and Sh. Sharp basal surfaces that are undulatory due to soft-sediment loading are common. Abundant plant debris, charcoal, and root traces are pervasive throughout this lithofacies. Beds are 0.01 to tens of meters thick (as covered sections) and are tens of meters long.

Interpretation: Massive mud is formed during suspension settling of a waning fluid gravity flow, and may represent vertical accretion deposits on a floodplain (Mathisen and Vondra, 1983; Bentham et al., 1993; Miall, 1996). Miall (1996) also suggests thinly bedded Fm is produced after channel abandonment in pools of standing water. This would result in mud drapes (Smith, 1987b). The abundant roots indicate bioturbation as a source for the structureless mudstone (Bentham et al., 1993). Another interpretation for massive mudstone is a very dilute mud flow (Waresback and Turbeville, 1990).

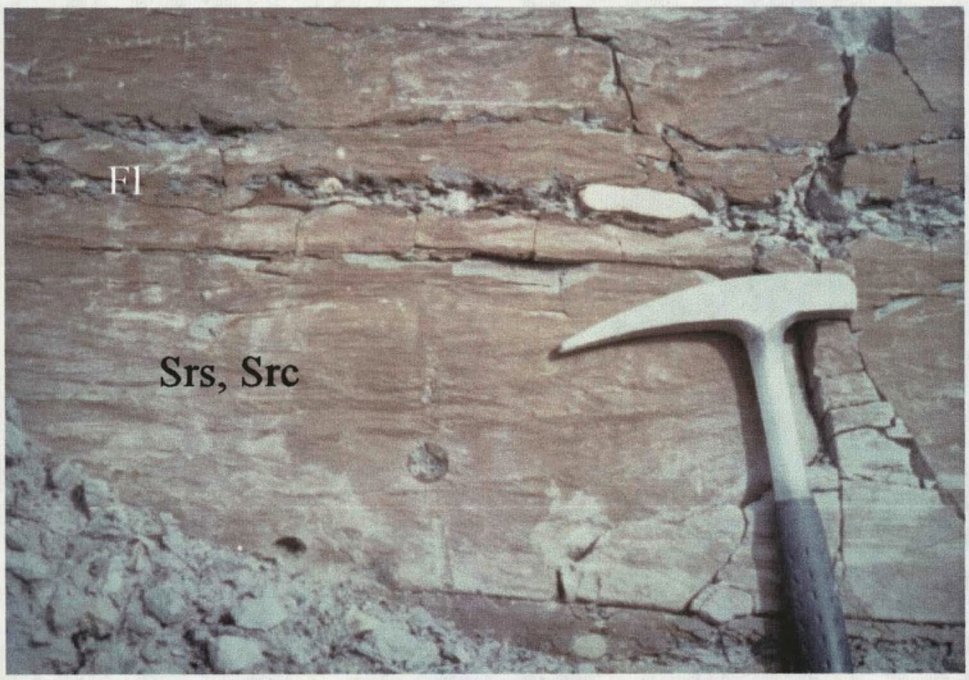


Figure 21: Ripple cross- and climbing ripple cross-laminated sandstones (Srs, Src) interbedded with laminated mudstone (Fl) are interpreted as wavy-flaser bedding. Exposed approximately 26 meters above the base of the measured stratigraphic section RE-Kte. Hammer for scale.

Root Beds of Silt and Mud (Fp)

Root beds of mudstone and siltstone that are well- to moderately sorted characterize this lithofacies (Figure 22). Bedding geometry is tabular, and basal surfaces are sharp or gradational. Abundant root traces, bioturbation, and mineral alteration (replacement) of roots are also characteristic. Roots in this facies are characteristically 0.10 to 0.15 meters long and less than 0.25 centimeters thick. Beds are 0.1 to 0.8 meters thick and laterally continuous for tens of meters.

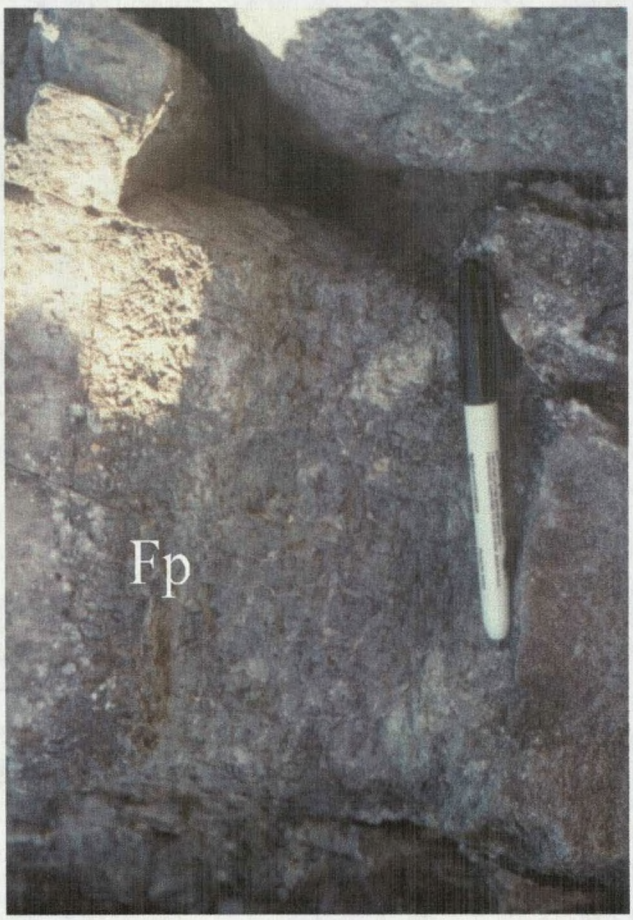


Figure 22: Thick rootbeds in blocky mudstone (Fp) in eastern facies, approximately 130 meters above the base of stratigraphic section RE-Kte. Sharpie marker for scale.

Interpretation:. Initially, deposition of fine-grained material occurs during waning fluid flow. Plants then take root, producing the "root beds". As such, Fp represents soil development within the floodplain (Miall, 1996).

Non-Clastic Lithofacies

Organic Deposits (O)

Coal is interbedded with iron oxides (hematite and limonite) and massive and laminated mudstone (Fm, Fl), and massive, very fine-grained sandstone (Sm). The coal is bituminous and thinly layered (less than 2 cm thick). Hematite and limonite form nodules throughout the fine-grained sand and mud. Bed geometry is tabular, and basal surfaces are gradational or sharp with massive mudstone (Fm) units below. Beds are 1.8 to 3 meters thick, and tens of meters long. Abundant plant debris is also evident.

Interpretation: The abundant plant debris and very fine grain size indicate low flow velocities, possibly standing water, and the iron oxides imply an oxidizing environment (Miall, 1996). The thin coal beds represent layers of plant debris that were interbedded with very fine-grained sediments. Transformation of the plant layers by heat and burial produced the thin coal layers.

Carbonate (Cl, Cn)

The carbonate is micritic, characterized by tabular and wedge-shaped geometries, and in some instances, is nodular (Cn) (Figure 23). Basal surfaces are gradational or sharp. Exposures are 0.4 to 3 meters thick and laterally continuous for 5 to tens of meters. Fresh

water fossils (gastropods and molluscs) and large (2-4 cm diameter) root casts are found with laminated micrite (Cl) and interbedded with Fm, Fl, and Sh. Fossils decrease in abundance in the uppermost portions of the laminated micrite.



Figure 23: Nodular carbonate mudstone (Cn) in eastern facies, approximately 33 meters above the base of stratigraphic section RE-Kte. Jacob's staff is 1.5 meters high.

Interpretation: The laminated micrite (Cl) may have formed in a shallow, fresh water lake or ponded water environment, based on the thinness of laminae, and lack of continuity. Micrite forms in shallow water with low sedimentation rates by either primary inorganic precipitation, calcareous production of shells and skeletons of organisms, carbonate grains deposited in a basin from an allochthonous source, or diagenesis (Allen and Collinson, 1986).

The nodular micrite (Cn) may represent soil development and the formation of caliche. Caliche is a product of weathering processes on a floodplain (Miall, 1996). Surficial water leaches ions from the surface, and concentrates them in the subsurface, forming carbonate nodules (Miall, 1996). The caliche in this area is underdeveloped; high sedimentation rates within the depositional system prevent or inhibit caliche development (Bentham et al., 1993).

Pyroclastic Lithofacies

Pyroclastic rocks may be analyzed using traditional sedimentologic techniques, such as lithofacies analysis. The violent expansion of gas during an explosive volcanic eruption produces fragmented material (such as glass shards, pumice, lithic clasts, and crystals). In addition, the gas behaves as water does in normal sedimentation processes, and transports pyroclastic debris as a fluidized flow, which results in gravity-driven deposits of flow, surge and fall. For this study, the pyroclastic lithofacies of unit C (rhyolitic to rhyolitic ash-flow tuff) were identified using detailed stratigraphic (vertical) sections. Facies are segregated by dominant (> 50%) grain size. Prefix T represents ash-sized material, and L describes lapilli-sized clasts. Facies were further separated by degree of sorting, grading, identification of sedimentary structures, and degree of welding. Sedimentary structures, basal contacts, grain size, and lateral variation also assisted in ascertaining pyroclastic lithofacies. Pyroclastic lithofacies aid in describing modifications of flow dynamics and transportation processes.

Additionally, pyroclastic rocks are deposited via flows similar in behavior to sediment gravity flows and hyperconcentrated flows. Therefore, the pyroclastic lithofacies

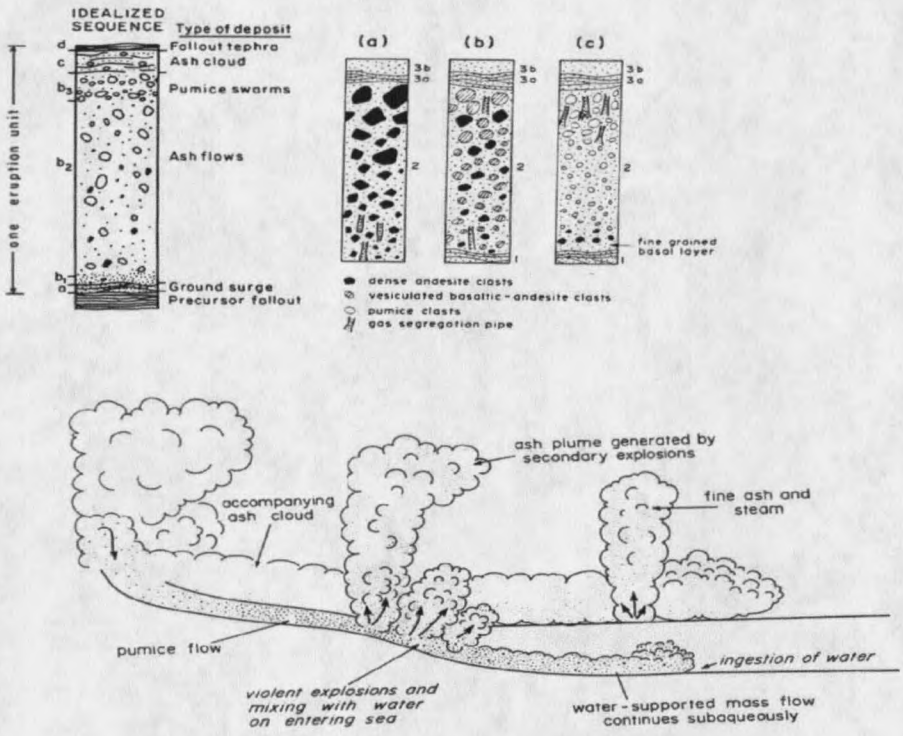


Figure 24: Schematic diagrams that illustrate possible pyroclastic flow deposits, and the mechanism for pumice flows that have a phreatic component. From Cas and Wright (1987, pg. 111 and 283).

interpretations are based on studies that document sedimentary flow processes involved with pyroclastic debris. One of the most significant differences between pyroclastic flow and fluid flow is the transport medium, gas versus water (Sparks, 1976). Sparks' (1976) pyroclastic flow model has been modified by other workers, and those variations are presented in Figure 24. In addition, models that apply debris flow transportation mechanisms to pyroclastic flow deposits are also used by volcanologists to interpret the flow processes (Figure 25).

Only unit C (rhyolite ash flow sheets) of the western facies and rare outcrops of the eastern facies contain pyroclastic units. One of the results of this study was that air-fall material was not observed; this may be due to poor preservation of air-fall detritus, and/or poor exposure of air-fall rocks. Autobrecciated rocks are not included in this section; they are discussed in the conglomerate and gravel facies at the beginning of this chapter.

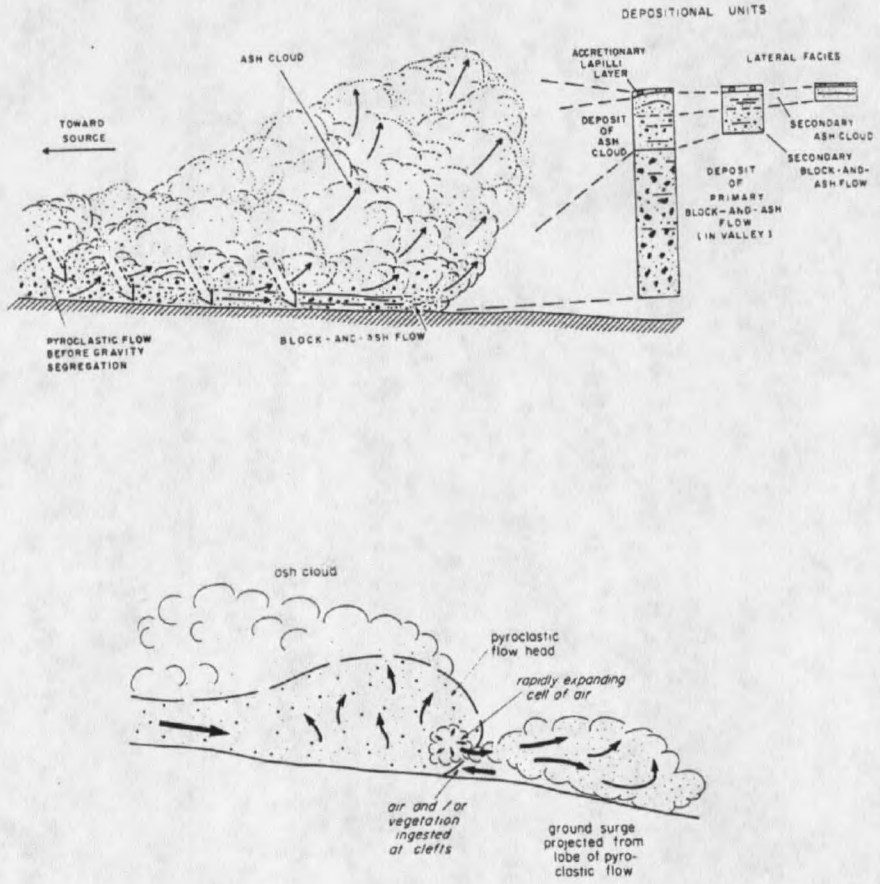


Figure 25: Schematic diagram illustrating possible pyroclastic flow mechanisms for producing pumice and block-and-ash flow deposits. From Cas and Wright (1987, pg. 253).

Matrix-Supported, Massive, Lapilli Tuff (Lmm)

Matrix-supported, massive lapilli tuff is dominated by sub-rounded to sub-angular pumice lapilli and accidental lithics, poor sorting, and a tabular geometry. The deposit is approximately 3 meters thick and is laterally extensive for tens of meters. The basal surface is sharp. This facies normally grades into matrix-supported, massive tuff (Tmm). Lithic clasts are normally graded, while pumice lapilli are ungraded.

Interpretation: Massive lapilli tuff is found only in the southern stratigraphic section. In this example, it grades normally into Tmm. One hypothesis is that Lmm is the result of an extremely fluid pyroclastic flow. Fluidization results in the elutriation of fines, and the deposition of lithic and pumice rich zones (Carey, 1991). Fluidization also allows the larger clasts to "sink" to the base of the flow. Another interpretation is that Lmm grading into the lapilli-depleted Tmm represents a normally graded pyroclastic flow.

Matrix-Supported, Massive Tuff
(Tmm), (Tmmg)

This lithofacies is characterized by more than 50% ash-sized material, poor sorting, and pumice and lithic lapilli that are sub-rounded to sub-angular. The conglomerate is matrix-supported, massive and ungraded (Tmm), or massive and graded (Tmmg). Matrix consists of glass shards and fine ash-sized pumice. Bed geometry is tabular, and the basal surface may be erosive or gradational. Laterally, units may extend for tens to hundreds of meters. Deposits are usually 0.75 to 13 meters thick. Typically, clasts are pumice and accidental lithic lapilli, with abundant crystal grains that are medium ash to small lapilli size. Lithic clasts are

mudstone, welded rhyolitic tuff, and aphanitic-porphyritic volcanic rock fragments. Tmm may consist of entirely lithic clasts or pumice lapilli. This facies is typically welded, as evidenced by the plastic deformation of glass shards in the matrix. In some instances, the upper part of these deposits are colored pink, and perhaps indicates high temperature emplacement (Fisher and Schmincke, 1984). Additionally, abundant lithophysae are found elongated oblique to flow banding, and are commonly found in zones throughout the deposits. Large, open vesicles are also elongated oblique to flow banding, but are more rare. Units that are density graded with normally graded lithic clasts at the base and reversely graded pumice lapilli at top are designated Tmmg. This unit can be unwelded or very weakly welded. Tmmg is further discussed below.

Interpretations: A pyroclastic flow is a dense, laminar fluidized flow (Rowley et al., 1985). Pyroclastic flows typically move in a nonturbulent manner and have high particle concentrations, similar to a debris flow; however, pyroclastic flows are hot (Carey, 1991). Poor sorting in pyroclastic flow deposits (Tmm) reflects the abundance of particles within the flow (Sparks, 1976). A high temperature emplacement for the pyroclastic flows is indicated by a pinkish upper contact, welding, and abundant lithophysae (Fisher and Schmincke, 1984). Welding of the unit is due to the heat of the deposit allowing the glass shards to become viscous and deform (Ross and Smith, 1961). Compaction of the deposit over time is also evident in the deformed glass and flattened pumice lapilli (Ross and Smith, 1961). Thin pyroclastic flows are attributed to small, dense surges, or the "tail" of a larger pyroclastic flow with a higher flow regime than true pyroclastic flows (See Figure 25) (Rowley et al., 1985).

Reverse grading (inverse coarse-tail) of pumice and normal grading (normal coarse-tail) of lithic clasts (Tmmg) are indicative of density contrasts between the clasts and the matrix (Sparks, 1976; Mathisen and Vondra, 1983). The pumice fragments "float" to the top of the flow unit, while the lithic fragments gravitationally "drop" to the base (Sparks, 1976; Rowley et al., 1985). Additionally, a high velocity flow allows the matrix to behave with increasing fluidity (Carey, 1991). This results in the floating of the pumice, and dropping of lithic clasts (Carey, 1991). The reverse grading of the pumice may also indicate dispersive pressures (shear stresses) between the pumice clasts (Rowley et al., 1985; Carey, 1991). The lithic clasts were possibly affected by turbulence, as suggested by the coarse-tail normal grading of clasts at the base of the deposit (Sparks, 1976).

Massive Tuff (Tm)

This lithofacies is characterized by poor sorting and dominant, coarse ash-sized particles. The matrix contains glass shards (plastically deformed and compressed) with medium to very coarse ash-sized crystals of feldspar and lithic clasts (mudstone, welded tuff, and volcanic rock fragments). The basal surface is typically gradational with Tmm or Tmmg, and the tabular deposits range from 0.2 to 9 meters thick, and tens to hundreds of meters long. This lithofacies is generally strongly welded.

Interpretations: This lithofacies has multiple possible interpretations. Elutriation of fines from the top of a pyroclastic flow can produce a deposit more fine-grained than the underlying pyroclastic flow (Fisher and Schmincke, 1984). However, lithofacies Tm is relatively coarse-grained, and poorly sorted, while elutriated fines are typically better sorted

(Fisher and Schminke, 1984). The gradational contact of Tm with Tmm and Tmmg indicates a continuous flow process, while elutriated deposits typically possess sharp basal contacts (Cole and Ridgway, 1993). In addition, using an analogy to the model for the emplacement of a debris flow plug, Tm may be the "tail" of the pyroclastic flow that overruns the "head" (Carey, 1991) (See Figure 25). However, this would require evidence of laminar deposition, and better sorting. Another possibility, and the most likely, is that Tm represents the uppermost, normally graded portion of a fluidized, low yield strength, pyroclastic flow. Normal grading within a flow is a result of decreasing eruption intensity (Vessel and Davies, 1981).

Tm may also represent a "basal layer" or ground surge (See Figure 24). This layer is typically poorly sorted, and grades upward into a coarser grained "ignimbrite" (Sparks, 1976). However, Tmm and Tmmg typically grade into Tm; hence, Tm most likely does not represent a ground surge. Additionally, Tm may represent a "layer 3", or ash-cloud surge (Sparks, 1976). Layer 3 deposits may be representative of a dust cloud that forms above pyroclastic flows (Sparks, 1976). Characteristically fine-grained, layer 3 may have a predominant coarse-tail grading (Sparks, 1976). Tm is generally coarse-grained ash, found at the top of Tmm and Tmmg, and strongly welded. Layer 3 deposits, though, are typically not well-preserved, due to fine-grain size (Sparks, 1976).

Antidunal Tuff (Ta)

This lithofacies is comprised of small (0.1 meters high and 0.2 meters long), swaley deposits with the stoss-side (foresets) preserved. The deposits are poorly sorted, and are

comprised of ash-sized glass shards, crystals, small pumice lapilli, and lapilli-sized lithic clasts. The unit is laterally extensive for up to tens of meters, and less than 1 meter thick. The basal surface is typically sharp, and the bed geometry is tabular.

Interpretation: Pyroclastic surges are turbulent, low concentration, fluidized debris flows that evidence recognizable sedimentary bedforms (Rowley et al., 1985). Antidunes are common structures formed in pyroclastic surges, due to the high particle content and the upper flow regime conditions that characterize pyroclastic surges (Sparks, 1976; Rowley et al., 1985). Additionally, antidunes form in high velocity flows, and deposit rapidly due to the cohesive, damp ash that commonly forms the deposits (Rowley et al., 1985). There are three types of pyroclastic surges. Base surges are formed during phreatomagmatic eruptions and are comprised of hydroclastic particles (Fisher and Schminke, 1984). They may occur during eruption column collapse (Fisher and Schminke, 1984). Ground surges form from eruption column collapse or by ingestion of air at the front of a pyroclastic flow (Fisher and Schminke, 1984). Ash-cloud deposits are due to elutriation of fines at the top of pyroclastic flows, or by normal gravity sorting of clasts (Fisher and Schminke, 1984). Fisher (1977) attributes antidunes to base-surges, and while Ta is found at the base of Tmm, evidence for hydroclastic or phreatomagmatic activity is lacking.

Climbing-Ripple Cross-Laminated Tuff (Trc)

This uncommon lithofacies is characterized by ash-sized glass shards, and pebbly, sub-angular lithic clasts that are climbing-ripple cross-laminated. The deposits are approximately one meter thick, and tens of meters long. The basal surface may be sharp or gradational.

Interpretation: Climbing ripples form from high particle concentrations, and Trc may be the result of a pyroclastic surge. As Trc is found in some instances at the base of Tmm, it is possible that Trc may have been deposited as a ground surge. However, in one instance, Trc is a gradational unit between Tmmg and Tmm. Trc may then be representative of flow transformation from a pyroclastic flow of high matrix strength to one that is more fluidized due to increasing velocity or another episode of column collapse (Carey, 1991).

Horizontally-Stratified Tuff (Th)

This lithofacies is characterized by fine ash-sized material that contains horizontally-stratified accretionary lapilli (0.1 to 0.5 cm in diameter). The deposit is approximately 0.4 meters thick and laterally continuous for 14 meters. The basal surface is sharp, and the bedding geometry may be wedge-shaped.

Interpretation: Th is most likely the result of a pyroclastic surge, but the accretionary lapilli add another dimension to the interpretation. Accretionary lapilli are found various distances from the source vent, form from rain drops or water within the surge (a base surge), and, therefore, can be the result of a pyroclastic surge. Th could be derived from an ash-fall, but this is difficult to ascertain. Being mostly ash, and with accretionary lapilli horizontally bedded in-between, Th is not gravity-sorted, while ash-fall material is. Therefore, Th most likely represents a pyroclastic surge that may have moved across a wet surface, or mixed with rain.

Vitrophyric Tuff (Tv)

This facies is characterized by a dense, black glass that contains variable amounts of feldspar crystals that are planarly aligned, and small pumice and lithic lapilli (Figure 26). In some instances, the glass is found as abundant stringers and pods in a fine ash matrix (Figure 27). Typically, the uppermost section of glass has hydrated to perlite. The deposits are 0.4 to 4.8 meters thick, and are laterally continuous for approximately tens of meters. The basal surface is typically gradational where observed, and bed geometry is tabular.

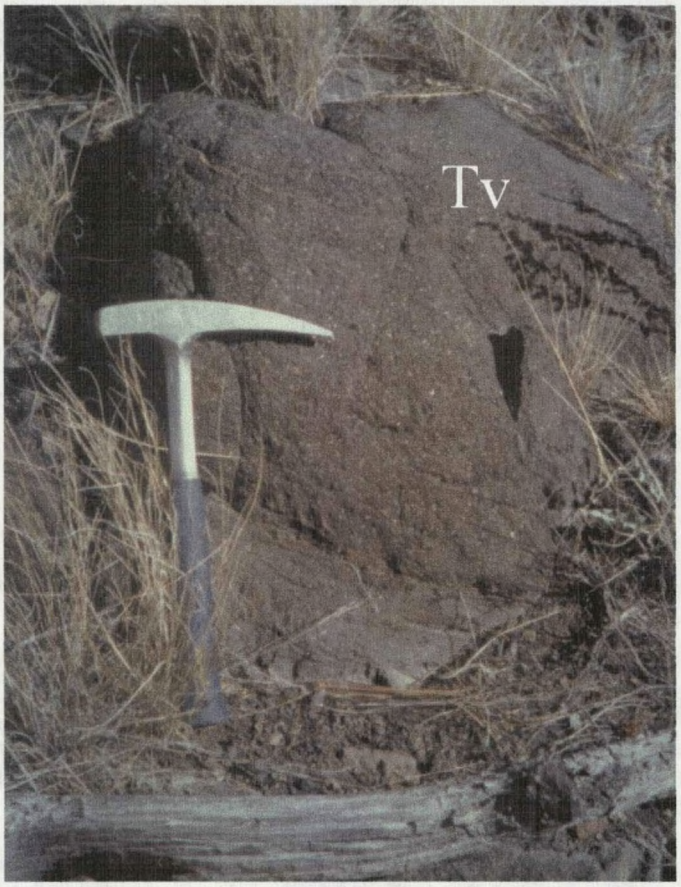


Figure 26: Vitrophyric tuff (Tv) in western facies, approximately 30 meters above the base of the southern stratigraphic section in unit C (S-C). Hammer for scale.

Interpretation: This lithofacies represents deformation by either extreme welding or extreme heat (Ross and Smith, 1961). Welding would produce flattening of pumice and glass to form a layered appearance; heat does not produce flattening (Ross and Smith, 1961). In most instances, the Tv is gradational with deposits attributed to pyroclastic flow deposits. Tv would therefore be indicative of the welded zone found in most pyroclastic flow models (Figure 28). However, one example of Tv is found at the known base of unit C. A pyroclastic surge deposit overlies the dense zone of Tv. Tv in this instance may represent an earlier pyroclastic flow that had been eroded prior to deposition of Ta.

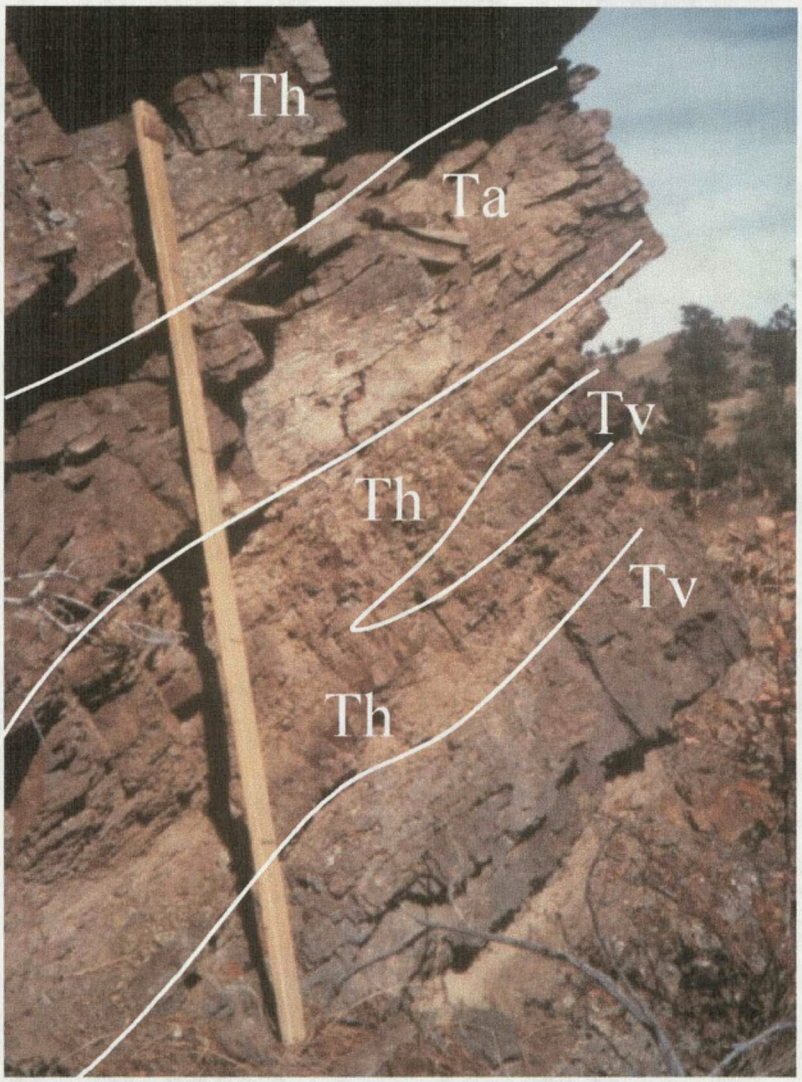


Figure 27: Interbedded vitrophyric tuff (Tv), horizontally-stratified tuff (Th), and swaley antidune tuff (Ta) in western facies, approximately 58 meters above the base of the central section in unit C (C-C). Jacob's staff is 1.5 meters tall. View to the north-northwest.

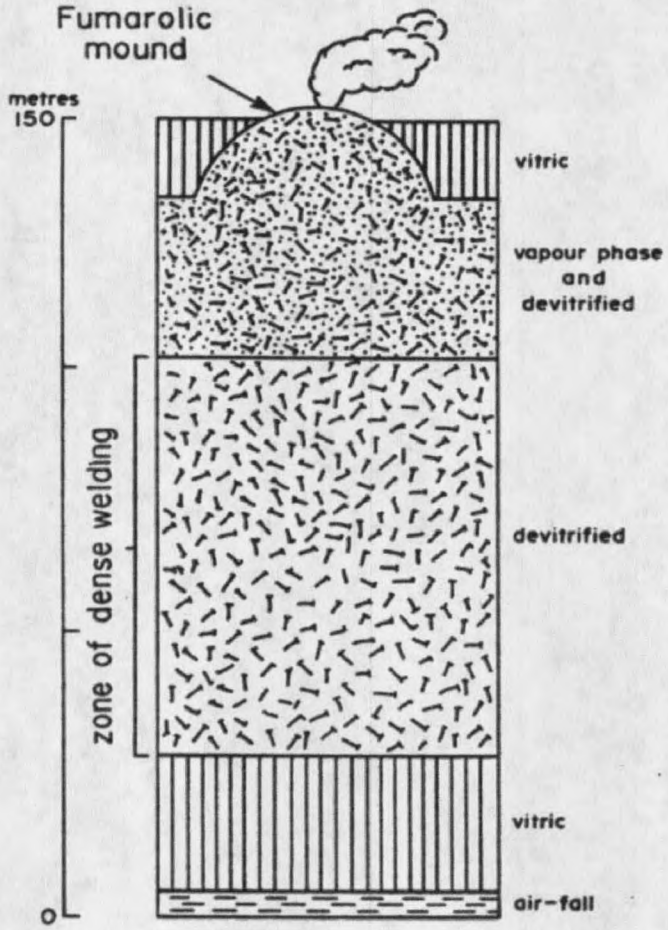


Figure 28: Diagram of alteration stratigraphy in pyroclastic flows, illustrating locations of welding, vapor phase crystallization, devitrification, and vitric zones. From Cass and Wright (1987).

VOLCANIC ROCK UNIT DESCRIPTIONS

Field analysis of volcanic units included measuring sections, sample collecting, identifying surface contacts between flows, and noting the abundance and occurrence of lithophysae, spherulites, pumice lapilli, lithic clasts, alteration zones, crystals, and vesicles. Additionally, flow banding, foliation, and mineral identification in hand sample were recorded. Thin section petrography of the volcanic rocks (units B, C, E, and the Adel Mountain Volcanics) was necessary for identifying major phenocrysts that may be found in epiclastic sandstones. Schmidt (1978) identifies the chemical composition of volcanic rock units B (latite), C (rhyolite-rhyodacite), E (trachyte), and Adel Mountain Volcanics (trachybasalt and trachyandesite), and observations made in this study were compared to his data. Utilizing thin section petrography, twenty-five samples were analyzed from latite, trachyte, and trachybasalt lava flows, and the rhyolite-rhyodacite ash-flow tuffs. Petrographic analysis aided in determining flow mechanisms, alteration characteristics, and identifying the number of individual flows.

Unit B- Latite Lava Flows

Latite lava flows in this study are characterized by abundant plagioclase feldspar phenocrysts set in a dark grey to grey-purple groundmass (Figure 29). The unit generally weathers orange brown, especially near the base. The tabular flows range in thickness from 30 to 75 meters, and are laterally continuous for hundreds of meters, only to pinch-out north

of the field area (Figure 30) (Schmidt, 1978). Lithophysae and vesicles occur in various amounts throughout the flows and aid in determining multiple flow units (Figure 31).



Figure 29: Porphyritic latite lava flow with abundant plagioclase feldspar phenocrysts in western facies, approximately 128 meters above the base of the central stratigraphic section in unit B (C-B). Sharpie marker for scale.

In thin section, the porphyritic latite lava flows consist of a finely-crystalline groundmass of feldspar (a rare instance showed penetrating twins). Specifically, the groundmass is microcrystalline andesine, sanidine, augite, quartz, magnetite, and apatite

(Schmidt, 1978). The phenocrysts are dominantly plagioclase feldspar and rare augite. Plagioclase phenocrysts range in size from 0.1 to 0.5 cm, and the augite phenocrysts are generally 0.2 to 0.4 cm. Schmidt (1978) identified the plagioclase feldspar phenocrysts as labradorite ranging in composition from An_{50} to An_{58}. The plagioclase phenocrysts are typically equigranular, albite twinned, discontinuously zoned, grouped in glomocrysts, heavily fractured in some instances, and may have microperthitic textures. Where altered, plagioclase phenocrysts are almost unrecognizable except for relict twinning. The plagioclase is replaced to various degrees by calcite, chlorite, clay, and zeolite (possibly clinoptilite), and sericite. The commonly equigranular augite phenocrysts are consistently zoned, and where altered, are replaced by zeolite, biotite, chlorite, and/or clay.



Figure 30: Exposure of latite lava flows (unit B) in western facies central stratigraphic section. View to the west from road leading into Rock Creek drainage. Uppermost rocks on left are ash-flow tuffs of unit C.

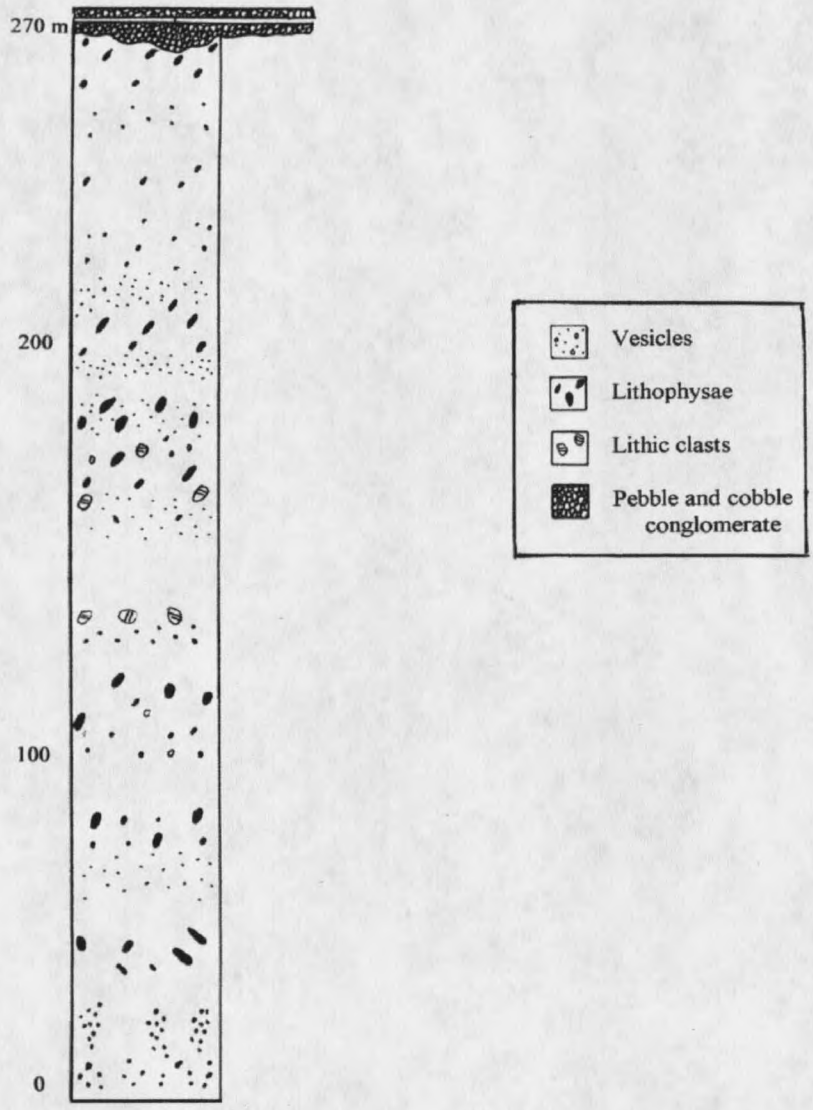


Figure 31: Schematic stratigraphic section of latite lava flows found in the western facies, unit B. Two flows are illustrated here, based on the location of lithic clasts approximately 130 meters from the base of the stratigraphic section.

Vesicles (up to 6 cm in diameter) are typically infilled by spherulitic chalcedony, macroquartz, chlorite, clay, and zeolites. Some amygdules contain multiple episodes of infilling. Rarer constituents of the latite lava flows are quartz, rock fragments (chert, micrite, and mudstone), nepheline? (may be K-spar), and analcime crystals. Hematite staining is prevalent, as are opaque minerals.

Interpretation

Multiple flows were distinguished where vesicles were concentrated (indicating the top of the flow), where a distinct, sharp upper surface occurred, and where squeeze-ups of altered, silicified mudstone indicated the presence of a basal surface. The northern measured section possibly contains two lava flows, while the central and southern sections consist of at least two or more flows.

Unit C- Rhyolitic Ash-Flow Tuffs

This unit is characteristically pink, tan, grey, purple, and white. The deposits include exposures of lapilli tuff, ash tuff, and vitric tuff (Figure 32). Tabular deposits range in thicknesses from 8 to 26 meters, and the unit thins to the north (Figure 33) (Schmidt, 1978). In hand sample, flow banding is evident, as are stretched, wispy pumice fragments (Figure 34). Non-welded deposits are poorly exposed and typically contain abundant biotite and pumice fragments. The pyroclastic structures observed in stratigraphic sections are discussed in the pyroclastic lithofacies section of the Lithofacies chapter.

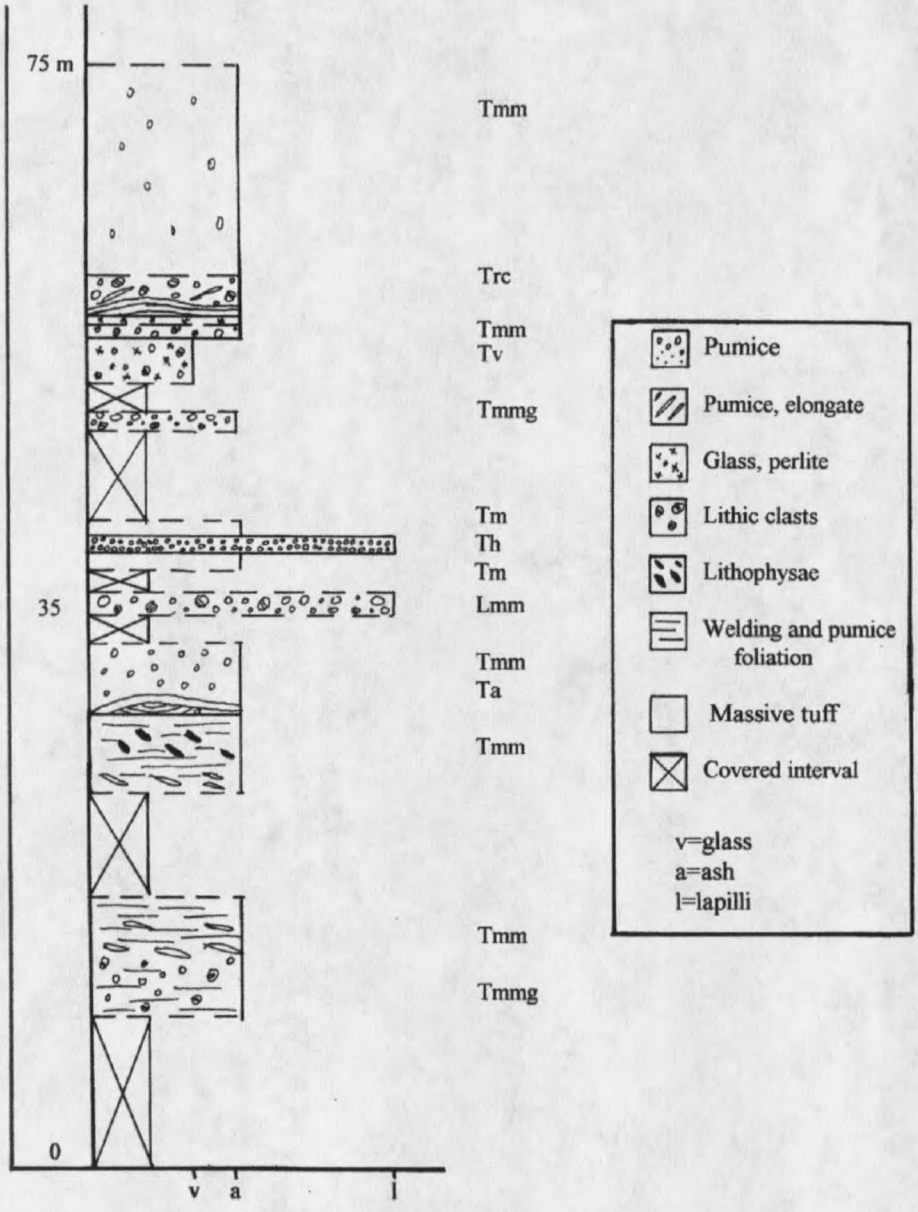


Figure 32: Schematic stratigraphic section of rhyolite-rhyodacite ash-flow tuffs found in the western facies. Pyroclastic lithofacies codes discussed in text and in Table 1.

In thin section, unit C is characterized by a vitric groundmass that has altered in most instances, to clay, chlorite, quartz, or zeolite. Relict shards are visible and retain bubble-wall texture. Glass in welded tuffs is compressed, with maximum compression localized at crystal contacts. Fragments include pumice, feldspar, biotite, quartz, and accidental lithics of mudstone, welded tuff, aphanitic volcanic rock, chalcedony, and plutonic rock.

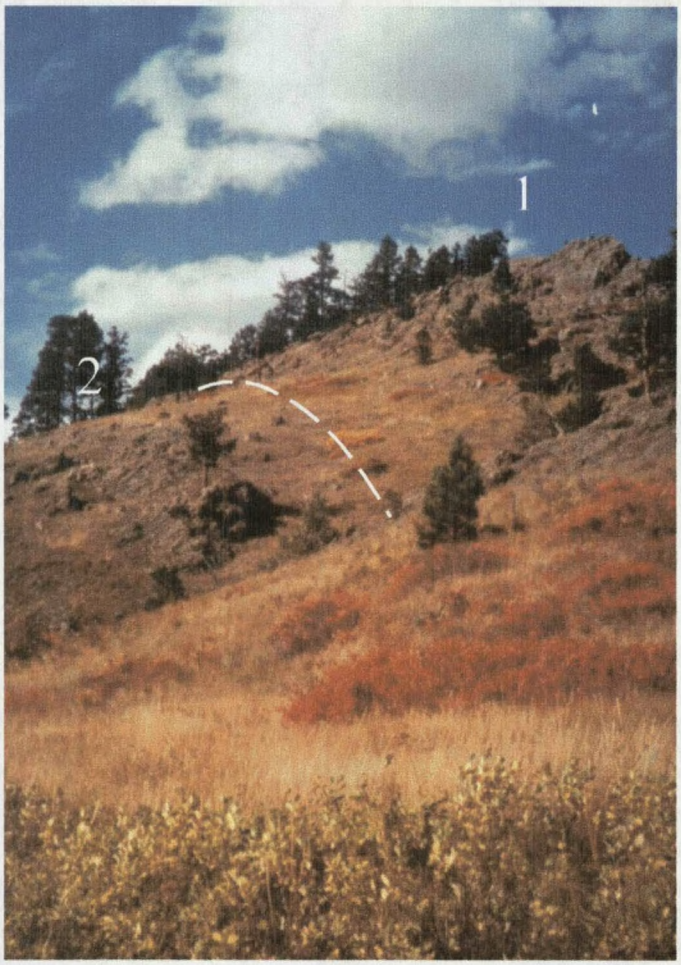


Figure 33: Exposure of rhyolite-rhyodacite ash-flow tuff sheets (unit C) in western facies, northern stratigraphic section (N-C). View to the northwest. Two flow units present (1, 2), separated by covered interval between.



Figure 34: Flow-banding in welded tuffs of the western facies, approximately 11 meters from the base of the northern stratigraphic section in unit C (N-C). Camera lens cap for scale.

Pumice fragments are generally wispy, and have been replaced to varying degrees by calcite, chlorite, microquartz, chalcedony, zeolite, and clay. In some instances, replacement is complete and the original pumice structure is difficult to identify. Some pumice clasts contain quartz, feldspar, and biotite in the vesicles. The quartz crystals found in compacted pumice commonly are strained, and contain abundant vacuoles.

Feldspar found in unit C is commonly broken along cleavage planes, equant, and may be altered to clay, chlorite, calcite, and zeolite. Typically, cores are more intensely altered, while rims may appear to be rounded due to clay replacement. Albite twinning on simple twins is most common, with rims of zoned plagioclase exhibiting simple twins. Rare, untwinned feldspar was also noted, and may have been sanidine. In one sample, feldspar is represented by multiple variations: plagioclase, potassium feldspar, perthite, and sanidine are present in one tuff sample. Atypically, this sample lacks alteration of feldspar. Feldspars range in size from 0.05 cm to 0.3 cm, and in one example, are glomocrysts. Quartz crystals are common to rare, and are found as broken, small (0.02 cm) fragments. Biotite is also less common than feldspar, and is typically deformed due to compaction during welding.

Lithic fragments are sub-rounded to sub-angular clasts of welded tuff, tuff, mudstone, aphanitic volcanic rock, and plutonic rock. All rock fragments contain crystals or groundmass altered to clay, chlorite, calcite, quartz, or zeolite. Mudstone grains are typically deformed. Rock fragments are found commonly in samples collected from the base of flows, and, in some instances, may be deformed or flattened.

Where vesicles are preserved, they are filled with chalcedony, microquartz, megaquartz, calcite, chlorite, clay, and zeolite. In some instances, quartz and feldspar are found in the vesicle cavity, and may represent vapor phase crystallization.

Unit E- Trachyte Lava Flows

Light grey groundmass, and trachytic texture characterize these aphanitic-porphyritic lava flows. The trachyte flows weather purple-grey, and in some cases are flesh colored. The

tabular flows range in thicknesses of 50 to 140 meters, and pinch out northwest of the field area (Schmidt, 1978) (Figure 35). The upper surface of the trachyte in the northern and central sections consists of a massive, matrix- and clast supported conglomerate (Gmm, Gcm) (Figure 36). Clasts are rounded to sub-rounded, scoriaceous, and severely stained by hematite. Matrix is difficult to discern from clasts, but appears to be hematitically-stained trachyte.



Figure 35: Exposure of trachyte lava flow of unit E in central stratigraphic section (C-E), western facies. View to the southeast.

In thin section, two distinct compositions were observed, and are interpreted as representing two distinct lava flows; a lower and upper lava flow. The lower lava flow is typified by an abundance of augite, rare and highly altered feldspar, and a finely-crystalline

groundmass. The groundmass consists of stubby, relict feldspar laths that have been altered to clay and perhaps zeolite or quartz, with abundant finely-crystalline opaque minerals. Schmidt (1978) determined that the groundmass is comprised of microcrystalline sanidine, andesine, augite, magnetite, and biotite. The augite phenocrysts are equigranular, fractured, show evidence of zoning and twinning, and are on average, 3 mm in diameter. The augite crystals are commonly intergrown and form glomocrysts. Only in a rare instance was an augite crystal found altered; the core of the augite crystal had been altered to clay. The feldspars are completely replaced by clay and chlorite, most likely after sericitization. The feldspars show relict albite twinning on simple twins. Schmidt (1978) provides a range in composition for the feldspars as andesine (An_{40}) to labradorite (An_{52}). The feldspars are rimmed with less-altered feldspar that display simple twinning. Some of the feldspars form penetrating intergrowths, or aggregates, which are on average 5 mm in diameter; individual crystals are 2 mm. There are also abundant opaque minerals. Hematite-rich clusters have "microlites" of quartz and feldspar, and may be accidental lithic clasts.

Amygdules are lined with clay, then filled with unaltered potassium feldspar that has simple and albite twins, and is zoned. Calcite in rare examples has replaced the amygdule core or has filled the entire vesicle. In other instances, the amygdules are spheroidal and are rimmed first with hematite, then clay, zeolite, clay again, and finally calcite. Calcite also fills pore spaces that may have originally been very irregularly shaped vesicles. In the southern section, the amygdules are filled with chlorite, macroquartz, chalcedony, and feldspar. The lower flow also has abundant hematite staining, especially along feldspar cleavage (twin) planes.

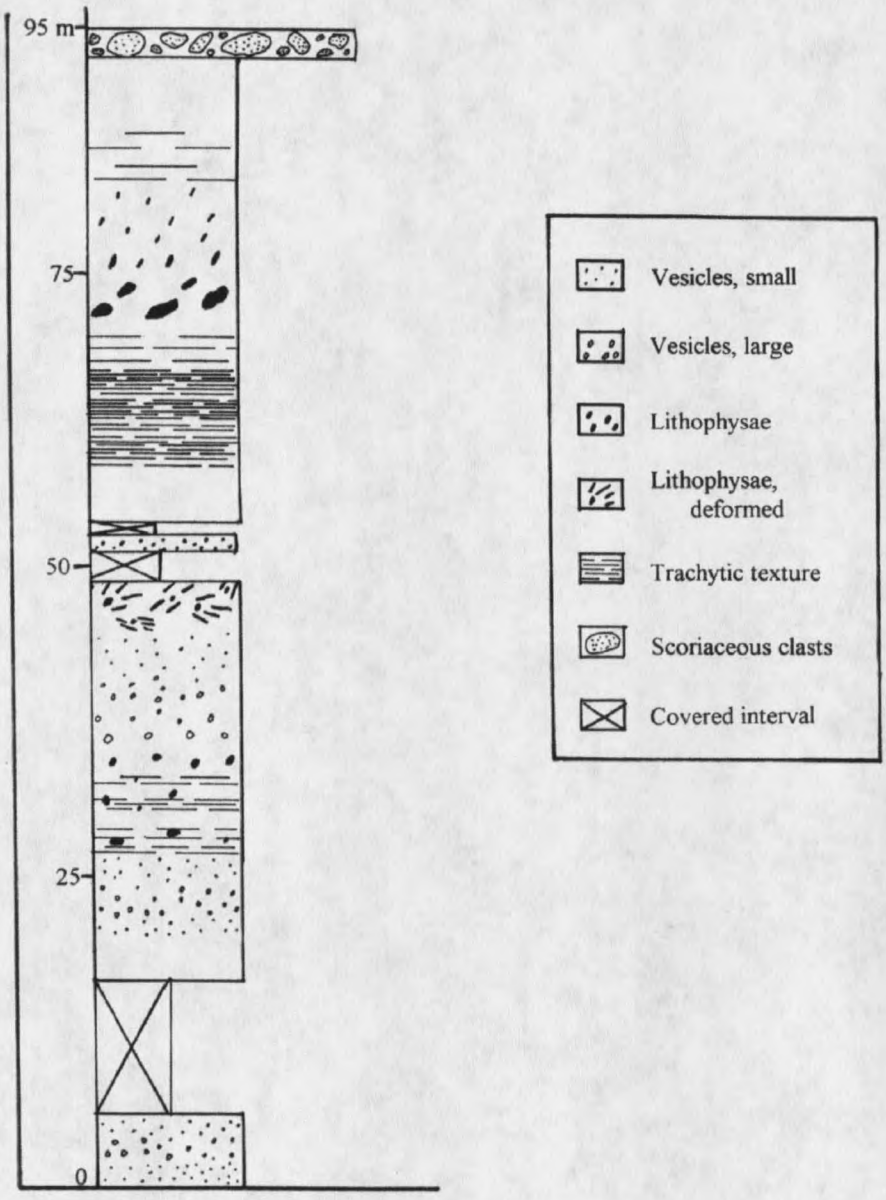


Figure 36: Schematic stratigraphic section through trachyte lava flow (unit E) found in western facies.

The uppermost lava flow, seen in all stratigraphic sections, has a more coarsely-crystalline groundmass than the lower flow. The groundmass consists of elongate feldspar laths altered to clay and possibly clinoptilite, augite crystals, and abundant opaque minerals. The groundmass exhibits evidence of flowage through preferential alignment of microlites around phenocrysts. Faint amounts of chlorite are visible, but alteration minerals are mainly clay and zeolites. A few of the groundmass feldspar laths show simple twins, and have undulatory extinction. The phenocrysts are predominantly zoned plagioclase feldspar, zoned augite, and biotite. Accidental lithic clasts are also present. The plagioclase feldspar phenocrysts have been sericitized, in addition to alteration of cores to clay, clinoptilite, and chlorite, and the rims completely to clay. Albite twinning is still evident, and the rims exhibit relict simple twinning. Chlorite alteration occurs along fractures. Simple twinned feldspars are uncommon. Many appear to be albite twinned where feldspar is intergrown with pyroxene. Feldspars are on average 3 mm long, and when in groups, the glomocrysts are on average 5 mm in diameter. Augite phenocrysts are equigranular, zoned, fractured, and mainly unaltered. Some are "embayed" into the feldspar crystals, and others seem to have intergrown with each other and feldspar. The augite crystals range in diameter from 2 to 5 mm. In one sample, a chlorite pseudomorph has replaced augite. Some biotite flakes occur, but are a minor accessory.

Amygdules are found only in the southern section, and they are comprised of chlorite rimmed in hematite. Hematite staining and chlorite replacement are prevalent throughout all sample localities. The conglomerate matrix in thin section displays feldspar laths that are sub-angular and altered to zeolite, and feldspar microlites that are unaltered and needle-like.

Interpretation

Two distinct flows were determined to be present through field analysis (sharp contact, lower flow had a pink upper surface, and vesicles), and through petrographic analysis (flow composition and textures differ slightly). The two flows occur together only in the central and southern measured sections. The northern section is comprised of only the uppermost lava flow. Additionally, the scoriaceous conglomerate is present in the central and northern sections only.

Adel Mountain Volcanics

Rocks of the Adel Mountain volcanic field were not extensively thin sectioned, and most of the information described here is from field observation. The Adel Mountain Volcanic rocks are aphanitic-porphyritic trachybasalt, and are characterized by a dark grey-green color that weathers to rust-orange or dark grey. The lava flows form columnar-jointed cliffs, have autobrecciated zones, and are interbedded with sandstones and conglomerates (Figure 37). The one identified and investigated lava flow is comprised of a broken basal surface that has baked the conglomerate below, a middle section with flow foliation and elongate amygdules (1cm to 5 cm long, and 0.25 cm wide), and an irregular upper surface that has a discontinuous sandstone lens above. The entire flow sequence is approximately 10 meters thick and tens of meters long.

In thin section, the groundmass consists of microcrystalline feldspar (some relict simple twinning) that has been altered to clay, abundant opaque minerals, and altered olivine (iddingsite pseudomorphs). Large (0.5 to 2 cm long) augite crystal appear visually to be the

most abundant phenocryst phase. The augite is fractured, zoned, and exhibits rare twinning. The iddingsite crystals are rimmed in hematite, are typically cored by vermicular chlorite or vermicular clay, and have a slight pleochroism of green to green-brown. The olivine phenocrysts are on average 2 mm in diameter. An isotropic phenocryst also exists that Schmidt (1978) suggests is analcime. The mineral in thin section is elongate, rectangular, and looks like altered feldspar as the rims are altered to clay. This same mineral fills the irregularly shaped amygdules as well, and is altered to clay near the edges of the amygdule. Rare, recognizable feldspar has been severely altered to clay.

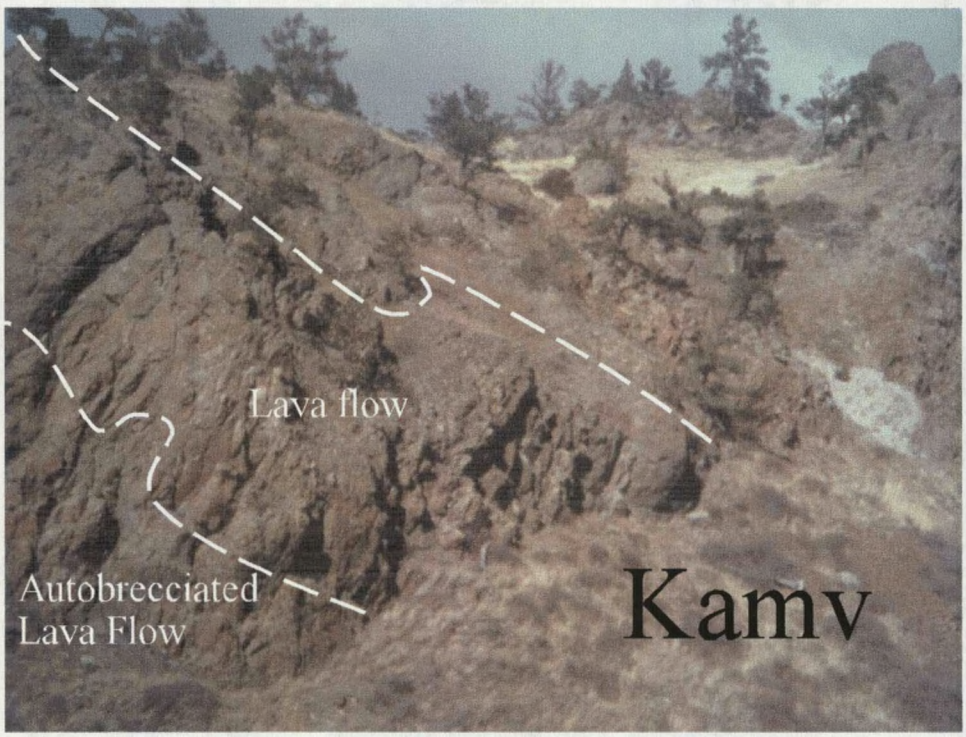


Figure37: Exposure of Adel Mountain Volcanics (Kamv) in measured sections of the eastern facies (RE-Kte). View to the north.

LITHOFACIES ASSOCIATIONS

Lithofacies associations were determined by identifying groupings of lithofacies from detailed stratigraphic section information that includes facies analysis, lateral facies relationships, and similarities among transportation processes. Delineating lithofacies associations allows interpretation of depositional environments found within larger, more generalized depositional systems. The lithofacies associations for the Upper Cretaceous Two Medicine Formation are separated into the western and eastern facies in order to facilitate understanding of the distinct depositional environments the western and eastern facies represent. The following analysis discusses sedimentary lithofacies, pyroclastic lithofacies, and characteristics of coherent lava flows from all units in the western and eastern facies. In some instances, however, units D and F are separately described to illustrate the differences between their sedimentary processes, lithofacies associations, and depositional environments.

Western Facies

Channel Association

Two Medicine Formation channel-fill deposits contain evidence of deposition from fluid gravity flow, hyperconcentrated flow, and debris flow. Lithofacies that represent channel-fill include trough cross-, low-angle cross-, and horizontally-stratified sandstones (St, Sl, Sh), ripple cross-laminated sandstone (Sr), massive sandstone (Sm, Smi), trough cross- and horizontally-bedded conglomerate (Gt, Gh), and massive- and clast-supported conglomerate

(Gmm, Gmmi, Gmin, Gcm, Gcmi, Gcms, Gcin) (Figures 38 and 39). Deposits are lenticular and tabular, and are generally laterally discontinuous. Beds of channel-fill deposits are 1 to 20 meters thick, and 5 to hundreds of meters in length. Carbonized vegetation is present at the base of unit D, and rarely found elsewhere.

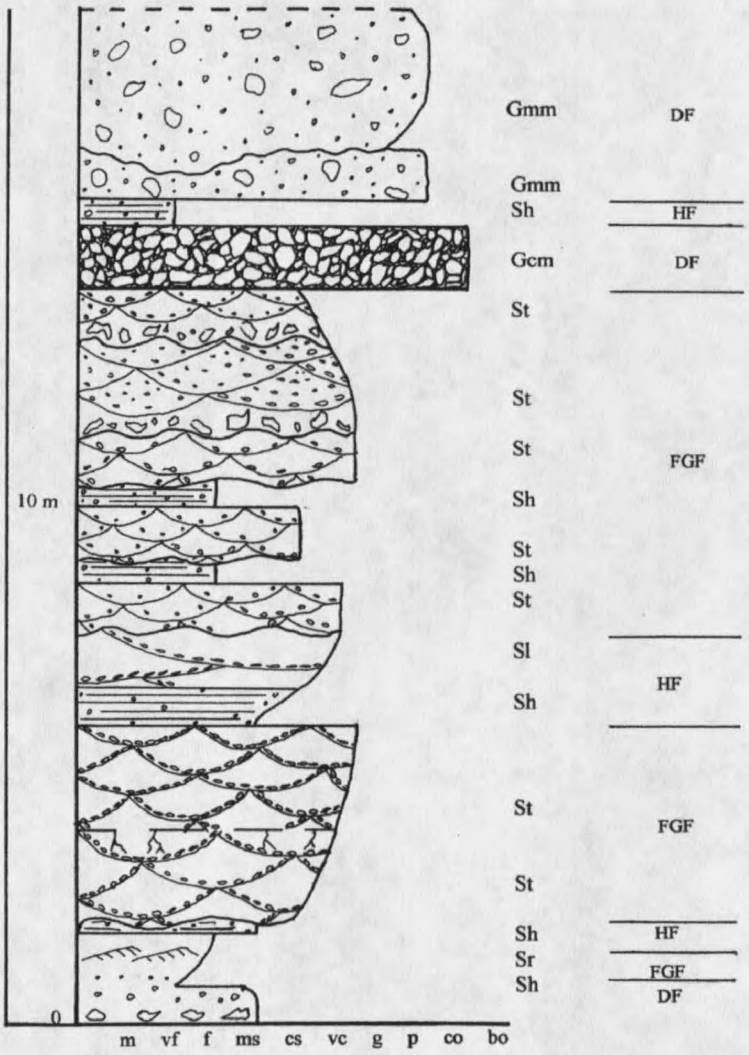


Figure 38: Schematic stratigraphic section of channel association found in unit D of the western facies. Lithofacies codes described in text and Table 1. DF= debris flow, HF= hyperconcentrated flow, and FGF= fluid gravity flow.

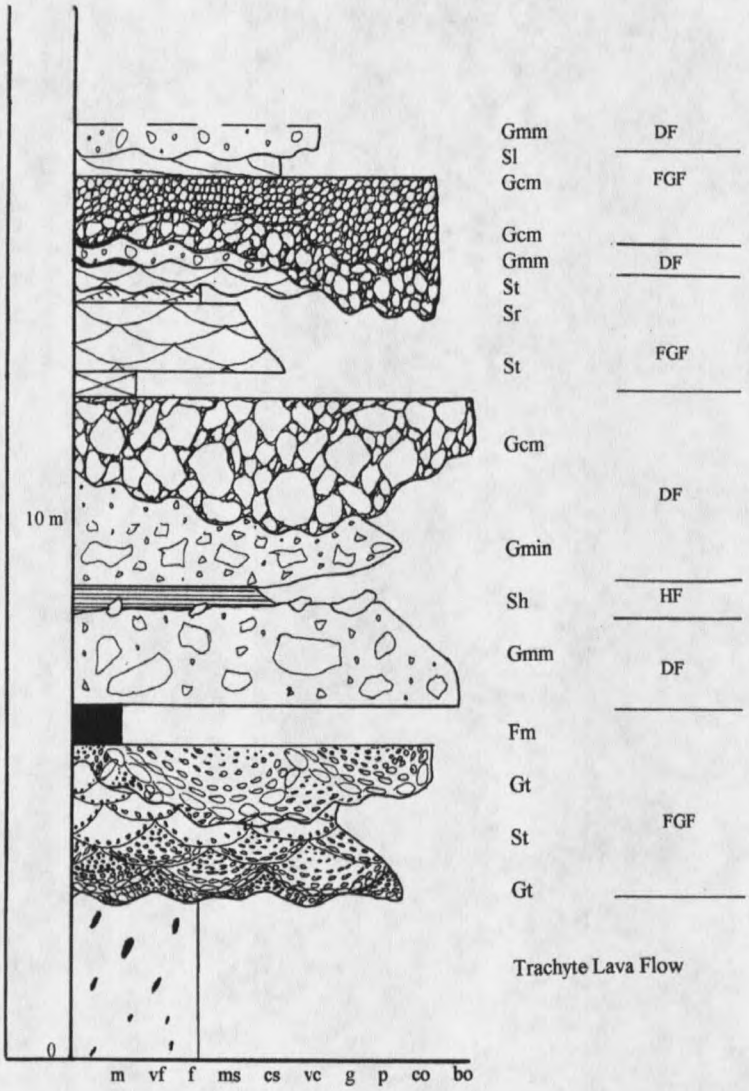


Figure 39: Schematic stratigraphic section of channel and floodplain associations for unit F of the western facies. Lithofacies codes are described in the text and in Table 1. DF= debris flow, HF= hyperconcentrated flow, and FGF= fluid gravity flow.

Fluid Gravity Flow (FGF): Trough cross-, low-angle cross-, and horizontally-stratified, and ripple cross-laminated tabular and lenticular sandstones (St, Sl, Sh, Sr), clast-supported, massive conglomerate (Gcm), and trough cross- and horizontally-bedded conglomerate (Gt, Gh) represent deposition and transport by fluid gravity flow and traction currents.

Coarsening upwards sets of St indicate increasing flow velocity over time (Miall, 1996). This is a common feature of unit D sandstones. St and Sr are found in lower regime fluid flows and the transition from St to Sr implies waning flow velocity (Harms and Fahnestock, 1965). Additionally, Sr could represent shallow stream flow. St interbedded with Sh may be the result of waning flow (for lower flow regime plane bed movement), or may indicate increased aggradation with higher flow velocities (upper flow regime plane bed movement) (Harms et al., 1982). The transition from Sl to Sh also indicates upper flow regime transformation in a shallow channel, or increased flow velocity (Orton, 1995).

The trough cross-bedded (Gt) conglomerates were deposited as dunes migrated down-channel. Fining upwards troughs indicate failure of the flow to transport the larger clasts (Miall, 1996). Therefore, flashy flow was most likely responsible for movement of the gravels. Migration of diffuse gravel sheets during pulses of high flow may have been responsible for producing horizontally-bedded conglomerates (Gh) (Hein and Walker, 1977). Finally, bimodal grain size distribution in clast-supported, massive conglomerate indicates deposition from streamflow. The larger clasts are deposited without orientation; matrix infiltrates the pore spaces to produce the bimodal grain size (Smith, 1986).

Debris Flow (DF): Debris flow deposits include matrix- and clast-supported, massive conglomerates (Gmm, Gmmi, Gmin, Gcm, Gcms, Gcin, Gcmi), and massive sandstones (Sm, Smi). Debris flows, being laminar, typically have sharp basal contacts. In a pre-existing channel, the basal contact may appear to be scoured. Several instances of matrix-supported conglomerates with erosive contacts found in unit F imply deposition in a channel scour. Matrix and clast-supported conglomerates transported by debris flows indicate pulses of volcaniclastic sediment into the fluvial system. The volcaniclastic sediment may have been derived from local volcanic edifices, or may be distal deposits of the Elkhorn Mountains volcanic field debris flows. Channelized volcanic debris flows may travel up to 100 kilometers, and may transform to hyperconcentrated flows as the debris flow loses velocity and large clasts (Smith, 1987a, 1987b). Massive sandstone may be indicative of rapid deposition from a high discharge flow (Fisher, 1971).

Hyperconcentrated Flow (HF): Hyperconcentrated flow produces thin Gcm deposits, coarse-tail normal graded conglomerate (Gcms), matrix-supported conglomerate (Gmm, Gmmi, Gmin), massive sandstone (Sm, Smi), and horizontally-stratified sandstone and conglomerate (Sh, Gh). In a channel, these most likely represent run-out from debris flows, or flow transformation due to fluidization of a debris flow as it encounters more water in the channel (Smith, 1987b). Massive sandstone and horizontally-stratified sandstone and conglomerate may be the result of high discharge flows that are sediment-rich and behave in a slightly turbulent manner (Miall, 1996).

Interpretation: Based on lithofacies, bedding geometries, abrupt vertical changes in grain size and lithofacies, and lack of evidence for lateral accretion, the fluvial systems of the Campanian Two Medicine Formation are interpreted to have been sandy and gravelly braided streams with well-defined floodplains or interchannel areas (Figure 40). Periodic influx of coarse volcaniclastic detritus in the form of debris flows and hyperconcentrated flows inundated fluvial channels. Episodes of abrupt aggradation on the fluvial plain were followed by periods of reworking by fluid gravity flows and channel entrenchment. This is especially noted in unit F, which is characterized by an abundance of debris flow and hyperconcentrated flow deposits relative to fluid gravity flow deposits.

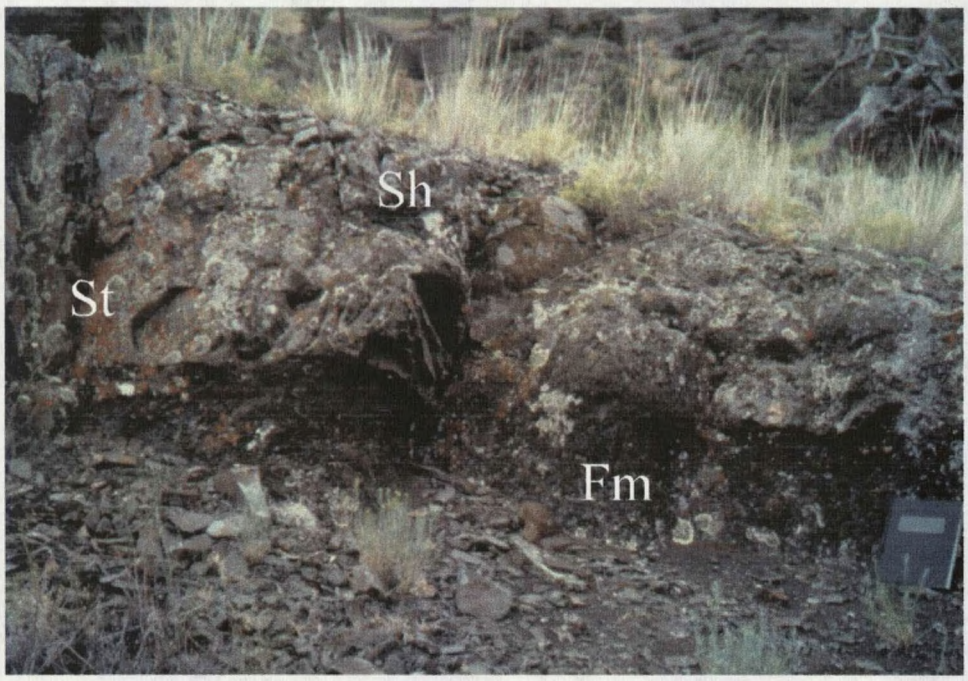


Figure 40: Channel-fill deposits of the western facies, unit D, approximately 80 meters above the base of the measured stratigraphic section. Trough cross-stratified sandstone (St) is capped by horizontally-stratified, hyperconcentrated flow-deposited sandstone (Sh). Note scour into floodplain-deposited mudstone (Fm). Notebook for scale (23.5 cm).

Floodplain Association

The floodplain association describes interchannel areas of the Two Medicine braided stream system. The lithofacies identified as representing deposition on the floodplain include massive and laminated mudstone (Fm, Fl), horizontally- and low angle trough cross-stratified sandstone (Sh, Sl), ripple cross-laminated sandstone (Sr), massive, matrix-supported conglomerate (Gmm), lava flows, and pyroclastic lithofacies of multiple ash-flow tuff sheets (Figures 39 and 41). Fm, Fl, Sh, and Sl are the most commonly interbedded deposits. Basal surfaces are commonly sharp, and erosional only rarely. Deposits of the floodplain association range in thicknesses of 2 to 15 meters (see Figure 40). Laterally, the deposits are continuous for distances up to 50 meters. Evidence for vegetation is conspicuously absent from all but the lowermost unit D floodplain deposits.

Fluid Gravity Flow (FGF): Deposition on the floodplain is typically by flood or high discharge flow that overflows channels. Thick sequences of massive and laminated mudstone (Fm, Fl) indicate that vertical accretion processes occurred on the floodplain. Horizontally-stratified and low-angle cross-stratified sandstones (Sh, Sl) exhibit coarsening upward sequences, are moderately to poorly sorted, and have sharp basal contact with the underlying laminated and massive mudstones (Fl, Fm). Deposits with these characteristics indicate overbank flow, crevasse splay, or waning channel-flow transportation mechanisms (Mathisen and Vondra, 1983; Smith, 1987b). Additionally, ripple cross-laminated sandstones (Sr) were noted at upper contacts of coarsening-upward crevasse splay deposits, and may indicate waning fluid flow (Harms and Fahnestock, 1965). Floodplain deposits, where exposed, were

approximately 0.5 to 3 meters thick, and laterally extensive for 10 to 30 meters. In addition, massive sandstone (Sm) beds are found in unit D with abundant root traces, implying stable interchannel areas (Lorenz, 1981).

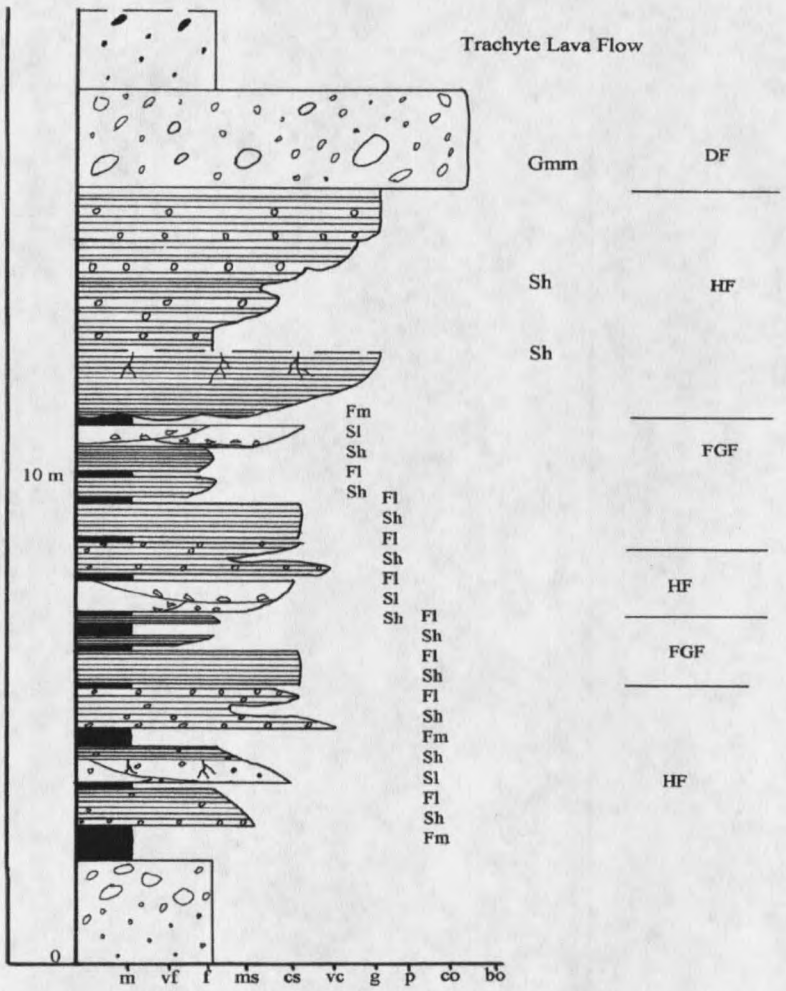


Figure 41: Schematic stratigraphic section of floodplain association for unit D of the western facies. Lithofacies codes are described in the text and in Table 1. DF= debris flow, HF= hyperconcentrated flow, and FGF= fluid gravity flow.

Debris Flow (DF): Episodic influx of sediment-laden flows in the fluvial systems likely over-ran channel banks and spread laterally over the fluvial plain. One example observed in unit F resembled "levee" deposits above a conglomerate-filled channel scour. The "levee" was a clast-supported, massive conglomerate (Gcm). Filling the channel scour was a coarse-tail inversely graded, clast-supported conglomerate (Gcmi). The floodplain-deposited conglomerate (Gcm) was observed laterally for approximately 20 meters, and then was covered. Other debris flow deposits (Sm, Smi, Gmm, Gmmi, Gcms, Gcin) were also found stratigraphically above "normal" floodplain deposits of vertically accreted, massive and laminated mudstone (Fm, Fl), and crevasse splay-deposited, horizontally-stratified, and ripple cross-laminated sandstone (Sh, Sr). In most examples, the basal contacts were erosional or sharp. Some of the mudstone lithofacies were also contorted by soft-sediment loading, which indicates deposition of coarse deposits *en masse* on a moderately wet surface (Smith, 1988). Debris flow deposits in the floodplain setting were typically 0.2 to 10 meters thick, and laterally extensive for 3 meters to 100 meters.

Hyperconcentrated Flow (HF): Hyperconcentrated flows on the floodplain behave similarly to sheetfloods on an alluvial fan (Blair and McPherson, 1994). Hyperconcentrated flows may result from the fluidization (flow transformation) of a debris flow as it encounters water in a channel, and proceeds to over-run the channel banks (Smith, 1986). This would be especially significant in the interchannel area of a fluvial plain, where high-discharge flows episodically avulse and inundate the floodplain. In unit F, horizontally-stratified conglomerate and sandstone (Gh, Sh) occur in "couplets" interbedded with debris flow deposits of massive

clast- and matrix-supported conglomerate (Gcm, Gmm). Couplets on alluvial fans occur as standing waves wash-out during a sheetflood event (Blair and McPherson, 1994). This definition is especially significant as couplets in unit F are found interbedded with low-angle cross-stratified sandstone (Sl); Sl has been interpreted as the result of scour-fill structures or antidunes (Miall, 1996). Sh and Gh are also found interbedded with massive and laminated mudstone (Fm, Fl), which also supports hyperconcentrated flow occurring on the vertical accretion deposits of the floodplain (Fm, Fl). Hyperconcentrated flow deposits generally are 0.05 to 2 meters thick, and laterally extensive for tens of meters.

Pyroclastic Flows/Surges: The lapilli- and ash-flow tuffs observed in unit C were deposited via pyroclastic flows and surges, as determined by lithofacies analysis. Pyroclastic lithofacies observed include massive tuff (Tm), climbing ripple cross- and horizontally-stratified tuff (Trc, Th), antidune-stratified tuff (Ta), vitrophyric tuff (Tv), and massive, matrix-supported tuff and lapilli tuff (Tmm, Tmmg, Lmm) (see Figure 32). Tuffs are tabular, laterally extensive, and occur almost exclusively in the western facies field area. Upper contacts with the fluvial deposits of unit D are covered, as are basal contacts with the underlying latite lava flows of unit B; however, in the southern section of unit C, a very poorly exposed, sharp, undulatory, basal surface was observed between a pyroclastic flow (Tmm) and a massive mudstone (Fm) (Figure 42). The pyroclastic units were deposited in a series of catastrophic events that inundated the fluvial plain; therefore, the pyroclastic lithofacies are placed in the floodplain association based on their tabular geometry and lack of channelization evidence.

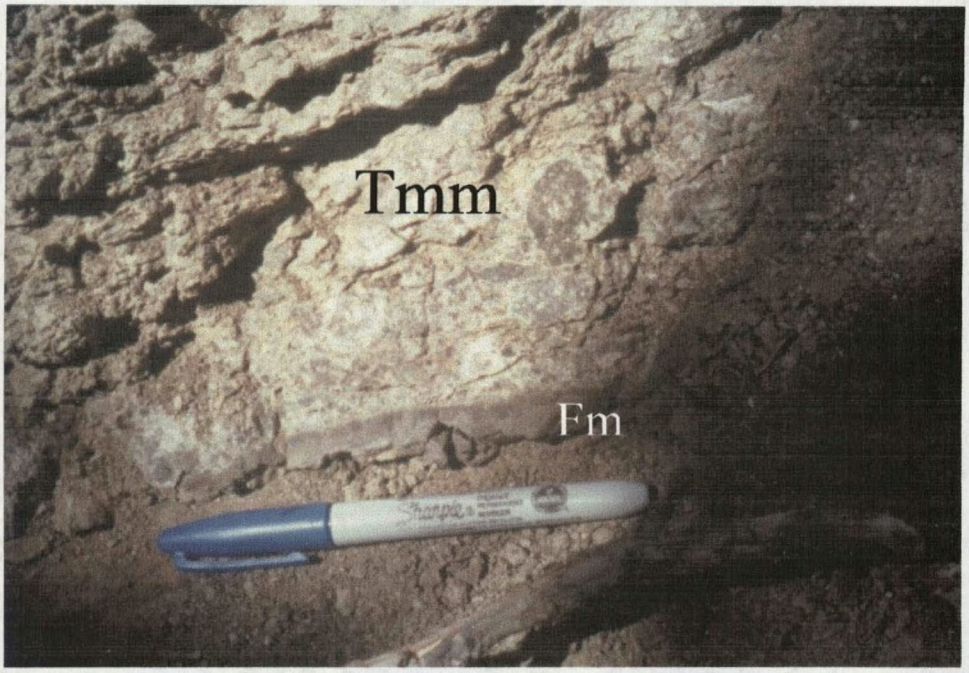


Figure 42: Pyroclastic flow deposit on floodplain mudstone (Fm). Lithic-rich base of pyroclastic flow (Tmm). Exposed in southern stratigraphic section of unit C (S-C), approximately 6 meters above the base of the measured section. Sharpie marker for scale.

On a broad fluvial plain, the lack of significant channelization results in attenuation of the pyroclastic flow, and may result in uncharacteristically thin, massive, matrix-supported tuff sheets (Tmm). In addition, attenuation results in a loss of yield strength (Costa, 1988), which may result in normally-graded lapilli tuff (Lmm, Tm). Deformed accidental mudstone (Fm, Fl) clasts were also observed in the field and petrographically, suggesting incorporation of "rip-ups" from the underlying substrate into the moving flow. This was especially evident in density graded, matrix-supported tuffs (Tmmg) where lithic lapilli were more concentrated and obvious.

Pyroclastic surges are represented by stoss-side dunes (Ta), horizontally-stratified tuff (Th), and climbing ripple cross-stratified tuff (Trc). Deposits are typically tabular, and dominantly grade upward into pyroclastic flow deposits. Poor exposure limits determination of lateral continuity; however, thicknesses of pyroclastic surge deposits range from 0.1 to almost 3 meters.

Lava Flow: The Two Medicine fluvial plain is unusual in that lava flows are interbedded with fluvial overbank deposits. Units B and E are comprised of multiple lava flows of latitic and trachytic composition. The lava flows range from 35 to 78 meters thick and are laterally continuous throughout the field area; although, Schmidt (1978) documents thinning of both lava flow units to the north. Basal and upper surfaces are covered; in one example (central section of unit B), conglomerates deposited by either hyperconcentrated flow or fluid gravity flow are found between units B and C. Silicified and altered accidental lithic clasts are found in the flows. The lithic clasts are generally very fine-grained, rounded to angular, and in some instances, appear to be "squeeze-ups" of underlying, muddy substrate. In one example, a large, laminated mudstone (Fl) accidental clast was found (Figure 43). A lava flow with these accidental lithic clasts indicates movement of the lava flow on the floodplain. The tabular geometry of the lava flows, their lateral continuity, and the incorporation of laminated mudstone (Fl) accidental lithic clasts permit inclusion of lava flows in the floodplain association.

Interpretation: Floodplain deposition was dominated by vertical accretion of massive and laminated mudstone (Fm, Fl); however, catastrophic floodplain inundation is indicated by wedge-, lenticular-, and tabular-shaped units of massive, clast- and matrix-supported conglomerate (Gcm, Gmm), and horizontally- and low-angle trough cross-stratified sandstones (Sh, Sl) deposited by debris flow and hyperconcentrated flow events. Presence of lava flows and ash-flow tuff sheets attests to direct influence of eruptive activity across the Two Medicine fluvial plain. It is hypothesized that fluvial channels were likely to have been also filled by lava flows and ash flow tuffs; however, evidence of this was never directly observed.

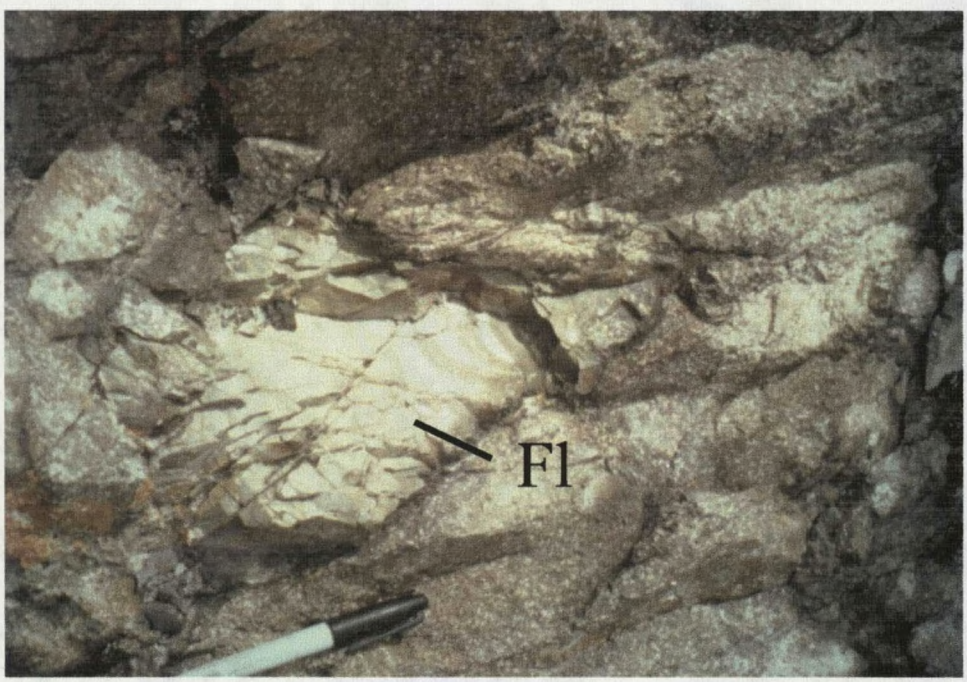


Figure 43: Laminated mudstone (Fl) accidental lithic clast in latite lava flow. Exposed in the central stratigraphic section of unit B (C-B), approximately 30 meters above the base of the measured section. Sharpie marker for scale.

Eastern Facies

Marsh Association

Organic material (O) is found interbedded with fine-grained, horizontally-stratified and massive sandstones (Sh, Sm), rootbeds (Fp), carbonate (Cn, Cl), and massive mudstone (Fm) in laterally discontinuous tabular deposits approximately 7 meters thick (Figure 44). Basal and upper surfaces are gradational between O, Fm, and Fp, but sharp between Sm, Sh, and (Cl). Thin coal beds (<0.1 meters thick), plant debris, and clay make up the organic material (O). Bioturbation results in massive sandstone and mudstone (Sm, Fm). Hematite and limonite nodules, concretions, and zones also occur in this association, indicating oxidation of the sediments.

Interpretation: The units described are interpreted to have been deposited in a marsh setting based on the interbedding of the carbonaceous mudstone and sandstones, and abundance of plant material (Weimer et al., 1982). In addition, the rootbeds (Fp) indicate a low energy environment that permits plant growth and sediment trapping (Dyer, 1994); sediment in this environment is deposited during waning flow, as evidenced by the fine-grain size and stratification observed in the sandstones and mudstones (Sh, Fm) (Weimer et al., 1982). Hematite and limonite nodules may be due to the replacement or infilling of decayed plant material by hydroxides; this is also typical of a marsh setting (Weimer et al., 1982). The carbonate mud may be the result of an enclosed or partially enclosed waterbody within the marsh (Reading and Collinson, 1996).

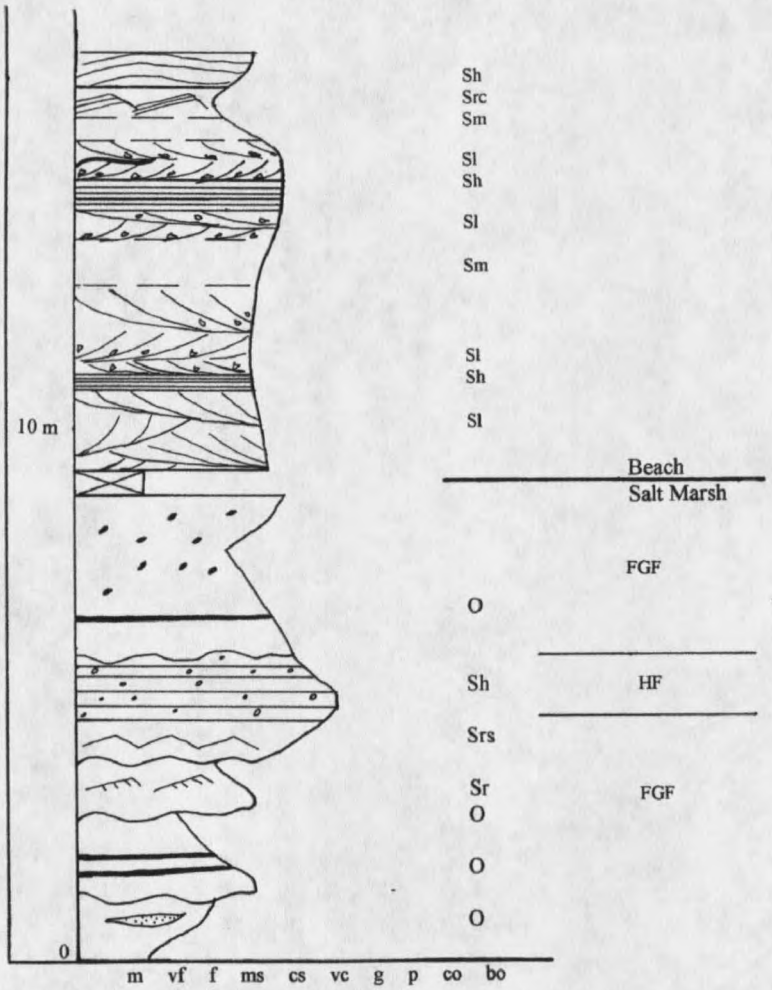


Figure 44: Schematic stratigraphic section of salt marsh and beach associations found in the eastern facies. Lithofacies codes are described in the text and in Table 1. DF= debris flow, HF= hyperconcentrated flow, and FGF= fluid gravity flow.

Beach Association

Interbedded low-angle cross- and horizontally-stratified (Sl, Sh), and massive sandstone (Sm) are capped by symmetric ripple cross-stratified (Srs) and swaley horizontally-stratified sandstone (Sh) (see Figure 44). Trough cross-stratified sandstone (St) is also present. Sl commonly exhibits "herringbone" stratification, which indicates bidirectional flow

(McCubbin, 1982). Tabular and lenticular deposits are 2 to 10 meters thick, and laterally continuous for hundreds of meters. Basal surfaces are sharp or gradational, with soft sediment deformation occurring in thin beds of Sh. Bioturbation is evident by the presence of worm burrows in the massive sandstone (Sm). Mud intraclasts (1 cm long, sub-flattened) are common along many of the trough bases of Sl and St. Heavy minerals (pyrite, magnetite) are prevalent in the lowermost deposits of Sl and Sh. The Sl and Sh deposits are also "cleaner", with less mud, clay, and zeolites, and typically weather a tan-white color (Figure 45).

Interpretation: Together, these lithofacies describe deposition in a beach or strandplain environment. Swash-backswash mechanisms produce horizontally- and low-angle cross-stratified sandstone in the beach backshore (McCubbin, 1982). In addition, heavy mineral concentrations, and bioturbation by roots and worm burrows are typically found in the beach backshore (McCubbin, 1982; Bibler and Schmidt, 1986). Trough cross-stratified sandstone (St) may be the result of migrating dunes in the upper shoreface (McCubbin, 1982; Reading and Collinson, 1996). Storm deposition in the lower shoreface may be responsible for the climbing ripple cross-stratification, the swaley geometry of the horizontally-stratified sandstone, and the low-angle cross-stratification (McCubbin, 1982; Reading and Collinson, 1996). In addition, the base of one of the beach association deposits has a basal lag of woody debris and mud intraclasts; this is also indicative of a storm deposit (McCubbin, 1982). However, the deposits are mostly fine and medium sand-sized, and therefore lack the characteristic silt and mud of the lower shoreface (McCubbin, 1982).

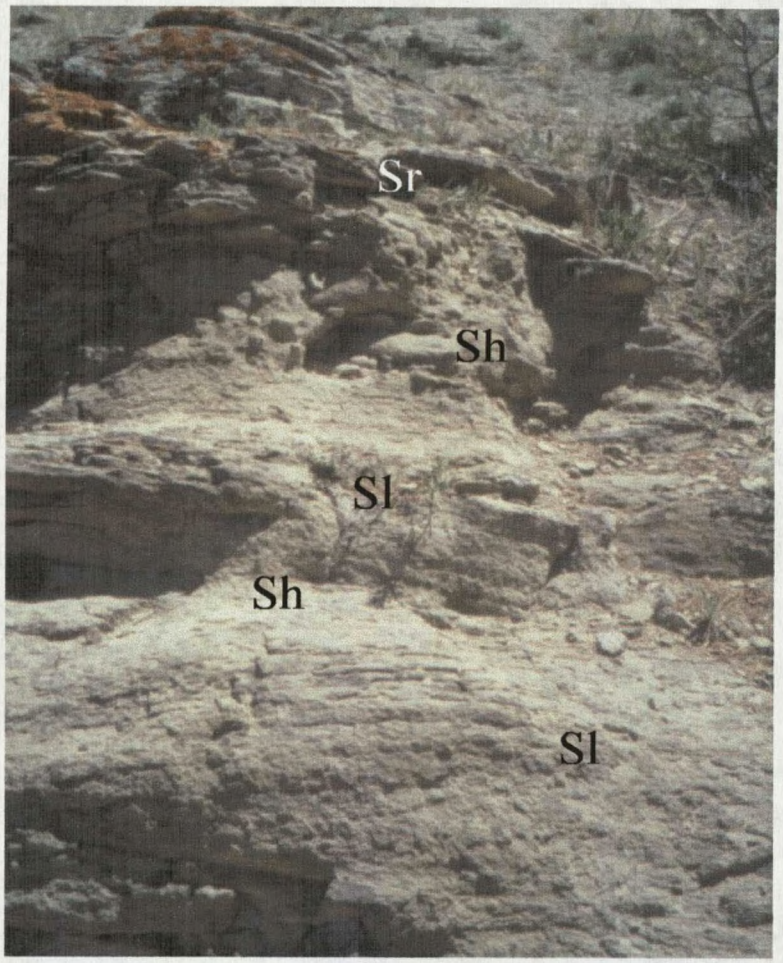


Figure 45: Beach sandstones in eastern facies exemplified by interbedded low-angle cross-, horizontally-, and ripple cross-stratified sandstones (Sl, Sh, Sr). Unit is 3 meters thick, and located approximately 14 meters from the base of stratigraphic section E2-Kte, and laterally, 20 meters along strike.

The deposits, if compared to other Late Cretaceous coastal plain sediments, may be interpreted as barrier islands rather than beaches. However, these coastal plain deposits lack thick (>10 meter), high-angle, trough cross- and planar-stratified sandstones (Bibler and Schmidt, 1986) and facies associated with barrier island formation (tidal delta, lagoon, and tidal inlet facies) (Reading and Collinson, 1996). Outcrops of the eastern facies definitely lack

thick high-angle trough cross- and planar-stratified sandstones. Tidal delta, lagoon, and tidal inlet facies may be present, but due to poor exposure of deposits, may not have been recognized.

Lacustrine Association

Thin (<1 meter), laterally discontinuous beds of carbonate mudstone (Cl) are interbedded with extremely fine-grained mudstone (Fl, Fm) (Figure 46). Basal surfaces are sharp, and one example shows evidence of deformation by loading from above. Laminae are the result of suspension settling, or may be due to ash-fall landing on the pond surface. Massive mudstone is interpreted as being bioturbated; freshwater gastropods and pelecepods (*Unio*) were found in two examples of the eastern facies.

Interpretation: The deposits were produced by shallow, ponded freshwater (Smith, 1987b; Waresback and Turbeville, 1990). Shallow waterbodies may also represent lacustrine deposits in an upper delta plain setting (Reading and Collinson, 1996). Lacustrine environments are characterized by fine-grained deposits, including abundant clay, and indicate deposition in a low energy environment (Reading and Collinson, 1996).

Distributary Channel Association

Facies deposited in this association include poorly-sorted, trough cross-, low-angle trough cross-, and horizontally-stratified sandstone (St, Sl, Sh), ripple cross-laminated sandstone (Sr), massive, bioturbated sandstone (Sm), trough cross-bedded conglomerate (Gt), and massive, matrix- and clast-supported conglomerate (Gmm, Gcm, Gcms) (see Figure 46).

Deposits are < 3 meters thick, are laterally discontinuous lenses (< 35 meters), and typically have erosive basal surfaces (Figure 47). Mud intraclasts typically form basal lags in St, Sl, and Gt. Many of the distributary channels laterally pinch out into the mudflat as crevasse splay deposits (Figure 48).

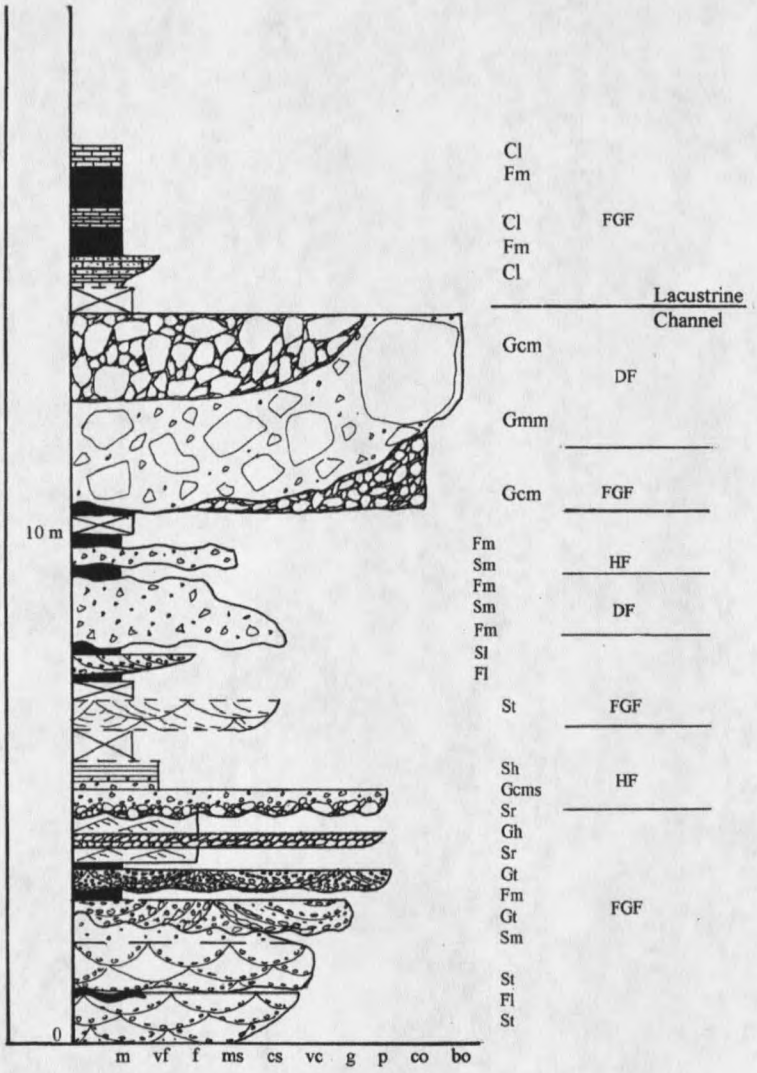


Figure 46: Schematic stratigraphic section of the lacustrine and distributary channel associations found in the eastern facies. Lithofacies codes are described in the text and in Table 1. DF= debris flow, HF= hyperconcentrated flow, and FGF= fluid gravity flow.

Fluid Gravity Flow (FGF): Interbedded low-angle trough cross-, horizontally-, and trough cross-stratified sandstone (Sl, Sh, St), ripple cross-laminated sandstone (Sr), and trough cross-stratified conglomerate (Gt) were deposited by fluid gravity flow in distributary channels that periodically experienced avulsion. In many instances, the distributary channels cut shallowly and broadly into mudflat deposits (discussed below), and the distributary channel deposits are commonly capped by mudflat deposits (Fm, Fl, Sr). Mud intraclast lags imply migration of the distributary channels across the mudflat (Weimer et al., 1982). Massive sandstones above distributary channel deposits are bioturbated by roots, and indicate channel abandonment. St is commonly capped by Sr, and this may indicate waning flow within the distributary channel (Harms and Fahnestock, 1965).

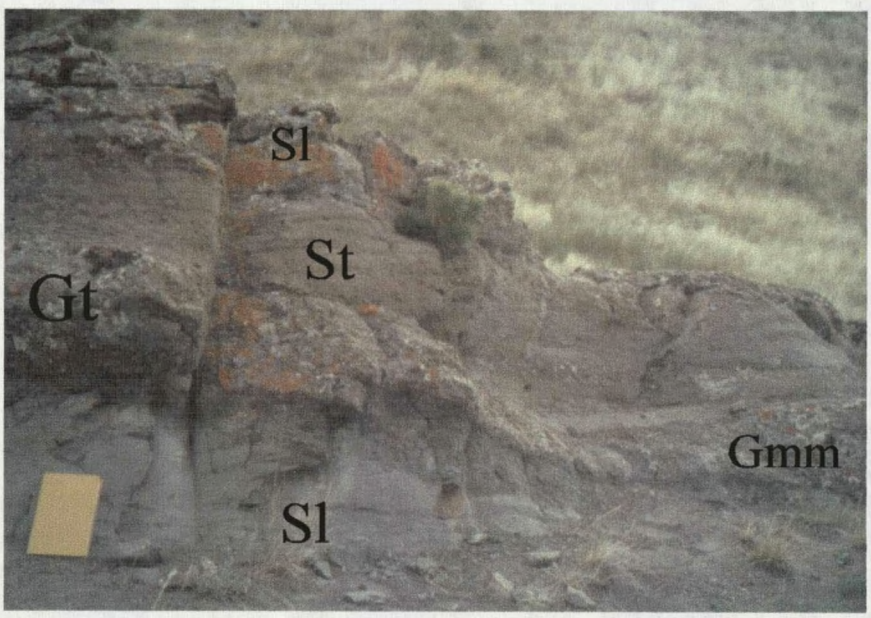


Figure 47: Distributary channel-fill deposits are trough cross-bedded, and matrix-supported, massive conglomerate (Gt, Gmm), and trough cross- and low-angle trough cross-stratified sandstones (St, Sl). Exposed approximately 139 meters above base of measured stratigraphic section RE-Kte.

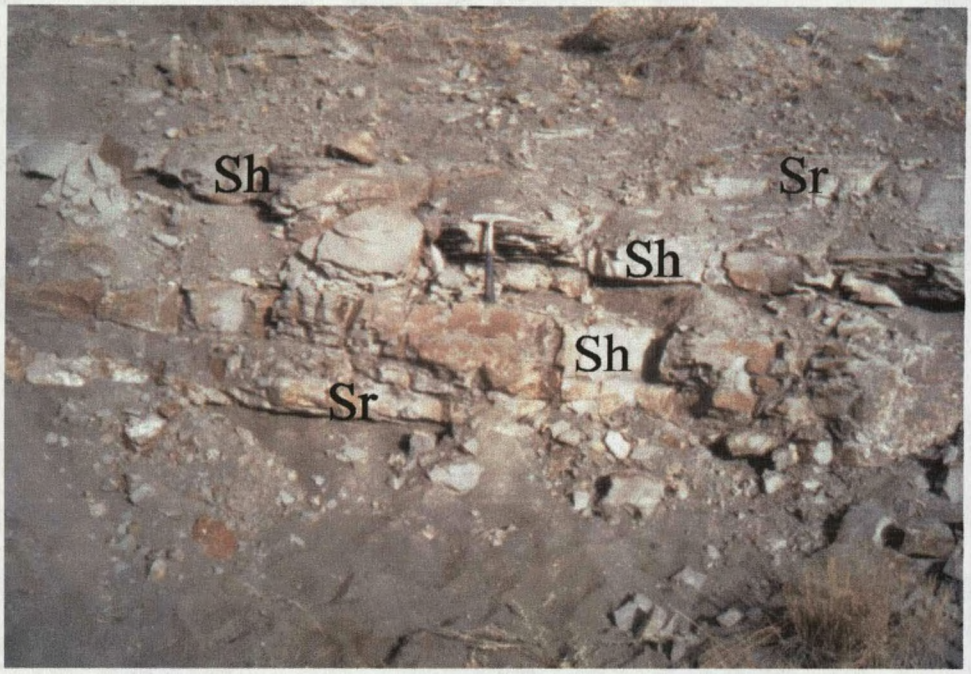


Figure 48: Crevasse-splay deposits found in the eastern facies. Lithofacies present are horizontally- and ripple cross-laminated sandstones (Sh, Sr) interbedded with laminated and massive mudstone (Fl, Fm). Exposed approximately 93 meters above the base of measured stratigraphic section RE-Kte. Hammer for scale.

Debris/ Hyperconcentrated Flow (DF/HF): As with western facies channel deposits, the distributary channels experienced periodic influx of volcanic debris in the form of volcanic debris flows and hyperconcentrated flows. Rare, matrix- and clast-supported massive conglomerate (Gmm, Gcm, Gcms) were found in channel sequences, with erosive bases, and interbedded with hyperconcentrated flow deposits of poorly sorted, horizontally-stratified sandstone (Sh). The Sh deposits may be run-out end members of larger volcanic debris flows derived from volcanic edifices to the west. As the debris flows reached the low-gradient coastal plain, they thinned and spread laterally across the mudflats, distributary channels, and possibly into the seaway (Orton and Reading, 1993). However, clast counts (See Provenance

Chapter and Appendix B) and observations of the deposits indicate that the coarser debris flow deposits may be monogenetic, and derived from the Adel Mountain volcanic field to the east.

Interpretation: The distributary channel association reflects normal fluvial deposition affected by episodic catastrophic processes on a coastal plain. Based on coarseness of grain-size (coarse sand to pebble), the lack of lateral accretion deposits, and the relatively thin (<3 meters) and discontinuous deposits, the distributary channels are interpreted to be low-sinuosity, braided, sandy-gravel "streams" that periodically received detritus from an explosive source (Smith, 1987b).

Tidal Mudflat Association

Thinly-bedded, tabular deposits of laminated and massive mudstone (Fl, Fm), ripple cross-, climbing-ripple cross-, and wave cross-laminated sandstones (Sr, Src, Srs), horizontally- and low-angle trough cross-stratified sandstones (Sh, Sl), massive sandstone (Sm), carbonate mudstone (Cn), and massive- and clast-supported conglomerate (Gmm, Gmmi, Gmin, Gcm, Gcmi, Gcms, Gcin) are found interbedded with each other, and have sharp and erosive basal surfaces (Figure 49). Deposits are typically poorly exposed, and deposits are 1 to 10 meters thick, and laterally continuous for tens of meters. In a few examples, the interbedding of the mudstone with the sandstone resembles wavy-flaser bedding and wavy bedding (See Figure 21) (Weimer et al., 1982). Trace fossils, including worm burrows of various orientations, vertical spreiten, and wasp burrows, are abundant in deposits of Fm, Fl, Sm, and Sr. Oyster hash (*Ostrea glabra*: Schmidt and Zubovic, 1966) of whole, seemingly unabraded oysters is also found interbedded with these deposits; disarticulate and articulate

oysters are commonly present in muddy deposits that are poorly exposed. Oysters are more abundant in the northernmost section of the eastern facies (E2-Kte). Deposits of Fm, Fl, Sr, and Sh exhibit soft-sediment deformation in the form of convoluted bedding, flame structures, and rare fluid-escape structures.

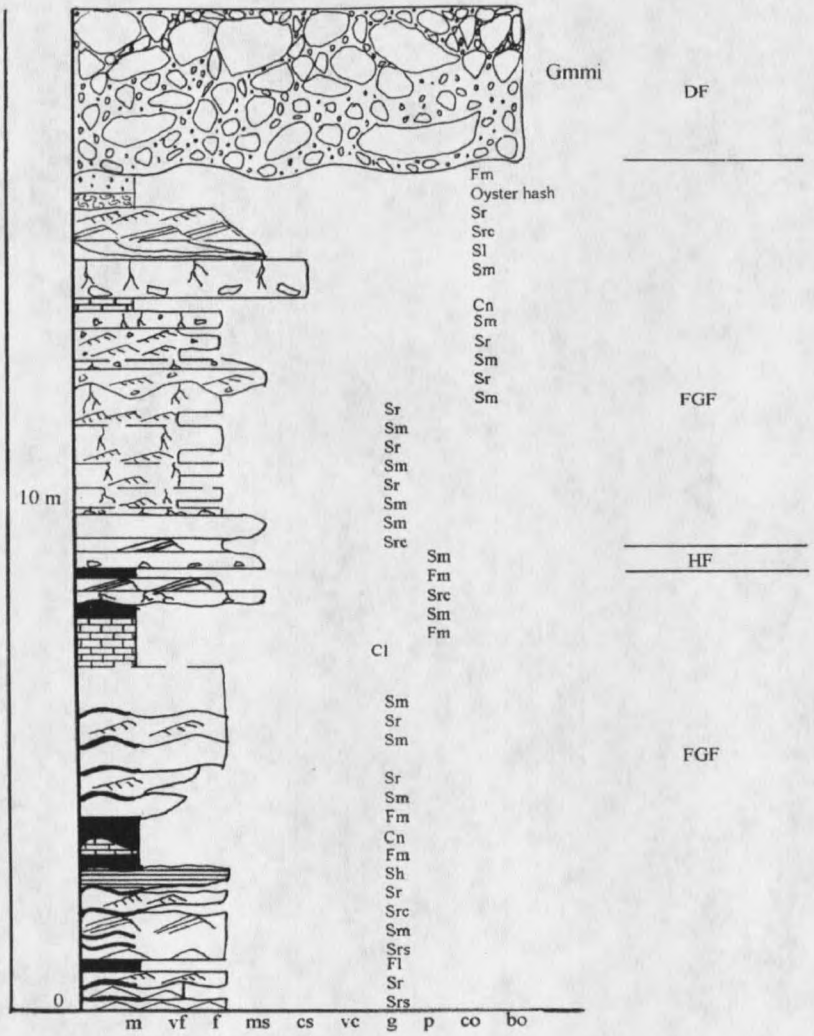


Figure 49: Schematic stratigraphic section of tidal mudflat association found in the eastern facies. DF= debris flow, HF= hyperconcentrated flow, and FGF= fluid gravity flow.

Fluid Gravity Flow (FGF): Tides deposit finer-grained sediment on the mudflat, producing wavy-flaser bedding (Dyer, 1994). Deposition by suspension settling, vertical accretion, and traction current transport resulted in interbedded laminated and massive mudstone (Fl, Fm) with massive, bioturbated sandstone (Sm), ripple cross-laminated sandstone (Sr, Src, Srs), and horizontally- and low-angle cross-stratified sandstone (Sh, Sl) (Weimer et al., 1982). Root traces are prevalent in massive sandstone beds (Sm). Nodular carbonate mudstone (Cn) is found in this association as well, and implies pedosol development, while laminated carbonate mudstone (Cl) in this association implies ponded water (Reading and Collinson, 1996). Disarticulate and articulate oysters are present in mudstone that is poorly exposed, and as well-cemented beds 1 meter thick. The associated deposits would be considered representative of a typical tidal flat environment (Weimer et al., 1982). Thin, discontinuous sheets of interbedded Fm, Fl, Sr, and Sh that lack tidal evidence are interpreted as crevasse splay deposits.

Debris Flow (DF): The mudflat also received debris flow detritus, evidenced by lenticular sheets of clast- and matrix-supported, massive conglomerate (Gcm, Gmm, Gmmi). The conglomerates are found interbedded with fluid gravity flow-deposited massive and laminated mudstone (Fl, Fm), ripple cross-laminated sandstones (Sr, Src, Srs), horizontally- and low-angle cross-stratified sandstone (Sh, Sl), and massive sandstone (Sm). Oysters (*Ostrea glabra*) and mud intraclasts (Fm, Fl) are found as clasts within the conglomerates. Soft sediment loading of the underlying mudstone occurred, indicating deposition of the debris flows on a wet, unconsolidated material. Clast- and matrix-supported breccias (Gcm, Gmm)

that are monogenetic, have evidence for emplacement at high temperatures (red discoloration of clasts, red discoloration of underlying unit, radially jointed clasts), and have a matrix of the same composition as the clasts are interpreted as hot debris flows when not associated with a lava flow.

Hyperconcentrated Flow (HF): Poorly sorted, massive sandstone (Sm) and horizontally- stratified sandstone (Sh) were deposited by hyperconcentrated flow on the mudflat. This is indicated by the sheet-like geometry of Sm and Sh, sharp basal contacts with underlying units of Fm and Fl, and the common bioturbation of the uppermost portions of the beds by roots and burrows. Deposits are thin (< 0.5 meters), tabular, and laterally discontinuous (15 to 25 meters).

Lava/Autobrecciated Flow: A single trachybasalt lava flow of the Adel Mountain volcanic field is interbedded with matrix- and clast-supported conglomerate (Gmm, Gcm) that may be of autobrecciated origin, and ripple cross-stratified (Sr) and horizontally-stratified sandstone (Sh). Laterally, deposits of Fm, Fl, and oysters in mudstone are found. The lava flow is interpreted to have been deposited on the mudflat based on the interbedded vertical accretion deposits (Fm, Fl), squeeze-ups of wet sediment from below (Figure 50), waning flow deposits (Sr, Sh), and the occurrence of oysters in mudstone underlying the lava flows. A wet substrate has been documented to cause phreatic explosions underneath a moving lava flow (Ricketts, 1985). Conglomerates and breccias interpreted to have been deposited by debris flows may be autoclastite lava flows, broken by the interaction of surface water with the lava flow.



Figure 50: Wet sediment loading and incorporation of tidal mudflat-deposited mud into the base of a lava flow of the Adel Mountain Volcanics. Jacob's staff for scale (1.5 meters). Exposed 330 meters above the base of measured section RE-Kte, and laterally along strike 100 meters to the south.

Interpretation: The fluid gravity flow deposits are commonly found in a tidally-influenced mudflat environment (Weimer et al., 1982). The presence of disarticulate *Ostrea glabra* indicates some transport; however, articulated shells do occur, and this implies short transport distances or in-growth preservation (Weimer et al., 1982; Bibler and Schmitt, 1986).

In addition, oysters live in brackish water settings (Feldmann and Palubniak, 1975). Burrow and root traces, brackish-water fauna, symmetric ripple cross-lamination (Srs), and laminated mudstones and sandstones (wavy, and wavy-flaser bedding) are indicative of an intertidal flat area of deposition (Weimer et al., 1982; Reading and Collinson, 1996). As seen in Figure 51, tidal mudflat lithofacies association is the most common of the associations found in the eastern facies. The stratigraphic placement of the eastern facies associations is represented in Figure 51.

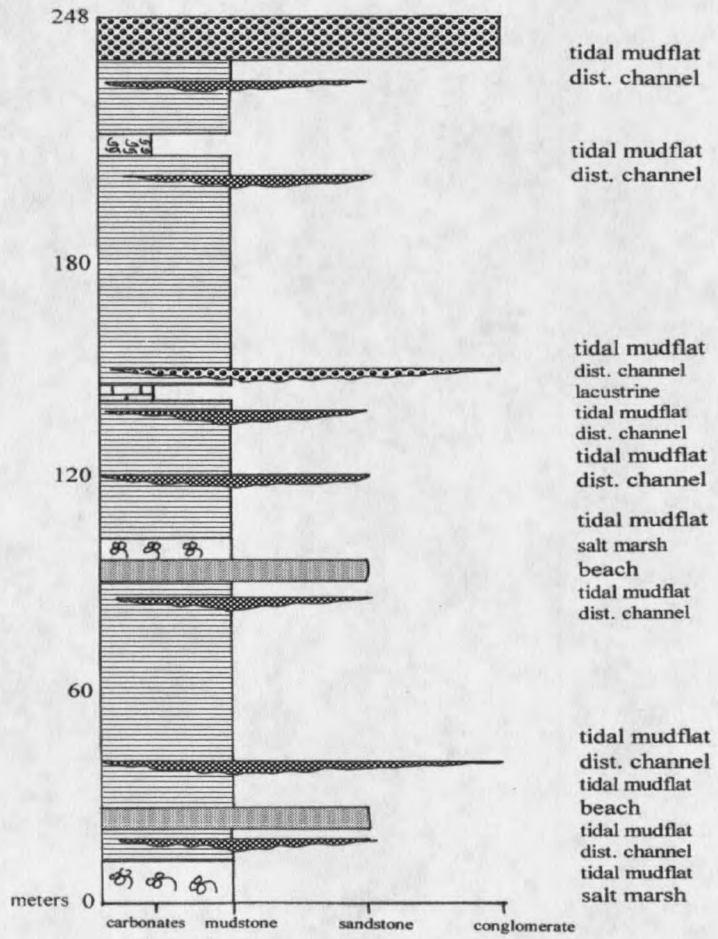


Figure 51: Schematic stratigraphic section of lithofacies associations found in the eastern facies. Data from RE-Kte and E2-Kte.

The deposition and transport of coarse, poorly sorted debris on the tidal flat are unusual occurrences, and rarely documented in the literature. The monolithologic, extremely coarse (boulder-sized) debris flow deposits of the eastern facies are comprised of Adel Mountain Volcanics clasts; this indicates a source to the east, rather than transport from the western facies, or the Elkhorn Mountains volcanic center. Additionally, the trachybasalt lava flow also must be derived generally from the east, as that is the only known location of trachybasalt.

PROVENANCE

In order to determine potential source areas for epiclastic material in the clastic sedimentary rocks and document the relative abundance of volcanic versus non-volcanic sediment, clast counts of conglomerate units and point counts of sandstone units were undertaken. Actual clast count and point count modal data are found in Appendices B, C, D, and E.

Conglomerate Composition

Clast counts were performed where coarse-grained deposits within the Two Medicine Formation were well-exposed; therefore, gravels transported by both debris flow and fluid gravity flow were counted. Five clast counts are from unit F of the western facies while only one is from a conglomerate in unit D. The lower eastern facies units lack well-exposed conglomerates; however, the uppermost section of the eastern facies is characterized by volcaniclastic breccias. Clasts in these were not counted due to their obvious monogenetic (trachybasalt) clast composition. Data are recorded in Appendix B, and histograms depicting relative modal percentages are in Appendix C.

Description

Conglomerates of the Two Medicine Formation are predominately sub-rounded to rounded, volcaniclastic-pebble to -boulder conglomerates. As platy or elongate clasts are rare

in the Two Medicine conglomerates, imbrication is uncommon. Clasts are typically volcaniclastic sandstone, undifferentiated volcanic rock (aphanitic, aphanitic-porphyritic), latite, trachyte, pumice, and mudstone. The volcaniclastic sandstone, latite, trachyte, and generic volcanic rock clasts are more durable than the pumice and mudstone clasts. Matrix is typically medium to very coarse sand, poorly sorted, and greenish in color due to alteration of volcanic rocks to chlorite and zeolites. Conglomerate framework is both clast- and matrix-supported. Clasts form lenticular and tabular beds 0.5 to 14 meters thick.

The volcaniclastic sandstone clasts are commonly sub-rounded to rounded, grey-green, poorly sorted, medium to coarse sand-size, and composed of aphanitic volcanic rock fragments and feldspar. In some instances, identification of volcanic rock clasts was restricted to the obvious phenocrysts in hand sample (i.e., plagioclase and pyroxene). Trachyte and latite clasts are sub-rounded and aphanitic-porphyritic. The latite was identified by a purple-grey color and large (1 cm) plagioclase phenocrysts, while trachyte clasts were identified by a light purple-grey color and bright green pyroxene phenocrysts. Pumice clasts are highly altered, rounded, green to whitish-green, friable, and usually in stringers at the top of conglomerate beds. Mudstone intraclasts form the base of many clast-supported conglomerates, and are usually angular or deformed.

Clast Composition Modes

Latite clasts are the dominant clast type for the unit D clast count, comprising almost two-thirds of the grains counted. The latite clasts are dominant in one outcrop of unit F; however, the occurrence of latite clasts decrease as trachyte clasts increase in abundance.

Trachyte (unit E) clasts are found only in unit F conglomerates, and increase in abundance upsection. Volcaniclastic sandstone clasts are present in every clast count, although in varying amounts. Pyroxene ± hornblende (mafic)- and feldspar-rich clasts are present in lithofacies Gt, Gcm, and Gmm, and although the clasts may be derived from other volcanic sources, they may actually be textural variations of the latite and trachyte lava flows. Pumice clasts are found in two units, S-F Gmm and Gt, and are abundant in S-F Gmm only. Mudstone clasts are uncommon, and are found in unit S-F Gcm. In unit S-F Gt, a single intrusive clast (diorite or granodiorite) was observed within a stream-laid conglomerate of unit F. Clasts grouped as "other" clasts were of unknown volcanic rock composition, some heavily altered to zeolite. The unidentifiable clasts may be altered rhyolitic clasts derived from the ash-flow tuffs of unit C. Rare boulder- and cobble-sized clasts of amphibolite and Cambrian Flathead Sandstone are found in an extensive breccia deposit of unit F, but the deposit was not included in a clast count due to poor exposure.

Sandstone Composition-Western Facies

Analysis of 13 western facies sandstones was necessary to determine the composition of sedimentary units, using approximately 300 point counts per thin section (Appendix D). The identified mineralogic content was then plotted on histograms to determine relative abundance of non-volcanic and volcanically derived grains (Appendix E). Figure 52 represents modal grain compositions for the western and eastern facies sandstones. Thin sections were chosen based on stratigraphic location; coverage of an entire unit was more desirable than repetitive counting of a single sandstone deposit.

Texture

Western facies sandstones are fine to very coarse-grained, very poorly sorted, and consist of angular to sub-rounded grains that in some examples appear to be floating, due to the amount of alteration. Other grain-to-grain contacts are concavo-convex, long, or tangential. Matrix is difficult to discern from the pervasive cement; however, hematite and clay typically form the matrix. The cement varies, and is most often clay, quartz, calcite, chlorite, zeolite, or some combination of these. Calcite typically replaces feldspar framework grains, although alteration varies from complete to slight. Volcanic rock fragments and feldspar grains are also altered to clay.

Framework Grains

Framework grains include monocrystalline quartz (Qm), feldspar (plagioclase (P) and potassium feldspar (K)), and lithic grains (primary volcanic rocks (Lv), pyroclastic rocks (Lp), and sedimentary rocks (Ls)). Point count data are presented on histograms illustrating the modal compositions for sandstones of the western facies (Appendix E). Framework grains were identified with petrographic microscope, and were counted as grains, rather than constituents.

Quartz, Monocrystalline (Qm): Monocrystalline quartz is rare to non-existent in western facies sandstones. Identified by lack of clay alteration, the few quartz grains counted had straight extinction, or were slightly undulatory.

Feldspar (F): Feldspar grains in the western facies are typically angular, broken, and altered to clay, calcite, chlorite, or zeolite. Perthitic textures are common, while microcline or tartan twinning is rare. Albite twinning is the most common, and may be found on simple twin planes. Feldspars are dominantly plagioclase, and are broken along cleavage planes. Thin sections were not stained for potassium feldspar. Rare potassium feldspar was identified by lack of albite twinning, and having clay, calcite, chlorite, or zeolite alteration, and possessing cleavage.

Lithic Fragments (Lv, Lp, Ls): Lithic fragments in the western facies sandstones include volcanic rock fragments that are aphanitic/porphyritic (Lv), pyroclastic rock fragments (Lp), and sedimentary rock fragments (Ls). Grains of volcanic rock (Lv) resemble latitic clasts; feldspathic groundmass encloses feldspar laths that may be altered to clay, calcite or chlorite, or may be completely unaltered. Other volcanic grains are wholly aphanitic. Pyroclastic rock fragments (Lp) include welded tuff, pumice, and glass particles that may be rounded to sub-angular, unaltered, or altered to clay, calcite, chlorite, zeolite, or varieties of quartz. Mudstone grains (Ls) are rounded or deformed around resistant grains.

Accessory Minerals: Other grains found in the sandstones include augite (M), biotite (Bi), muscovite (Mi), and opaque (D) minerals. Analcime (A) was observed, but rare. Augite, muscovite, and biotite are always broken, and in the case of the micas, deformed around more resistant grains. The accessory minerals are less likely to be found altered, though if alteration has occurred, augite was replaced by chlorite or calcite, and biotite was replaced by chlorite.

Sandstone Composition Modes

Point counts of 13 western facies sandstones plot on a Q-F-L ternary diagram in a generally linear cluster (Figure 52). Values were obtained from relative modal percentages of framework grains described previously. All of the western facies sandstones are low in quartz, and have moderate to low feldspar contents. Lithic grain content seems to be inversely related to feldspar content; otherwise, lithic grains are the most dominant in most of the western facies sandstones. Sandstone composition ranges from lithic arkoses (uncommon) to feldspathic litharenites (very common) and litharenites (common), using terminology from Folk (1970). The litharenites are primarily volcanic litharenites, as volcanic and pyroclastic lithic fragments (Lv, Lp) comprise the majority of lithic grains (Lv + Lp=90-95% of lithic grains). The litharenites completely lack quartz (Q=0%), and feldspars are only present in the 4-25% range. The feldspathic litharenites contain more feldspar than the litharenites (F=30-50%), and have a small quartz component that is monocrystalline (Qm=2-5%). The lithic fragments in the feldspathic litharenites are also dominantly volcanic (Lv) and pyroclastic (Lp) (Ls=4%). The single lithic arkose sample is feldspar-rich (F=64%), while quartz is lacking (Q=0%), and lithic fragments are solely volcanic (Lv=36%).

Sandstone Composition-Eastern Facies

Analysis of 15 sandstone thin sections from the eastern facies was performed in order to document compositional differences between the western and eastern facies sandstones, and to identify compositional variations within the eastern facies. Modal point count data are found in Appendix D, and histogram plots of the data are found in Appendix E.

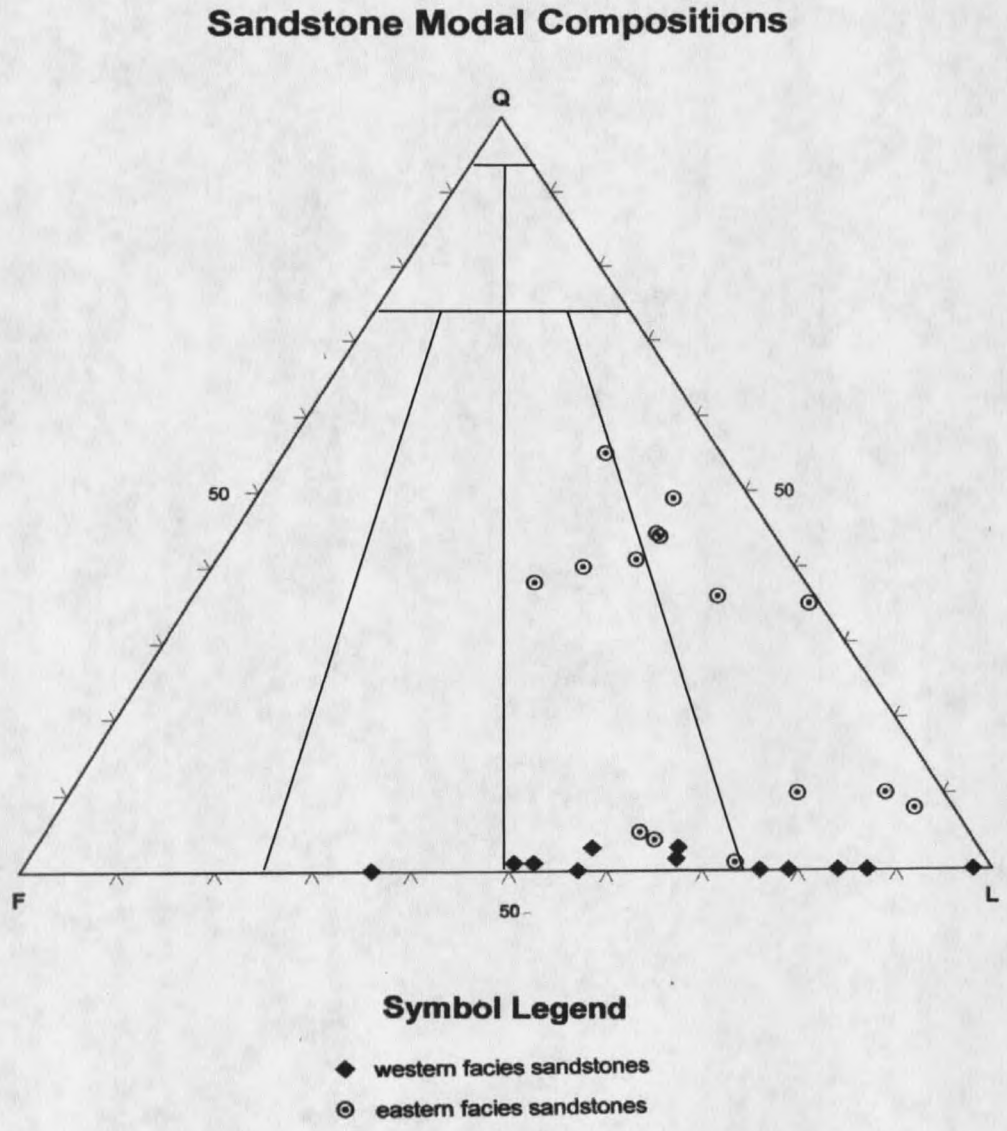


Figure 52: Ternary diagram of modal composition for western and eastern facies sandstones. Sandstone classification boundaries from Folk et al. (1970). Q= total quartz, F= total feldspar, and L= total lithics. See text for full discussion.

Texture

Eastern facies sandstones are very fine to very coarse-grained, very poorly to poorly sorted, and have angular to sub-rounded grains. Cementation may be by clay, quartz, zeolite, calcite, chlorite, glass, or a combination of these. Matrix may be clay or hematite. Grain contacts are tangential, floating, long, or concavo-convex. Calcite typically replaces feldspar grains; feldspar is recognized by calcite pseudomorphs, or by residual twinning evident in the grains.

Framework Grains

Framework grains were identified by petrographic microscope, and were counted as whole grains, rather than as constituents of a grain. Identified framework grains include monocrystalline (Qm) and polycrystalline (Qp) (chert and metasedimentary) quartz, feldspar grains (F), and lithic grains (Lv, Lp, Ls). Accessory grains were also identified, and are described herein.

Quartz, Monocrystalline (Qm): Monocrystalline quartz may be angular, broken, and shard-like (Q1), or sub-angular to sub-rounded (Q2). In a few examples, the quartz is volcanic; embayed edges are rounded and globular. Straight extinction characterizes both varieties of monocrystalline quartz, although slight undulatory extinction may be found. Rare to uncommon features include vacuoles and inclusions.

Quartz, Polycrystalline (Qp): Polycrystalline quartz includes both chert fragments and metasedimentary quartz. Polycrystalline quartz grains are typically rounded. Chert grains are microcrystalline quartz, and may be confused with zeolite or silica replacement of pumice grains. Metasedimentary quartz was recognized by sutured grain contacts.

Feldspar (F): Plagioclase feldspars are often broken along cleavage planes. Plagioclase feldspar grains were identified by albite and composite twinning. Rare examples of microcline and possible potassium feldspar were also observed. Thin sections were not stained, so potassium feldspar was identified by presence of cleavage and clay alteration. In some instances, plagioclase has been completely replaced by calcite or microquartz; chalcedony is often the cement in these examples. Alteration intensities for feldspars in the eastern facies are as varied as the western facies feldspars.

Lithic Fragments (Lv, Lp, Ls): Volcanic rock fragments (Lv) include aphanitic/porphyritic grains that are sub-rounded, and may be altered to clay or zeolites. Some may have also been replaced by calcite and chlorite. The groundmass is feldspathic, and visible phenocrysts are feldspar laths. The most abundant rock fragments are pyroclastic (Lp) (welded tuff, pumice, and ash). Alteration of pumice and ash is prevalent; calcite, chlorite, clay, and zeolites are the most common replacement minerals, with micro- and macroquartz rare. Unfortunately, it is difficult to discern the pumice and ash (glass) due to the severity of the alteration; the grains in the sandstone commonly appear to be "floating" rather than in grain-to-grain contact. Sedimentary lithic grains (Ls) are mudstone and are most often hematite stained and rounded, and deformed mudstone grains were also observed.

Accessory Minerals: Mafic grains (M) include augite and orthopyroxene that are typically equant, and may be broken. The augite is unaltered, twinned, and zoned, while the orthopyroxene is unaltered and untwinned. Other accessory minerals are biotite (Bi), muscovite (Mi), analcime (A), and opaques (D). Chlorite-based clays were also more prevalent in the eastern facies sandstones than the western facies.

Sandstone Composition Modes

Point counts of 15 eastern facies sandstones reveal two distinct composition clusters on a ternary diagram (See Figure 52). Relative percentages of modal composition for framework grains described above were plotted on a ternary diagram in order to compare composition of the eastern facies sandstones with the western facies sandstones. As seen from the diagram, less than half (six) of the point counted eastern facies sandstones plot with the western facies sandstones, although with a distinct increase in the quartz content (Qt=2-12%). The lower cluster is distinctly lithic-rich (Lt=60-90%), and has a moderate to low feldspar content (F=4-39%). The sandstones correspond with the feldspathic litharenites (F>25%) and volcanic litharenites of the western facies. Quartz in the sandstones includes chert and metasedimentary types (Qp). Chert and metasedimentary quartz are typically included in the lithic fragments total; however, in order to document a recycled origin for the eastern facies sandstones, all quartz was plotted together.

The upper cluster is well-distributed between lithic grains (Lt=40-65%) and quartz (Qt=35-42%), with a feldspar content that ranges from Ft=2-37%. The sandstones are also feldspathic litharenites and litharenites, although not as rich in volcanic rock fragments. Total

quartz is composed of both polycrystalline and monocrystalline quartz grains (Qp, Qm), with monocrystalline quartz commonly occurring in all sandstones (Qm=3-35%). Lithic fragments are more pyroclastic in origin than the western facies sandstones, and pyroclastic lithic fragments (Lp) are inversely related to the abundance of volcanic lithic grains (Lv).

Paleocurrents

Paleocurrent data are lacking from the western and eastern facies sandstones due to poor exposure, lack of three dimensional exposure, and incomplete exposure of cross-bed limbs. The paleocurrent indicators that were measured include trends of parting lineations from the eastern facies (measured section RE-Kte), and trough cross-stratification from sandstones in both facies. The parting lineations revealed a north-south trend for the beach sandstone measured, and the trends measured for the channel sandstones indicate an east-to-west direction of transport. The paleocurrent measurements are too few to be a statistically large enough representation of the transportation direction for the Two Medicine Formation, thus, they are not considered further.

Potential Sediment Source Areas

Conglomerate Sources

Based on relative percentages of clast composition, the latite lava flows (unit B) generated debris for coarse-grained volcaniclastic deposition throughout units D and F. Pumice clasts are present in several conglomerate units that are stratigraphically higher than unit C (ash-flow tuff unit). Pumice, although perhaps from the uppermost deposits of the ash-

flow tuffs of unit C, may have been from various sources; primary pumice may have been deposited as lapilli-fall and subsequently reworked, or may have been transported via rafting in the fluvial system.

Clast counts of coarse-grained deposits in the Two Medicine Formation reveal volcaniclastic sediments are predominant over non-volcaniclastic detritus. The lack of obvious thrust-derived clasts indicates volcanically-derived deposits overwhelmed the sedimentary basin. Volcanic debris may have been incorporated into thrust sheets; thus, the preponderance of volcaniclastic clasts in the Two Medicine Formation may disguise an actual thrust-sheet source. In addition, the observance of angular Flathead clasts in unit F may indicate nearby thrust activity (the Flathead clasts were boulder-size and angular) during deposition of the volcaniclastic conglomerates of unit F.

The roundness of the volcanic cobbles in the conglomerates of the Two Medicine Formation may imply long transport distances (Davies et al., 1979); however, others have determined that rounding in volcanic rock fragments (larger than granule size) may occur in short transport distances (Pearce, 1971). Abrasion of cobbles and boulders occurs by the transport of smaller detritus impacting the stationary larger clasts (Cameron and Blatt, 1971; Pearce, 1971). A transport distance of 2 miles was hypothesized as necessary for rounding of volcanic cobbles in the conglomerates of the Early Cretaceous Crowsnest Formation in Alberta, Canada (Pearce 1971). Climate is also considered to be an important factor in producing roundness; however, the climate in the Campanian of western Montana is not well known (Viele and Harris, 1965; Lorenz, 1981; Roberts and Kirschbaum, 1995). Resilicified volcanic rocks are considered to be durable, and less likely to chemically weather (Cameron

and Blatt, 1971; Abbot and Peterson, 1978). The clasts in this study were not evaluated petrographically; thus, it is difficult to determine if resilicification was a factor, if abrasion of the cobbles occurred, or if the clasts were actually transported long distances.

The latite and trachyte clasts are locally-derived from the erosion of the volcanic carapace that sourced the latite and trachyte lava flows. Pumice may be farther-traveled; a source from the Elkhorn Mountains volcanic center may be possible, or transport of pumice from the Sleeping Giant rhyodacitic volcanic center.

Western Facies Sandstone Sources

Point counts of western facies sandstones reflect the proximity of the western facies volcaniclastic deposits to a volcanic source. The abundance of rock fragments and "fresh" crystals (plagioclase, augite, biotite) in western facies sandstones indicates erosion from nearby sources; unaltered sand-size crystals indicate short residence times in fluvial systems (Self, 1975). The different alteration intensities among the plagioclase feldspars may be interpreted as representing various cycles of feldspar transport (Davies et al., 1979). Feldspar derived from a far source (the Elkhorn Mountains Volcanics) may have had more opportunities to be altered to clay and abraded. In addition, crystals may have been added to the fluvial system by ash-fall, which may also explain the occurrence of relatively fresh plagioclase feldspar with completely altered plagioclase. Pyroclastic fragments may be derived from erosion of the volcanic edifice at Sleeping Giant, or from the Elkhorn Mountains volcanic center. Latite and trachyte grains most likely represent erosion of the volcanic carapaces once around Wolf Creek.

Eastern Facies Sandstone Sources

Eastern facies sandstones are finer-grained than the western facies. Point-counted grain sizes range from very fine to very coarse sand, and samples are predominantly very fine- to fine-grained. Petrographic observations indicate a preponderance of pyroclastic and volcanic rock fragments in the coarse grain size, while quartz occurs mainly in the fine grain size samples. Chert is a component of the uppermost coarse-grained sandstones. Medium-grained sandstones have both abundant volcanic lithic fragments and quartz. As volcanic lithic fragments breakdown, their components would be considered "fine-grained"; thus, the very coarse samples may represent deposits of local volcanically-derived sediment, or sediment that was transported only short distances. The fine-grained samples would therefore be indicative of longer transport or more active, high energy transport, necessary for breakdown of volcanic fragments. Quartz, however, is found in angular and sub-rounded forms, and is not an abundant constituent of the primary volcanic rocks found in this setting. Based on the roundness of the pyroclastic rock fragments and common occurrence of hematite staining of the clasts, some transport and exposure occurred before deposition (Davies et al., 1979). Angular and shard-like quartz (Q2) is characteristic of ash-fall or impact shattering of quartz grains, while round quartz grains (Q1) are indicative of current transport (Viele and Harris, 1965). Rounded quartz grains may also be the result of magmatic resorption or multiple cycles of transport (Garzanti, 1986). Fresh and unaltered pyroxenes imply a single-cycle of transport (Davies et al., 1979). In addition, fresh pyroxene also indicates short residence time in the transport systems (Self, 1975); thus, the pyroxenes are likely derived from the nearby Adel Mountain volcanic field or from erosion of the Wolf Creek volcanic center. Compositional

comparisons between pyroxenes found in the Adel Mountain Volcanics and the western facies lava flows was not conducted, nor was it possible with petrographic microscope, as they are augite in both units. Chemical analysis would need to be conducted on the mineral grains.

The eastern facies sandstones likely had multiple sources. If time-correlative, the eastern facies sandstones may represent the distal deposits of the western facies braid-plain. Other sources of sand may include longshore current transport of grains along the coastal plain, or from erosion and reworking of the Adel Mountain volcanic rocks derived from the east. Rounded quartz grains may imply longshore current transport. Grains typically derived from unroofing of thrust sheets include chert, limestone, sandstone, quartzite, and metamorphic and igneous lithic grains and mineral constituents. The sandstones of the eastern facies have a small component of rounded chert, sandstone, mudstone, and metasedimentary quartz grains, in addition to rare occurrences of microcline (a plutonic feldspar). As the Sevier thrust belt was active during this time, it is possible that longshore currents transported durable grains from the actively eroding thrust-belt northward into western Montana. Concurrently, the Montana section of the Sevier thrust belt was actively shedding Paleozoic and Mesozoic strata into basins of southwestern Montana to form the Beaverhead Group (Wilson, 1970). It is also possible, therefore, that the sediments typically derived from unroofing of thrust sheets may be delivered by fluvial transport of debris from the west, rather than longshore current transport from the south. Finally, the volcanic grains have multiple source area possibilities. Pyroclastic lithic fragments may be derived from erosion of the rhyolitic-rhyodacitic volcanic carapace near Sleeping Giant, or the Elkhorn Mountains volcanic center. The volcanic rock fragments may be derived from the erosion of the latite and trachyte

volcanic carapaces of the western facies, or from the Adel Mountain volcanic center. For the latter, it would require erosion of earlier Adel Mountain volcanic rocks, since the sandstones are stratigraphically below the Adel Mountain Volcanics.

VOLCANIC ROCK SOURCE AREAS

Latite Lava Flows

A latite intrusion 0.10 miles north of Wolf Creek, Montana, is of the same chemical composition as the latite lava flows (Schmidt, 1978). Schmidt (1978), therefore, implies that the source for the latite lava flows in unit B is this latite intrusion; the latite lava flows also thin to the north, away from the intrusion. The latite intrudes the Telegraph Creek Formation, Virgelle Sandstone, and the sedimentary member and unit A of the Two Medicine Formation; the contact with the latite lava flows (unit B) is mapped as sharp (Schmidt, 1972a).

Rhyolite Ash-Flow Tuffs

Pyroclastic rocks (unit C) were deposited by eruption-induced flows and surges; air-fall deposits may be present but are poorly exposed. Deposits of unit C are laterally continuous, with abrupt variations in lithofacies visible in well-exposed outcrops. Pyroclastic deposits are preserved as pinching out tabular sheets ranging from 8 to 20 meters thick; unit C thins to the north (Schmidt, 1978). Schmidt (1978) identified five sheets in the southern exposures near Wolf Creek, three to four sheets above Rock Creek, and two to three sheets near Electric Mountain. Lithofacies and petrographic analyses in this study reveal two sheets in the northern section, four sheets in the central section, and three sheets in the incomplete southern section.

Information regarding the source areas for the pyroclastic rocks is sparse. Rhyolitic intrusives (sills and dikes) are found throughout the western facies; however, Schmidt (1978) has mapped these as Tertiary. Additionally, the rhyolite intrusives are compositionally dissimilar from the rhyolitic tuffs (Schmidt, 1978). The Elkhorn Mountains volcanic field to the southwest is interpreted as the source area for the rhyolite to rhyodacite tuffs found near Wolf Creek (Schmidt, 1978). Thrust faulting during Late Cretaceous-early Tertiary time shortened the actual distance between the Elkhorn Mountains Volcanics and Wolf Creek depositional area. Wolf Creek is presently 50 km from the northern part of the Elkhorn Mountains Volcanics. The original, restored distance may be on the order of 150 km. This greater distance may account for the thinness of the pyroclastic flows, the low abundance of pyroclastic surges, and thinning of the deposits to the north. Conversely, the source area may be directly to the south; the Sleeping Giant rhyodacite intrusion is approximately 17 km from the study area (Cannon et al., 1996). This may be the more likely source area; although, conclusive evidence would require chemical analysis of the intrusion and ash-flow tuffs to determine if they are similar.

Trachyte Lava Flows

The trachyte lava flows have a possible source area approximately one mile west of the latite intrusion. A trachyte intrusion is solely within the sedimentary rocks of unit D; Schmidt (1972a) has mapped trachyte dikes that are fed by the intrusion and truncated by the trachyte lava flows of unit E. Field and petrographic analyses reveal two lava flows at the southern and central stratigraphic sections, while the northern section contains only one flow; thus, the

trachyte lava flows thin to the north, away from the trachytic intrusion. Schmidt (1978) also states that the trachyte lava flows thin to the north, and describes the trachyte intrusion as a possible source for these flows.

Trachybasalt Coherent and Autobrecciated Lava Flows

The trachybasalt lava flow and associated autobrecciated flows found in the eastern facies are mapped as deposits of the Adel Mountain Volcanics (Lyons, 1944; Schmidt, 1978); however, Lyons (1944) and Schmidt (1978) describe these rocks as part of the volcanic breccia unit of the Adel Mountain Volcanics, which is the most voluminous of the Adel Mountain Volcanics rocks. The source area for lava flows of the Adel Mountain Volcanics is hypothesized to be the Three Sisters stock (vent) in sections 30, 31, 32, and 33 of T16N, R1W (Lyons, 1944). The Three Sisters stock is approximately 15 miles (24 km) from this study's eastern facies measured sections, and was determined to be the vent for the Adel Mountain Volcanics based on radiating dike patterns that emanate from the Three Sisters stock (Lyons, 1944).

DEPOSITIONAL SYSTEMS

Western Facies

Based on lithofacies associations, vertical stratigraphic profiles, and observed lateral relationships, the western facies of the Two Medicine Formation near Wolf Creek, Montana, is interpreted to be the deposit of a volcanically-influenced, possibly unconfined, sandy-gravel, braid-plain (Figure 53). The fluvial systems were characterized by in-channel gravel and sand dune migration, vertical accretion on extensive floodplains, and hyperconcentrated flow, debris flow, lava flow, and pyroclastic flow and surge occurring on floodplains and within channels.

Braid-Plain Deposits

As described in previous chapters, the western facies is comprised of poorly sorted, sub-angular to sub-rounded volcaniclastic channel-fill, and poorly sorted, volcaniclastic floodplain deposits. Thick, laterally continuous floodplain strata envelope tabular, coarse-grained sand and gravel channel-fill deposits. Episodic debris flow and hyperconcentrated flows contributed high concentrations of sediment to the fluvial systems, as evidenced in the common occurrence of matrix- and clast-supported, massive conglomerates (Gmm) intercalated with channel sandstones and overbank mudstones. Mud intraclasts form lags at the base of channel-fill deposits, and may imply that flashy, high discharge fluid gravity flow resulted in bank collapse, or channel scour on the floodplain (Lorenz, 1981; Suydam, 1988).

Vegetated floodplains are suggested by the abundance of root traces within floodplain mudstones. Floodplain deposits typically are overlain by channel sandstones or by floodplain-deposited debris flow and hyperconcentrated flow conglomerates. This implies that stable interchannel areas experienced periodic inundation from volcanic debris flow and hyperconcentrated flow.

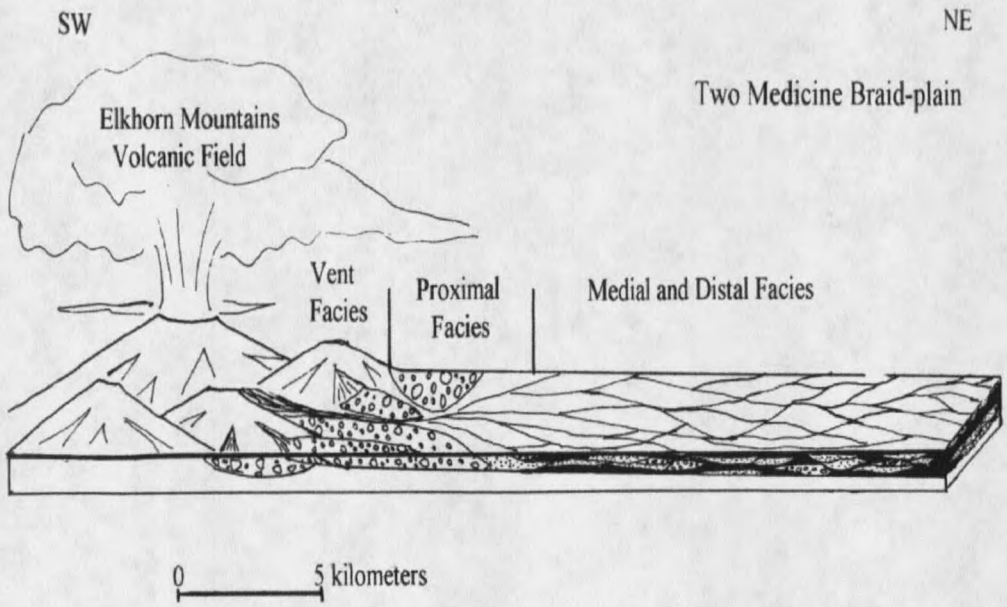


Figure 53: Schematic diagram illustrating the Two Medicine braid-plain, and associated volcanic facies related to the Elkhorn Mountains volcanic field. Note fining of units away from the source, and the geometry of the sandstone beds enveloped within floodplain mudstones in the braid-plain.

Depositional Model

Traditional braided stream facies models are based on modern braided streams which lack fine-grained sedimentation on adjacent floodplains (Miall, 1996). In contrast, the channel

deposits in the Two Medicine Formation near Wolf Creek, Montana, are tabular, coarse-grained, and very poorly sorted. The channel deposits lack lateral accretion surfaces, are laterally continuous for tens of meters, and are surrounded by floodplain deposits, which may imply rapid aggradation, high subsidence rates (to create accommodation space), and/or an unconfined braid-plain (Lorenz, 1981; Suydam, 1988; Bentham et al., 1993). With a volcanically-influenced fluvial system, the episodic and voluminous influx of detritus (syn-eruption) would result in high sedimentation rates; in fact, the actual cause for the preservation of the vertical accretion deposits may be high sedimentation rates (Smith, 1987a; Runkel, 1990). On an unconfined alluvial plain, the voluminous volcaniclastic debris would be reworked by braided streams during inter-eruption periods (Smith, 1987b; Orton, 1995). The channels of the Two Medicine Formation responded to the high sedimentation rates by reworking volcanic detritus (as evidenced by bimodal conglomerates), and depositing fine-grained sediment on floodplains during high discharge avulsion events.

Eastern Facies

Based on vertical stratigraphic profiles, lithofacies assemblages and associations, and lateral relations between lithofacies, the eastern facies of the Two Medicine Formation is interpreted to be representative of braid-delta deposition (Figure 54). Deposition occurred by vertical accretion on mudflats and marshes, sand and gravel dune migration within distributary channels, and debris flow, hyperconcentrated flow, lava flow, and autobrecciated flow on marshes, tidal mudflats, and in distributary channels.

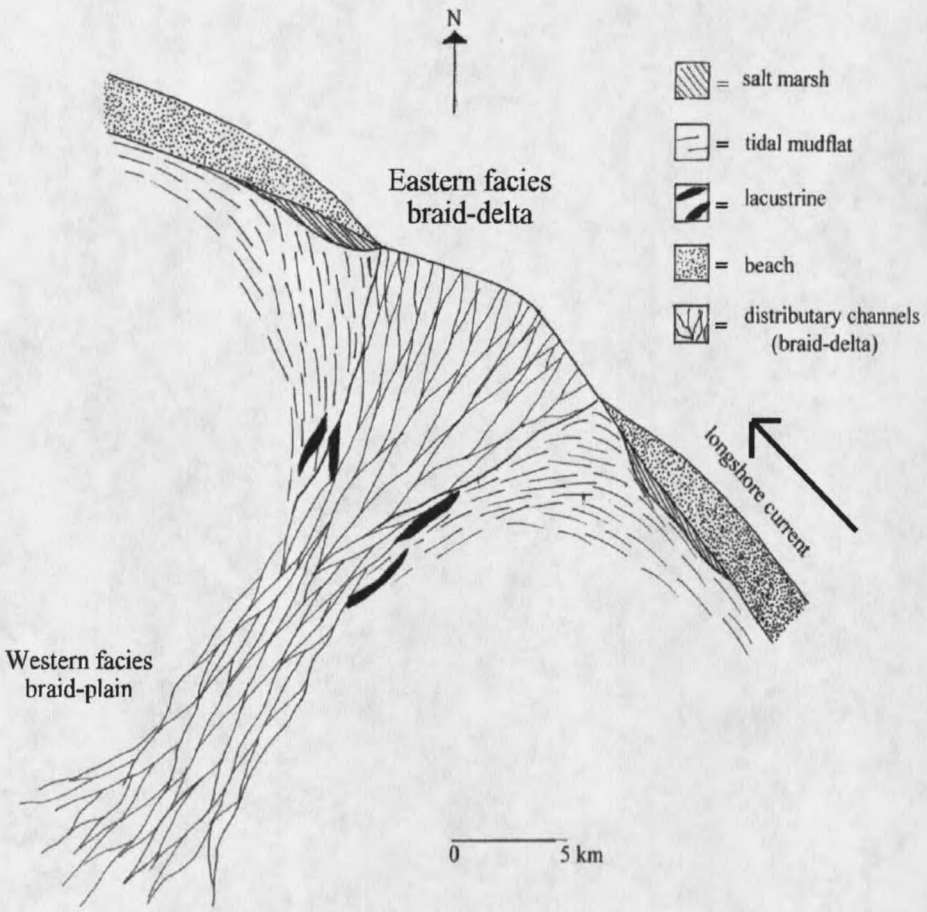


Figure 54: Schematic map-view diagram illustrating the proposed relationships between the lithofacies associations of the eastern facies, before eruption of the Adel Mountain volcanic field, approximately at 74 Ma. Volcaniclastic sediment that is fluvially transported to the Western Interior Cretaceous Seaway is interpreted to be derived from erosion of the Elkhorn Mountains and Wolf Creek volcanic fields to the southwest.

Braid-Delta Deposits

As with the western facies, episodic, volcanically-derived debris flow and hyperconcentrated flow periodically inundated the coastal plain, documented by the interfingering of matrix-supported, massive conglomerate (Gmm) with tidal mudflat sandstone

and mudstone. Laminated mud intraclasts are found at the bases of channel deposits, indicating erosion of the marsh by undercutting distributary channels (Dyer, 1994). Beach deposits are thin, lacustrine deposits are laterally discontinuous, and marsh deposits are underdeveloped. Distributary channel and tidal mudflat deposits are the primary units observed.

Depositional Model

The marsh, tidal mudflat, beach, distributary channel, and lacustrine deposits of the eastern facies are interpreted to be components of a braid-delta. This is due to the presence of braided channel facies (distributary channel and mudflat deposits), the lateral continuity of the deposits, the lack of boulder-sized clasts, and the association with a braid-plain to the west, which fulfill certain criteria of braid-deltas as defined by McPherson et al. (1987). McPherson et al. (1987), define fan-deltas as being very coarse-grained, having lenticular channel bodies, and being laterally discontinuous. Fan-deltas are characterized by debris flow and hyperconcentrated flow (McPherson, et al., 1987). However, the Two Medicine braid-delta experienced hyperconcentrated flow and debris flow, and yet maintains the original characteristics of the braid-delta as defined above. The differences between the Two Medicine braid-delta and the McPherson et al. (1987) model are due to the episodic and intense nature of volcanism, and the abundant debris volcanism produces, compared to typical fan-deltas which are formed as proximal highlands erode. In contrast, the uppermost eastern facies contains very coarse breccias of the Adel Mountain Volcanics. The breccia units are wedge-shaped and laterally discontinuous, and are interpreted to be the deposits of debris flows. The

debris flows were derived from the Adel Mountain volcanic center; therefore, transport was from the east-southeast. The breccia units found in the upper eastern facies are interpreted to have been deposited on a fan-delta that episodically interfingered with braid-delta deposits derived from the west (Figure 55).

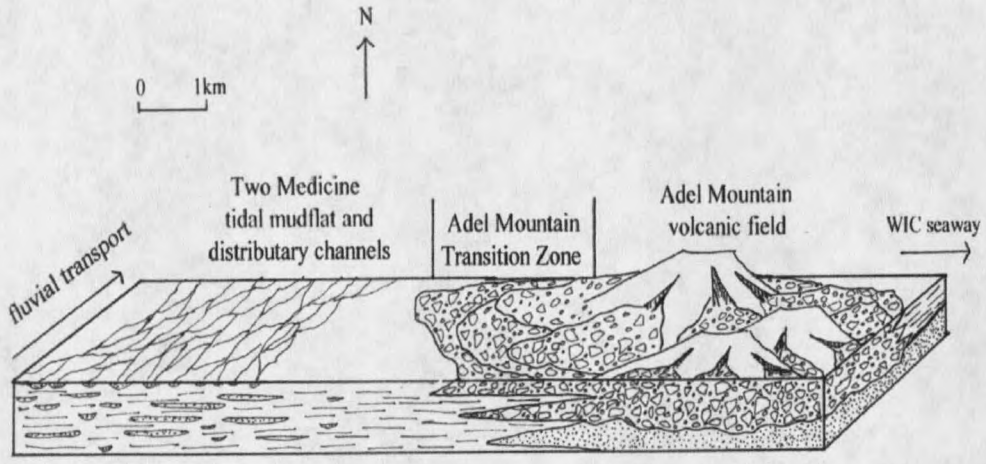


Figure 55: Schematic block diagram illustrating proposed relationships between the distributary channel, tidal mudflat, and beach lithofacies associations of the eastern facies after eruption of the Adel Mountain volcanic field, post-74 Ma. Braid-delta distributary channels were most likely diverted around the Adel Mountain volcanic field, thus, the Adel Mountain fan-delta interfingered with tidal mudflat deposits of the eastern facies. This is proposed to be representative of an Adel Mountain transition zone between the Two Medicine Formation and the Adel Mountain Volcanics.

The beach, marsh, and mudflat deposits may be interpreted as being the deposits of estuarine or lagoonal settings; however, evidence for drowned valleys or barrier islands is lacking (Bibler and Schmitt, 1986). The depositional environment was most likely influenced by the amount of sediment fed into the system, or how fluvially-influenced the braid-delta was

at a given time (Orton, 1988; Ballance, 1988). Rapid changes of depositional environment may have occurred, influenced by the amount of volcaniclastic sediment entering the system. Evidence for the addition of volcanically-derived detritus into the depositional system is found with sandstone point counts (see Figure 52). The eastern facies sandstones have both volcanic and non-volcanic sources. The eastern facies most likely received volcanic-rich sediment from the western facies braid-plain. During syn-eruptive episodes, debris flows and hyperconcentrated flows traveled down braided channels, and reached the coastline at the braid-delta. The volcaniclastic sedimentation from episodic debris flow and hyperconcentrated flow resulted in progradation of the braid-delta into the beach, tidal mudflat, and marsh settings. The deposition of voluminous volcanic debris produced rapid changes in depositional environments, indicated by the thinness of the beach deposits, lacustrine deposits produced by the ponding of water behind choked distributary channels, and by the decrease in marsh settings over time. In fact, when compared to equivalent Upper Cretaceous rocks, the Two Medicine Formation eastern facies most likely interfingers with at least two beach sandstones that have to be Horsethief Formation (Figure 56). The only other transgressive beach sandstone is the Parkman Formation, which in addition to not being exposed in this part of Montana, is also too low stratigraphically to be found in the eastern facies (See Figure 56). An example of fluvial influence on beach formation is found in the late Jurassic Huriwai delta, in New Zealand. The Huriwai Formation lacks beach facies, which Ballance (1988) attributes to the high occurrence of fluvial sedimentation derived from the denudation of a volcanic center. The beach facies in the Two Medicine Formation are thinner than normally observed, and this may be due to pulses of sustained volcanism.

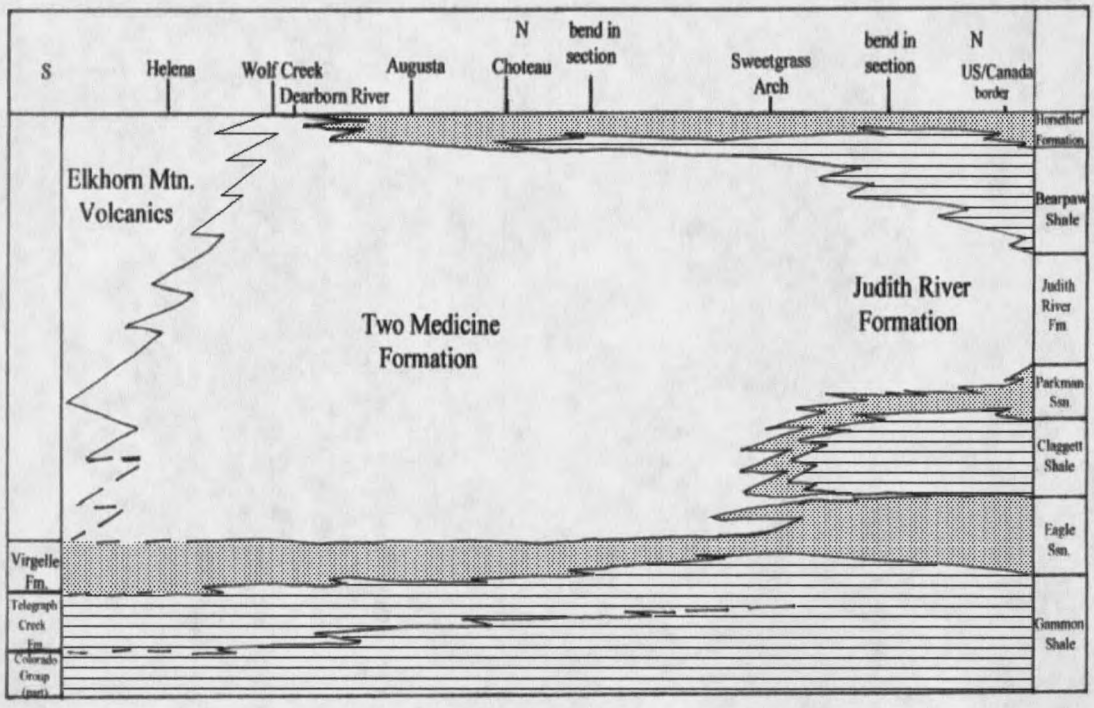


Figure 56: Schematic stratigraphic cross-section illustrating interfingering relationship between the Two Medicine Formation and equivalent Upper Cretaceous rocks in western, central, and northern Montana, and southern Alberta. See Figure 4 for cross-section information. Modified from Gill and Cobban (1973), Lorenz (1981), Rogers et al. (1993), and Rogers (1998).

DISCUSSION

The Campanian Two Medicine Formation near Wolf Creek, Montana, provides important insight into the development of the Sevier foreland basin and resultant paleogeography with respect to volcanic processes. As such, sedimentologic and stratigraphic data presented in this study, when associated and compared to correlative Late Cretaceous deposits, suggest depositional environments were highly varied regionally due to intermittent volcanism. In addition, volcanism may have increased aggradation rates across local basins, and resulted in varied fluvial responses during syneruptive and intereruptive periods.

Volcanic Influences on Sedimentation

Explosive and effusive volcanism resulted in sedimentary facies and deposits that are atypical for braided stream depositional sequences (Smith, 1987b; Waresback and Turbeville, 1990; Miall, 1996). Hyperconcentrated and debris flows provided sediment from distant and local sources, and dispersed this sediment into fluvial and coastal systems. The result of this episodic influx was choking of stream channels and increasing fluvial influence on coastal environments.

Choking of streams by pulses of sediment is typical in volcanic fluvial environments (for example, Smith, 1987a, b; Waresback and Turbeville, 1990; Riggs et al., 1997). Debris flows commonly experience flow transformation to hyperconcentrated flows as the debris flow encounters increasing amounts of water and attenuates (Smith, 1987a; Runkel, 1990).

Attenuation may also occur as the debris flows leave high gradient, proximal channels when they reach distal, lower gradient braid-plains and transform to hyperconcentrated flows (Smith, 1987a). Thick accumulations of hyperconcentrated flow deposits on floodplains indicate rapid aggradation rates due to the low preservation potential of floodplain deposits in an active braided channel system (Smith, 1987a; Smith, 1988b; Palmer, 1997). In addition, sheets of hyperconcentrated and debris flow deposits are indicative of syn-eruptive induced aggradation (Smith, 1988a). In western facies deposits, unit D commonly contains an abundance of hyperconcentrated flow deposits and minor debris flow deposits, while unit F is comprised of abundant debris flow deposits. Both units have hyperconcentrated and debris flow deposits in channel-fill and floodplain associations. Hyperconcentrated flow deposits preserved in channel-fill sequences indicates channel migration (Smith, 1987a). Paleosols are an indicator of sedimentation rates; neither unit D nor unit F display evidence of well-developed paleosols. For instance, unit D contains root traces in the exposed lower half, while unit F lacks any evidence for vegetation. Thick paleosols imply low sedimentation rates (Smith, 1987a); therefore, sedimentation increased as volcanism increased throughout the basin.

In addition to debris and hyperconcentrated flows affecting the morphology of braid plains, lava flows and ash flows also influenced sedimentation on the Two Medicine alluvial plain. Catastrophic influx of voluminous debris instantaneously alters the gradient, topography, and base level of the basin (Smith, 1988a; Riggs et al., 1997). The tabular geometry of the flows and their tapering to the north imply that the pre-eruption gradient was generally low. Viele and Harris (1965) and Schmidt (1978) report a thick accumulation of conglomerate (stream-laid) cut into the lava flows and pyroclastic flows of units B and C,

north of this study. Significantly, this implies erosion and downcutting of the fluvial systems into the lava and pyroclastic flows, which was not directly observed in the study area. However, point-counts of sandstones in units D and F indicate erosion of the volcanic highlands continued throughout deposition of fluvial sandstones.

Inter-eruption periods (terminology of Smith (1987a)) are identified by channels incised into lava, pyroclastic, debris, and hyperconcentrated flow deposits (Riggs et al., 1997). The implications are that streams attempt to return to the previous gradient, by incising channels into the volcanic rocks (Smith, 1987a, b; Waresback and Turbeville, 1990; Riggs et al., 1997). Additionally, fluvial channels rework deposits by transporting finer-grained material downstream, developing channel margins, and eroding less-consolidated volcanic debris (Smith, 1987b; Riggs et al., 1997). For this area, only once was a sedimentary deposit found atop a primary flow. Therefore, inter-eruption episodes are identified by fluid gravity flow deposits that may have debris and hyperconcentrated flow deposits intercalated within. However, it is possible that the hyperconcentrated flows and debris flows may be associated with eruptions upstream, and are not locally-derived (Smith, 1987b). In addition, inter-eruptive deposits are considered to be those that contain syn-orogenic grains from tectonically active environments (Riggs et al., 1997); however, it is possible that for this study area, syn-orogenic grains may actually be volcaniclastic due to the overwhelming of thrust sheets by volcanic debris, or the incorporation of volcanic detritus into thrust sheets.

The presence of thick floodplain deposits in the western facies of the Two Medicine Formation indicates rapid vertical accretion or aggradation due to normal or volcanism-induced flood events (Waresback and Turbeville, 1990; Palmer, 1997). Aggradation within

channels during syn-eruptive events may cause avulsion of channels onto the floodplain (Waresback and Turbeville, 1990; Palmer, 1997). When addition of voluminous volcanic detritus occurs concurrent with foredeep subsidence, the preservation of sediments is more likely (Lorenz, 1981).

For the eastern facies, the affect of volcanism on sedimentation is seen in the occurrence of volcaniclastic, fluvially-influenced braid-delta deposits interfingered with tidal mudflat and beach deposits. Fluvial deposits (distributary channels of the braid delta) were likely derived from the west, based on the abundant pyroclastic fragments, large feldspar crystals, and low quartz (monocrystalline, angular) content. Additionally, the point-counted samples for beach sandstones in the lowermost eastern facies exhibit compositions similar to the fluvial sandstones. This may be due to air-fall derived pyroclastic fragments being added to the nearshore environment. The uppermost eastern facies deposits sampled are tidal mudflat sandstones that are also pyroclastic-rich, and contain low amounts of rounded quartz grains and analcime crystals. This may reflect the addition of air-fall material to the low-energy mudflat environment. Analcime is found in the Adel Mountain Volcanics (Schmidt, 1978); however, small amounts are also found in the rhyolite-rhyodacite ash-flow tuffs of the western facies (Schmidt, 1978). Thus, analcime is not indicative of source.

As volcanism increased (whether from the east or west), it produced a prograding wedge of volcaniclastic material. The initial deposits of the eastern facies are marsh and beach deposits, possibly indicating a higher sea level (base level) than the later braid-delta deposits. The beach and marsh deposits are then overlain by tidal mudflat deposits, which may imply an increase in volcanic activity causing progradation of littoral sediments. Evidence for

progradation is found in sediment composition becoming increasingly pyroclastic and more coarse-grained upsection (Smith, 1987b, 1988b). Thus, during syn-eruption episodes, volcanism increased the fluvial influence on the coastal plain, producing a prograding braid delta (Orton, 1995). An increase in channel depth and width, and a decrease in sediment sorting indicate a fluvial system attempting to rework and attain grade after an eruption (Riggs et al., 1997). With a decrease in volcanism over time, the braid delta either migrated or the fluvial influence decreased sufficiently to allow the development of a tidal mudflat (Lorenz, 1981; Orton, 1995). During this seemingly quiescent period, the Adel Mountain volcanic field produced debris flow breccias that inundated the tidal mudflat from the east, incorporating oysters as clasts, and producing chaotic soft-sediment loading. Within the Adel Mountain Volcanics (further upsection), mudflat and channel deposits are intercalated with lava flows, autobrecciated flows, and debris flow deposits. The coastal plain deposits are laterally discontinuous, and appear to represent deposition in local paleotopographic low areas. The coastal plain, therefore, was affected by a west-facing volcaniclastic fan derived from erosion of the proximal Adel Mountain volcanic center, and by a volcanically-influenced braid-delta prograding to the east.

Tectonic Implications

During Late Cretaceous time, the Sevier fold-thrust belt was actively propagating eastward into its associated foreland basin. Synorogenic conglomerates and sandstones in alluvial fan settings are the characteristic deposits that demonstrate thrust belt movement (Pivnik, 1990). Shallow thrusts typically caused denudation of Paleozoic and Mesozoic strata.

The sediment derived from the uplifted areas was then transported and deposited into wedge-top and foredeep depozones (Lawton et al., 1997) (See Figure 1). The Sevier thrust belt extended from Nevada into Canada, and syn-orogenic conglomerates and sandstones are found along the length of the orogenic belt (Steidtmann and Schmitt, 1988); however, in western Montana, these synorogenic deposits are only found in the hinterland (Golden Spike Formation), or along reentrants (Beaverhead Group). This may be due to volcaniclastic processes being more dominant than tectonic processes.

The Elkhorn Mountains Volcanics and possible volcanic sources that have subsequently been eroded (Viele and Harris, 1965), were erupted along and within the thrust belt. Synchronous with volcanism, thrusting and folding occurred along the Sevier orogenic front to the north and south of the area now occupied by the Boulder batholith. Deposits in the volcanic member of the Two Medicine Formation near Wolf Creek, lack any identifiable syn-orogenic deposits. Debris flow and hyperconcentrated flow deposits of conglomerates and sandstones exist; however, as they are almost exclusively volcaniclastic, they are not derived from exhumed Paleozoic or early Mesozoic strata. These deposits are interpreted as representing episodes of slope failure on volcanic edifices, and are not orogenically produced.

The lack of identifiable syn-orogenic deposits does not preclude thrusting in this area at this time. Folding of foredeep deposits is evidenced in the disconformity between the Adel Mountain Volcanics and the Two Medicine Formation along the southwestern edge of the Adel Mountain volcanic field (Viele and Harris, 1965; Schmidt, 1978). The prodigious volume of volcanic material deposited in the Two Medicine Formation fluvial systems, in conjunction with the local magmatic intrusions, may have overwhelmed thrust sheets by mantling

topography, thereby, preventing denudation of thrust sheets. This would indicate that aggradation was volcanism-induced (Smith, 1987a). Conversely, thrusting may have produced erosion of uplifted volcanic material that was then transported and deposited into the foredeep. The appearance of quartzite boulders, an amphibolite cobble, and volcaniclastic sandstone pebbles and cobbles in the upper deposits of the Two Medicine Formation volcanic member may imply thrust activity, and most likely indicates uplift along the Steinbach thrust to the west late during Two Medicine deposition.

CONCLUSIONS

Sedimentologic and petrographic analyses of the Two Medicine Formation near Wolf Creek, Montana, suggest the following conclusions regarding the response of alluvial systems to intra-basinal explosive and effusive volcanism:

1) The western facies of the Campanian Two Medicine Formation was deposited by braided fluvial systems. Braided systems were characterized by interconnected channels that experienced episodic sedimentation associated with explosive volcanism, and normal streamflow processes (vertical accretion), producing tabular channel bodies within extensive floodplain deposits.

2) The eastern facies of the Campanian Two Medicine Formation was deposited by a braid-delta system. The braid-delta was characterized by braided distributary channels that experienced episodic avulsion associated with increased sedimentation from terrestrial volcanism, which resulted in tabular distributary channel bodies within tidal mudflat deposits. As volcanic eruptions declined, the dominance of the braid-delta decreased, resulting in the production of beach, marsh, and lacustrine deposits.

3) Lava flow, pyroclastic flow and surge, debris flow, and hyperconcentrated flow are found within channel deposits, and intercalated with floodplain deposits of the western facies, indicating that active volcanism within the retroarc foreland basin was concurrent with braid-plain sedimentation.

4) Fluvial channels responded to volcanism and volcanically-derived sedimentation events by reworking the debris and incising floodplain deposits in order to attain original grade.

5) Coastal plain response to volcanism and volcanically-produced sedimentation events (syn-eruption) was progradation of the braid-delta. Progradation occurred as pulses of debris flow and hyperconcentrated flow traveled down braided channels and reached the coastline, depositing coarse, poorly sorted material, and overwhelming normal coastal processes. During inter-eruptive events, distributary channels reworked debris. As volcaniclastic sedimentation declined, beach, marsh, and tidal mudflat environments were reestablished.

REFERENCES CITED

REFERENCES CITED

Abbott, P.L., and Peterson, G.L., 1978, Effects of abrasion durability on conglomerate clast populations: examples from Cretaceous and Eocene conglomerates of the San Diego area, California: Journal of Sedimentary Petrology, v. 48, n. 1, p., 31-42.

Allen, P.A., Collinson, J.D., 1986, Lakes: *in* H.G. Reading, ed., Sedimentary Environments and Facies, Blackwell Science, Oxford, p. 63-94.

Arguden, A.T., and Rodolfo, K.S., 1990, Sedimentologic and dynamic differences between hot and cold laharic debris flows of Mayon Volcano, Philippines: Geological Society of America Bulletin, v. 102, p. 865-876.

Ballance, P.F., 1988, The Huriwai braidplain delta of New Zealand: a late Jurassic, coarse-grained, volcanic-fed depositional system in a Gondwana forearc basin: *in* W. Nemec and R.J. Steel, eds., Fan Deltas: Sedimentology and Tectonic Settings, Blackie and Sons, Glasgow and London, p. 431-444.

Bentham, P.A., Talling, P.J., and Burbank, D.W., 1993, Braided stream and flood-plain deposition in a rapidly aggrading basin: the Escanilla Formation, Spanish Pyrenees: *in* J.L. Best and C.S. Bristow, eds., Braided Rivers, Geological Society Special Publication No. 75, p. 177-194.

Bibler, C.J., and Schmitt, J.G., 1986, Barrier-island coastline deposition and paleogeographic implications of the Upper Cretaceous Horsethief Formation, Northern Disturbed Belt, Montana: The Mountain Geologist, v. 23, n. 4, p. 113-127.

Blair, T.C., and McPherson, J.G., 1994, Alluvial fans and their natural distinction from rivers based on morphology, hydraulic processes, sedimentary processes, and facies assemblages: Journal of Sedimentary Research, v. A64, no. 3, p. 450-489.

Borrero P., C.A., and Naranjo H., J.L., 1990, Casabianca Formation: a Colombian example of volcanism-induced aggradation in a fluvial basin: Journal of Volcanology and Geothermal Research, v. 41, p. 253-267.

Buesch, D.C., 1991, Changes in depositional environments resulting from emplacement of a large-volume ignimbrite: in R.V. Fisher, and G.A. Smith, eds., Sedimentation in volcanic settings: Society of Economic Paleontologists and Mineralogists Special Publication, No. 45, p. 139-153.

Calvache, M.L.V., 1990, Pyroclastic deposits of the November 13, 1985 eruption of Nevado del Ruiz volcano, Colombia: Journal of Volcanology and Geothermal Research, v. 41, p. 67-78.

Cameron, K.L., Blatt, H., 1971, Durabilities of sand size schist and "volcanic" rock fragments during fluvial transport, Elk Creek, Black Hills, South Dakota: Journal of Sedimentary Petrology, v. 41, n. 2, p. 565-576.

Cannon, J.L., Thompson, G.G., and Warne, J.R., 1996, Second day river log: Boat trip from Upper Holter Lake through Gates of the Mountains: *in* E.J. Sterne and J.R. Warne, eds., Thrust Systems of the Helena Salient, Montana Thrust Belt, Rocky Mountain Section Field Trip #4, American Association of Petroleum Geologists Rocky Mountain Section Meeting, Billings, p. 45-49.

Carey, S.N., 1991, Transport and deposition of tephra by pyroclastic flows and surges: *in* R.V. Fisher and G.A. Smith, eds., Sedimentation in Volcanic Settings, Society of Economic Paleontologists and Mineralogists (Society for Sedimentary Geology) Special Publication, n. 45, p. 39-58.

Cas, R.A.F., and Wright, J.V., 1988, Volcanic Successions, Modern and Ancient, A geological approach to processes, products, and successions: Chapman and Hall, London, 528 p.

Chadwick, R.A., 1981, Chronology and structural setting of volcanism in southwestern and central Montana: Montana Geological Society Field Conference Southwest Montana, 1981, p. 301-310.

Christiansen, E.H., Kowallis, B.J., and Barton, M.D., 1994, Temporal and spatial distribution of volcanic ash in Mesozoic sedimentary rocks of the Western Interior: an alternative record of Mesozoic magmatism, *in* M.V. Caputo, J.A. Peterson, and K.J. Franczyk, eds., Mesozoic systems of the Rocky Mountain region, USA: Rocky Mountain Section, Society of Economic Paleontologists and Mineralogists, Denver, p. 73-94.

Cole, R.B., and Ridgeway, K.D., 1993, The influence of volcanism on fluvial depositional systems in a Cenozoic strike-slip basin, Denali fault system, Yukon Territory, Canada: Journal of Sedimentary Petrology, v. 63, no. 1, p. 152-166.

Collinson, J.D., 1986, Alluvial sediments: *in* H.G. Reading, ed., Sedimentary Environments and Facies, Blackwell Science, Oxford, p. 20-54.

Costa, J.E., 1988, Rheologic, geomorphic, and sedimentologic differentiation of water floods, hyperconcentrated flows, and debris flows: *in* V.R. Baker, R.C. Kochel, and P.C. Patton, eds., Flood Geomorphology, p. 113-122.

Cronin, S.J., Neall, V.E., Lecointre, J.A., and Palmer, A.S., 1997, Changes in Whangaehu river lahar characteristics during the 1995 eruption sequence, Ruapehu volcano, New Zealand: Journal of Volcanology and Geothermal Research, v. 76, p. 47-61.

Davies, D.K., Vessell, R.K., Miles, R.C., Foley, M.G., and Bonis, S.B., 1979, Fluvial transport and downstream sediment modifications in an active volcanic region: *in* A. Miall, ed., Fluvial Sedimentology, Society of Canadian Petrologists and Geologists Memoir, v. 5, p. 61-83.

DeCelles, P.G., and Giles, K.A., 1996, Foreland basin systems: Basin Research, v.8, p. 105-123.

Dickinson, W..R., 1974, Plate tectonics and sedimentation: *in* W.R. Dickinson, ed., Tectonics and Sedimentation: Society of Economic Paleontologists and Mineralogists Special Publication 22, p. 1-27.

Dyer, K.R., 1994, Estuarine sediment transport and deposition: *in*, K. Pye, ed., Sediment transport and depositional processes, Oxford, Blackwell Scientific Publications, p. 193-218.

Elder, W.P., 1988, Geometry of Upper Cretaceous bentonite beds: Implications about volcanic source areas and paleowind patterns, western interior, United States: Geology, v. 16, p. 835-838.

Feldmann, R.M., and Palubniak, D.S., 1975, Palaeoecology of Maestrichtian oyster assemblages in the Fox Hills Formation: *in* W.G.E. Caldwell, ed., The Cretaceous system in the western interior of North America, The Geological Association of Canada Special Paper No. 13, The proceedings of an international symposium organized by the Geological Association of Canada and held at the University of Saskatchewan in Saskatoon, May 23-26, 1973.

Fisher, R.V., 1971, Features of coarse-grained, high concentration fluids and their deposits: Journal of Sedimentary Petrology, v. 41, n. 4, p. 916-927.

Fisher, R.V., and Schmincke, H.-U., 1984, Pyroclastic rocks: Berlin, Springer-Verlag, 472p.

Fisher, R.V., and Smith, G.A., 1991, Volcanism, tectonics, and sedimentation: Sedimentation in Volcanic Settings, Society of Economic Paleontologists and Mineralogists Special Publication, No. 45, p. 1-5.

Fisher, R.V., and Schmincke, H.-U., 1994,Volcaniclastic sediment transport and deposition: *in* K. Pye, ed., Sediment transport and depositional processes, London, Blackwell Scientific Publications, p. 351-388.

Folk, R.L., Andrews, P.B., and Lewis, D.W., 1970,, Detrital sedimentary rock classification and nomenclature for use in New Zealand: New Zealand Journal of Geology and Geophysics, v. 13, fig. 8, p. 955, and fig. 9, p. 959.

Furnes, H., Sturt, B.A., 1976, Beach/shallow marine hyaloclastite deposits and their geological significance- an example from Gran Canaria: Journal of Geology, v. 84, p. 439-453.

Garzanti, E., 1986, Source rock versus sedimentary control on the mineralogy of deltaic volcanic arenites (Upper Triassic, northern Italy): Journal of Sedimentary Petrology, v. 56, n. 2, p. 267-275.

Gill, J.R., and Cobban, W.A., 1973, Stratigraphy and geologic history of the Montana Group and equivalent rocks, Montana, Wyoming, and North and South Dakota: United States Geological Survey Professional Paper 776, 37p.

Gunderson, J.A., and Sheriff, S.D., 1991, A new Late Cretaceous paleomagnetic pole from the Adel Mountain, west-central Montana: Journal of Geophysical Research, v. 96, no. B1, p. 317-326.

Gwinn, V.E., and Mutch, T.A., 1965, Intertongued Upper Cretaceous volcanic and nonvolcanic rocks, central-western Montana: Geological Society of America Bulletin, v. 76, p. 1125-1144.

Hackett, W.R., and Houghton, B.F., 1989, A facies model for a Quaternary andesitic composite volcano: Ruapehu, New Zealand: Bulletin of Volcanology, v. 51, p. 51-68.

Hamblin, A.P., 1997a, Stratigraphic architecture of the Oldman Formation, Belly River Group, surface and subsurface of southern Alberta: Bulletin of Canadian Petroleum Geology, v. 45, No. 2, p. 155-177.

Hamblin, A.P., 1997b, Regional distribution and dispersal of the Dinosaur Park Formation, Belly River Group, surface and subsurface of southern Alberta: Bulletin of Canadian Petroleum Geology, v. 45, No. 3, p. 377-399.

Hamblin, A.P., and Abrahamson, B.W., 1996, Stratigraphic architecture of "Basal Belly River" cycles, Foremost Formation, Belly River Group, subsurface of southern Alberta and southwestern Saskatchewan: Bulletin of Canadian Petroleum Geology, v. 44, No. 4, p. 654-673.

Harlan, S.S., Geissman, J.Wm., Lageson, D.L., and Snee, L.W., 1988, Paleomagnetic and isotopic dating of thrust-belt deformation along the eastern edge of the Helena salient, northern Crazy Mountains Basin, Montana: Geological Society of America Bulletin, v. 100, p. 492-499.

Harlan, S.S., Mehnert, H.H., Snee, L.W., and Meen, J.K., 1991, Preliminary isotopic (K-Ar and $^{40}Ar/^{39}Ar$) age determinations from selected Late Cretaceous and Tertiary igneous rocks in Montana: in D.W. Baker, and R.P. Berg, eds., Guidebook of the Central Montana Alkalic Province: Geology, ore deposits, and origin, Montana Bureau of Mines and Geology Special Publication 100, p. 136-137.

Harlan, S.S., Mehnert., H.H., Snee, L.W., Sheriff, S., and Schmidt, R.G., 1991, New $^{40}Ar/^{39}Ar$ isotopic dates from the Adel Mountain Volcanics: Implications for the relationship between deformation and magmatism in the Montana Disturbed Belt, western Montana: Geological Society of America Abstracts with Programs, v. 23, p. 136.

Harms, J.C., and Fahnestock, R.K., 1965, Stratification, bed forms, and flow phenomena (with an example from the Rio Grande): *in* G.V. Middleton, ed., Primary Sedimentary Structures and Their Hydrodynamic Interpretation, Society of Economic Paleontologists and Mineralogists Special Publication No. 12, p. 84-115.

Harms, J.C., Southard, J.B., and Walker, R.G., 1982, Structures and sequences in clastic rocks: Society of Economic Paleontologists and Mineralogists, Short Course No.9, Ch. 3, p. 1-51.

Hein, F.J., and Walker, R.G., 1977, Bar evolution and development of stratification in the gravelly, braided, Kicking Horse River, British Columbia: Canadian Journal of Earth Sciences, v. 14, p. 562-570.

Irving, A.J., and O'Brien, H.E., 1991, Isotopic and trace-element characteristics of Late Cretaceous to Oligocene mafic volcanics from west-central Montana: Implications for Tertiary tectonics and magma genesis: *in* D.W. Baker, and R.P. Berg, eds., Guidebook of the Central Montana Alkalic Province: Geology, ore deposits, and origin, Montana Bureau of Mines and Geology Special Publication 100, p. 140-142.

Ivy, S.D., 1989, Source, evolution, and eruptive history of the Cold Spring Creek Volcanics, Beaverhead County, Montana: Master's Thesis, Oregon State University, 132 p.

Jordan, T.E., 1995, Retroarc foreland and related basins, in C.J. Busby, and R.V. Ingersoll, eds., Tectonics of Sedimentary Basins: Blackwell Science, Cambridge, p. 331-362.

Klepper, M.R., Robinson, G.D., and Smedes, H.W., 1971, On the nature of the Boulder batholith of Montana: Geological Society of America Bulletin, v. 82, p. 1563-1580.

Kokelaar, P., 1986, Magma-water interactions in subaqueous and emergent basaltic volcanism: Bulletin of Volcanology, v. 48, p. 275-289.

Kuenzi, W.D., Horst, O.H., and McGehee, R.V., 1979, Effect of volcanic activity on fluvial-deltaic sedimentation in a modern arc-trench gap, southwestern Guatemala: Geological Society of America Bulletin, v. 90, p. 827-838.

Lorenz, J.C., 1981, Sedimentary and tectonic history of the Two Medicine Formation, Late Cretaceous (Campanian), northwestern Montana: unpublished Doctoral Dissertation, Princeton University, 215 p.

Lyons, J.B., 1944, Igneous rocks of the northern Big Belt range, Montana: Geological Society of America Bulletin, v. 55, p. 445-472.

Mackie, T.L., 1986, Tectonic influences on the petrology, stratigraphy and structures of the Upper Cretaceous Golden Spike Formation, central-western Montana: unpublished Master's Thesis, Washington State University, 132 p.

Mathisen, M.E., and Vondra, C.F., 1983, The fluvial and pyroclastic deposits of the Cagayan Basin, Northern Luzon, Philippines-an example of non-marine volcaniclastic sedimentation in an interarc basin: Sedimentology, v. 30, p. 369-392.

McCubbin, D.G., 1982, Barrier-island and strand-plain facies: *in* P.A. Scholle and D. Spearing, eds., Sandstone Depositional Environments, American Association of Petroleum Geologists Memoir 31, p. 247-280.

Miall, A.D., 1996, The geology of fluvial deposits: sedimentary facies, basin analysis, and petroleum geology: Berlin, Springer-Verlag, 582p.

Mudge, M.R., and Sheppard, R.A., 1968, Provenance of igneous rocks in Cretaceous conglomerates in northwestern Montana: United States Geological Survey Professional Paper 600-D, p. D137-D146.

Mudge, M.R., and Earhart, R.L., 1980, The Lewis thrust fault and related structures in the Disturbed Belt, northwestern Montana: United States Geological Survey Professional Paper 1174, 18 p.

Munoz, J.B., and Stern, C.R., 1989, Alkaline magmatism within the segment 38°-39°S of the Plio-Quaternary volcanic belt of the southern South American continental margin: Journal of Geophysical Research, v. 94, No. B4, p. 4545-4560.

Naranjo, J.A., and Francis, P., 1987, High velocity debris avalanche at Lastarria volcano in the north Chilean Andes: Bulletin of Volcanology, v. 49, p. 509-514.

O'Neill, J.M., Schmidt, C.J., and Genovese, P.W., 1990, Dillon cut-off--Basement-involved tectonic link between the disturbed belt of west-central Montana and the overthrust belt of extreme southwestern Montana: Geology, v. 18, p. 1107-1110.

Orton, G.J., 1988, A spectrum of Middle Ordovician fan deltas and braidplain deltas, North Wales: a consequence of varying fluvial clastic input: *in* W. Nemec and R.J. Steel, eds., Fan Deltas: Sedimentology and Tectonic Settings, Blackie and Sons, Glasgow and London, p. 23-49.

Orton, G.J., 1995, Facies models in volcanic terrains: time's arrow versus time's cycle: *in* A G. Plint, ed., Sedimentary Facies Analysis, A tribute to the research and teaching of Harold G. Reading, International Association of Sedimentologists Special Publications, v. 22, p. 157-193.

Orton, G.J., 1996, Volcanic environments: *in* H.G. Reading, ed., Sedimentary Environments: Processes, Facies, and Stratigraphy, p. 485-567.

Orton, G.J, and Reading, H.G., 1993, Variablility of deltaic processes in terms of sediment supply, with particular emphasis on grain size: Sedimentology, v. 40, p. 475-512.

Palmer, B.A., 1997, Sedimentary record of caldera-forming eruptions, Eocene Challis volcanic field, Idaho: Geological Society of America Bulletin, v. 109, no. 2, p. 242-252.

Palmer, B.A., and Shawkey, E.P., 1997, Lacustrine sedimentation processes and patterns during effusive and explosive volcanism, Challis volcanic field, Idaho: Journal of Sedimentary Research, v. 67, no. 1, p. 154-167.

Palmer, B.A., Purves, A.M., and Donoghue, S.L., 1993, Controls on accumulation of a volcaniclastic fan, Ruapehu composite volcano, New Zealand: Bulletin of Volcanology, v. 55, p. 176-189.

Pearce, T.H., 1971, Short distance fluvial rounding of volcanic detritus: Journal of Sedimentary Petrology, v. 41, n. 4, p. 1069-1072.

Peterson, J.A., 1981, General stratigraphy and regional paleostructure of the western Montana overthrust belt: Montana Geological Society Field Conference, Southwest Montana, 1981, p. 5-35.

Pierson, T.C., and Costa, J.E., 1987, A rheologic classification of subaerial sediment-water flows: Geological Society of America, Reviews in Engineering Geology, v. 7, p. 1-12.

Pierson, T.C., Janda, R.J., Thouret, J-C., and Borrero, C.A., 1990, Perturbation and melting of snow and ice by the 13 November 1985 eruption of Nevado del Ruiz, Colombia, and consequent mobilization, flow and deposition of lahars: Journal of Volcanology and Geothermal Research, v. 41, p. 17-66.

Punongbayan, R.S., Newhall, C.G., and Hoblitt, R.P., 1996, Photographic record of rapid geomorphic change at Mount Pinatubo, 1991-1994: *in* C.G. Newhall and R.S. Punongbayan, eds., Fire and Mud, Eruptions and Lahars of Mount Pinatubo, Philippines, Seattle and London, University of Washington Press, p. 21-66.

Reading, H.G., and Collinson, J.D., 1996, Clastic shorelines: *in* H.G. Reading, ed., Sedimentary Environments and Facies, 2nd edition, Blackwell Science, Oxford, p. .

Ricketts, B.D., 1985, Volcanic breccias in the Isachsen Formation near Strand Fiord, Axel Heiberg Island, District of Franklin: Geological Survey of Canada Current Research Part A 85-1A, p. 609-612.

Riggs, N.R., Hurlbert, J.C., Schroeder, T.J., and Ward, S.A., 1997, The interaction of volcanism and sedimentation in the proximal areas of a mid-Tertiary volcanic dome field, central Arizona, U.S.A.: Journal of Sedimentary Research, v. 67, no. 1, p. 142-153.

Roberts, A.E., 1963, The Livingston Group of south-central Montana: United States Geological Survey Professional Paper 475-B, p. B86-B92.

Roberts, L.N.R-, and Kirschbaum, M.A., 1995, Paleogeography of the Late Cretaceous of the Western Interior of middle North America- coal distribution and sediment accumulation: United States Geological Survey Professional Paper 1561, 115 p.

Robinson, G.D., and Marvin, R.F., 1967, Upper Cretaceous volcanic glass from western Montana: Geological Society of America Bulletin, v. 78, p. 601-608.

Rodolfo, K.S., 1989, Origin and early evolution of lahar channel at Mabinit, Mayon Volcano, Philippines: Geological Society of America Bulletin, v. 101, p. 414-426.

Rogers, R.R., 1998, Sequence analysis of the Upper Cretaceous Two Medicine and Judith River Formations, Montana: non-marine response to the Claggett and Bearpaw marine cycles: Journal of Sedimentary Research, v. 68, no. 4, p. 615-632.

Rogers, R.R., Swisher, C.C., and Horner, J.R., 1993, Ar/Ar age and correlation of the non-marine Two Medicine Formation (Upper Cretaceous), northwestern Montana, U.S.A.: Canadian Journal of Earth Sciences, v. 30, p. 1066-1075.

Roobol, M.J., Smith, A.L., and Wright, J.V., 1987, Lithic breccias in pyroclastic flow deposits on St. Kitts, West Indies: Bulletin of Volcanology, v. 49, p. 694-707.

Ross, C.S., and Smith, R.L., 1961, Ash-flow tuffs: their origin, geologic relations, and identification: United States Geological Survey Professional Paper 366, 81p.

Rowley, P.D., MacLeod, N.S., Kuntz, M.A., and Kaplan, A.M., 1985, Proximal bedded deposits related to pyroclastic flows of May 18, 1980, Mount St. Helens, Washington: Geological Society of America Bulletin, v. 96, p. 1373-1383.

Runkel, A.C., 1990, Lateral and temporal changes in volcanogenic sedimentation: Analysis of two Eocene sedimentary aprons, Big Bend region, Texas: Journal of Sedimentary Petrology, v. 60, no. 5, p. 747-760.

Schmidt, R.G., 1972a, Geologic map of the Wolf Creek quadrangle, Lewis and Clark County, Montana: United States Geological Survey Geologic Quadrangle Map GQ-974.

Schmidt, R.G., 1972b, Geologic map of the Coburn Mountain quadrangle, Lewis and Clark and Cascade Counties, Montana: United States Geological Survey Geologic Quadrangle Map GQ-975.

Schmidt, R.G., 1978, Rocks and mineral resources of the Wolf Creek Area, Lewis and Clark and Cascade Counties, Montana: United States Geological Survey Bulletin 1441, 91 p.

Schmidt, R.G., and Zubovic, 1961, Cobern Mountain overthrust, Lewis and Clark County, Montana: United States Geological Survey Research Short Papers 211, p. C-175-177.

Schmitt, J.G., and Steidtmann, J.R., 1990, Interior ramp-supported uplifts: Implications for sediment provenance in foreland basins: Geological Society of America Bulletin, v. 102, p. 494-501.

Self, R.P., 1975, Petrologic changes in fluvial sediments in the Rio Nautla drainage basin, Veracruz, Mexico: Journal of Sedimentary Petrology, v. 45, n. 1, p. 140-149.

Sheriff, S.D., and Gunderson, J.A., 1990, Age of the Adel Mountain volcanic field, west-central Montana: ISOCHRON/WEST, no. 56, p. 21-23.

Shultz, A.W., 1984, Sub-aerial debris flow deposition in the Upper Paleozoic Cutler Formation, western Colorado: Journal of Sedimentary Petrology, v. 54, n. 3, p. 759-772.

Skipp, B. and McGrew, L.W., 1977, The Maudlow and Sedan Formations of the Upper Cretaceous Livingston Group on the west edge of the Crazy Mountains Basin, Montana: United States Geological Survey Bulletin 1422-B, 68 p.

Smedes, H.W., 1966, Geology and igneous petrology of the Northern Elkhorn Mountains, Jefferson and Broadwater Counties, Montana: United States Geological Survey Professional Paper 510, 116p.

Smith, G.A., 1986, Coarse-grained nonmarine volcaniclastic sediment: Terminology and depositional process: Geological Society of America Bulletin, v.97, p. 1-10.

Smith, G.A., 1987a, Sedimentology of volcanism-induced aggradation in fluvial basins: Examples from the Pacific Northwest, U.S.A.: *in* F. G. Ethridge, R.M. Flores, and M.D. Harvey, eds., Recent Developments in Fluvial Sedimentology, Contributions from the Third International Fluvial Sedimentology Conference, Society of Economic Paleontologists and Mineralogists Special Publication, No. 39, p. 217-228.

Smith, G.A., 1987b, The influence of explosive volcanism on fluvial sedimentation: The Deschutes Formation (Neogene) in central Oregon: Journal of Sedimentary Petrology, v. 57, no. 4, p. 613-629.

Smith, G.A., 1988a, Neogene synvolcanic and syntectonic sedimentation in central Washington: Geological Society of America Bulletin, v. 100, p. 1479-1492.

Smith, G.A., 1988b, Sedimentology of proximal to distal volcaniclastics dispersed across an active foldbelt: Ellensburg Formation (late Miocene), central Washington: Sedimentology, v. 35, p. 953-977.

Smith, G.A., 1991, Facies sequences and geometries in continental volcaniclastic sediments: *in* R.V. Fisher, and G.A. Smith, eds., Sedimentation in volcanic settings, Society of Economic Paleontologists and Mineralogists Special Publication, No. 45, p. 109-121.

Smith, G.A., and Lowe, D.R., 1991, Lahars: Volcano-hydrologic events and deposition in the debris flow- hyperconcentrated flow continuum: *in* R.V. Fisher, and G.A. Smith, eds., Sedimentation in volcanic settings, Society of Economic Paleontologists and Mineralogists Special Publication, No. 45, p. 59-70.

Smith, R.C.M., 1991, Landscape response to a major ignimbrite eruption, Taupo volcanic center, New Zealand: *in* R.V. Fisher, and G.A. Smith, eds., Sedimentation in volcanic settings: Society of Economic Paleontologists and Mineralogists Special Publication, No. 45, p. 123-137.

Sparks, R.S.J., 1976, Grain size variations in ignimbrites and implications for the transport of pyroclastic flows: Sedimentology, v. 23, p. 147-188.

Suydam, J.D., 1988, Sedimentology, provenance, and paleotectonic significance of the Cretaceous Newark Canyon Formation, Cortez Mountains, Nevada: unpublished Master's Thesis, Montana State University, 90 p.

Thouret, J-C., Salinas, R., and Murcia, A., 1990, Eruption and mass-wasting-induced processes during the late Holocene destructive phase of Nevado del Ruiz volcano, Colombia: Journal of Volcanology and Geothermal Research, v. 41, p. 203-224.

Tilling, R.I., 1974, Composition and time relations of plutonic and associated volcanic rocks, Boulder batholith region, Montana: Geological Society of America Bulletin, v. 85, p. 1925-1930.

Todd, S.P., 1989, Stream-driven, high-density, gravelly traction carpets: possible deposits in the Trabeg Conglomerate Formation, SW Ireland and some theoretical considerations of their origin: Sedimentology, v. 36, p. 513-530.

Turbeville, B.N., Waresback, D.B., and Self, S., 1989, Lava-dome growth and explosive volcanism in the Jemez Mountains, New Mexico: Evidence from the Plio-Pleistocene Puye alluvial fan: Journal of Volcanology and Geothermal Research, v. 36, p. 267-291.

Valentine, G.A., Palladino, D.M., Agosta, E., Taddeucci, J., and Trigila, R., 1998, Volcaniclastic aggradation in a semiarid environment, northwestern Vulcano Island, Italy: Geological Society of America Bulletin, v. 110, no. 5, p. 630-643.

Vessel, R.K., and Davies, D.K., 1981, Nonmarine sedimentation in an active fore arc basin: in F.G. Ethridge and R.M. Flores, eds., Recent and ancient nonmarine depositional environments: models for exploration: Society of Economic Paleontologists and Mineralogists Special Publication 31, p. 31-45.

Viele, G.W., and Harris, F.G., III, 1965, Montana Group stratigraphy, Lewis and Clark County, Montana: American Association of Petroleum Geologists Bulletin, v. 49, n. 4, p. 379-417.

Wallace, C.A., Lidke, D.J., and Schmidt, R.G., 1990, Faults of the central part of the Lewis and Clark line and fragmentation of the Late Cretaceous foreland basin in west-central Montana: Geological Society of America Bulletin, v. 102, p. 1021-1037.

Walton, A.W., 1986, Effect of Oligocene volcanism on sedimentation in the Trans-Pecos volcanic field of Texas: Geological Society of America Bulletin, v. 97, p. 1192-1207.

Walton, A.W., and Palmer, B.A., 1988, Lahar facies of the Mount Dutton Formation (Oligocene-Miocene) in the Marysvale Volcanic Field, southwestern Utah: Geological Society of America Bulletin, v. 100, p. 1078-1091.

Waresback, D.B., and Turbeville, B.N., 1990, Evolution of a Plio-Pleistocene volcanogenic-alluvial fan: The Puye Formation, Jemez Mountains, New Mexico: Geological Society of America Bulletin, v. 102, p. 298-314.

Weimer, R.J., and Land, C.B., 1975, Maestrichtian deltaic and interdeltaic sedimentation in the Rocky Mountain region of the United States: *in* W.G.E. Caldwell, ed., The Cretaceous system in the western interior of North America, The Geological Association of Canada Special Paper No. 13, The proceedings of an international symposium organized by the Geological Association of Canada and held at the University of Saskatchewan in Saskatoon, May 23-26, 1973, p. 633-666.

Weimer, R.J., Howard, J.D., and Lindsay, D.R., 1982, Tidal flats: *in* P.A. Scholle and D. Spearing, eds., Sandstone Depositional Environments, American Association of Petroleum Geologists Memoir 31, p. 191-246.

White, J.D.L., 1991, The depositional record of small, monogenetic volcanoes within terrestrial basins: in R.V. Fisher, and G.A. Smith, eds., Sedimentation in volcanic settings: Society of Economic Paleontologists and Mineralogists Special Publication, No. 45, p. 155-171.

White, J.D.L., 1996, Pre-emergent construction of a lacustrine basaltic volcano, Pahvant Butte, Utah (USA): Bulletin of Volcanology, v. 58, p. 249-262.

Williams, P.F., and Rust, B.R., 1969, The sedimentology of a braided river: Journal of Sedimentary Petrology, v. 39, p. 649-679.

Wilson, M.D., 1970, Upper Cretaceous-Paleocene synorogenic conglomerates of southwestern Montana: American Association of Petroleum Geologists Bulletin, v. 54, no. 10, p. 1843-1867.

Woodward, L.A., 1981, Tectonic framework of disturbed belt of west-central Montana: American Association of Petroleum Geologists Bulletin, v. 65, p. 291-302.

APPENDICES

APPENDIX A

LOCATIONS OF STRATIGRAPHIC SECTIONS

APPENDIX A: Detailed stratigraphic section locations for the area north of Wolf Creek, Montana (centered around Rock Creek), and the area north of the Dearborn River off of Highway 287.

1. Western facies, northern stratigraphic section: Using Wolf Creek Quadrangle map, begin at northern base of the peak just southeast of Electric Mountain in NW ¼, NW ¼, NE ¼, SW ¼, sec. 34, T16N, R4W. Continues perpendicular to strike to Dry Creek drainage. Moves southeast along drainage approximately 40 meters. Continues up outcrop, still perpendicular to strike towards the prominent peak at 4634 ft on map. Now move to the southeast along the rim to SE ¼, NW ¼, NE ¼, NE ¼, sec. 4, T15N, R4W. Continue perpendicular to strike down towards the Rock Creek drainage. Section ends at SW ¼, SW ¼, SE ¼, NE ¼, sec. 4, T15N, R4W.

2. Western facies, central stratigraphic section: Using the Wolf Creek Quadrangle map, begin at NW ¼, SE ¼, SE ¼, SE ¼, sec. 14, T15N, R4W. Continues in a southwesterly step perpendicular to strike to the ridge top located at SE ¼, SE ¼, SW ¼, SE ¼, sec. 14, T15N, R4W. Moves directly downslope, perpendicular to strike towards the reservoir. Continues directly north approximately 500 meters, then across the Dry Creek drainage. Begins again at the NW ¼, NW ¼, SE ¼, NW ¼, sec. 14, T15N, R4W. Continues for 25 meters perpendicular to strike, then moves laterally 50 meters directly north along strike. Now in the NW ¼, SE ¼, NW ¼, NW ¼, sec. 14, T15N, R4W. Continues perpendicular to strike up to ridge crest, and then moves laterally south to SE ¼, NE ¼, SW ¼, NW ¼, sec. 14, T15N, R4W. Continues perpendicular to strike directly downslope into the Rock Creek drainage. Section ends at NW ¼, SW ¼, SW ¼, NW ¼, sec. 14, T15N, R4W.

3. Western facies, southern stratigraphic section: Using the Wolf Creek Quadrangle map, begin at SW ¼, SW ¼, SE ¼, SW ¼, sec. 23, T15N, R4W. Continues perpendicular to strike up the ridge to elevation 4916 ft. Moves perpendicular to strike downslope, towards unnamed drainage. Moves northeast along drainage 25 meters. Begins again at the NE ¼, SE ¼, SW ¼, NE ¼, sec. 22, T15N, R4W. Moves upslope, perpendicular to strike to elevation 4506 ft. Moves laterally southwest along the ridge for 500 meters. Begins again at SE ¼, NW ¼, SE ¼, NW ¼, sec. 22, T15N, R4W. Continues downslope, perpendicular to strike in a northeasterly direction. Follows second drainage from the bottom to the northeast for 600 meters. Begins again at SE ¼, NE ¼, NW ¼, SE ¼, sec. 15, T15N, R4W. Moves perpendicular to strike to NW ¼, NE ¼, NW ¼, SE ¼, sec. 15, T15N, R4W. Then moves laterally along strike to the southwest, along the anticlinal trend, to NE ¼, SW ¼, NE ¼, SW ¼, sec. 15, T15N, R4W, where it ends.

APPENDIX A, Continued:

4. Eastern facies, stratigraphic section RE-Kte: Using the Coburn Mountain Quadrangle map, begin at SE ¼, NE ¼, SW ¼, NE ¼, sec. 27, T17N, R4W. Continue perpendicular to strike in an east-northeast direction. Move laterally to SW ¼, NE ¼, SE ¼, NE ¼, sec. 27, T17N, R4W. Continue perpendicular to strike. Move laterally to SE ¼, SW ¼, NW ¼, SW ¼, sec. 26, T17N, R4W. Continue perpendicular to strike to base of Adel Mountain Volcanics (Elephant Mountain). Move laterally to SW ¼, NW ¼, NW ¼, NW ¼, sec. 26, T17N, R4W. Continue perpendicular to strike up into the narrow canyon. Section ends at SW ¼, NE ¼, NW ¼, NW ¼, sec. 26, T17N, R4W.

5. Eastern facies, stratigraphic section E2-Kte: Using the Coburn Mountain Quadrangle map, begin at the SE ¼, SE ¼, SW ¼, NE ¼, sec. 27, T17N, R4W. Continue perpendicular to strike, laterally moving along the drainage to NE ¼, SE ¼, SE ¼, SE ¼, sec. 22, T17N, R4W. Continue upslope perpendicular to strike to large outcrops of NW ¼, NE ¼, SE ¼, SE ¼, sec. 22, T17N, R4W. Section ends there.

APPENDIX B

CLAST-COUNT DATA

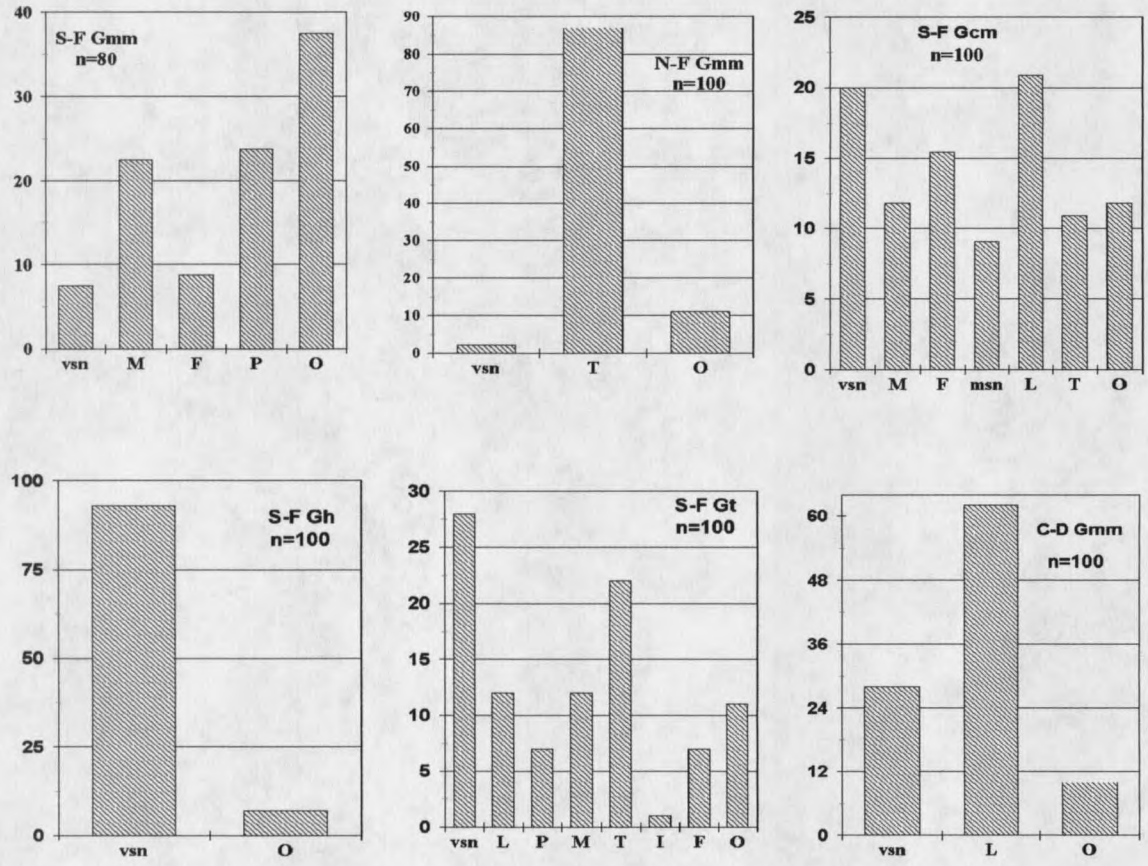
APPENDIX B: Table 2. Clast-count data from Two Medicine Formation conglomerates. Sample number refers to stratigraphic section location, unit, and lithofacies type. VSS = volcaniclastic sandstone clasts, latite = latite lava flow clasts, trach = trachyte lava flow clasts, MSN = mudstone clasts, INT = plutonic clasts, PUM = pumice clasts, FELD = feldspar-rich clasts, MAF = mafic-rich clasts, and other = unidentifiable clasts.

Sample	n	VSS	Latite	Trach.	MSN	INT	PUM	FELD	MAF	Other
C-D Gmm	100	28	62	0	0	0	0	0	0	10
S-F Gt	88	28	12	22	0	1	7	7	0	11
S-F Gcm	110	22	23	12	10	0	0	17	13	13
S-F Gmm	80	6	0	0	0	0	19	7	18	30
S-F Gh	100	93	0	0	0	0	0	0	0	7
N-F Gmm	100	2	0	87	0	0	0	0	0	11

APPENDIX C

HISTOGRAM PLOTS OF CLAST-COUNT DATA

APPENDIX C: Histogram plots of relative percentages for clast composition in conglomerates of the western facies of the Two Medicine Formation. Sample number refers to stratigraphic section location, unit, and lithofacies type. VSS = volcaniclastic sandstone clasts, latite = latite lava flow clasts, trach = trachyte lava flow clasts, MSN = mudstone clasts, INT = plutonic clasts, PUM = pumice clasts, FELD = feldspar-rich clasts, MAF = mafic-rich clasts, and other = unidentifiable clasts.



APPENDIX D

POINT-COUNT DATA

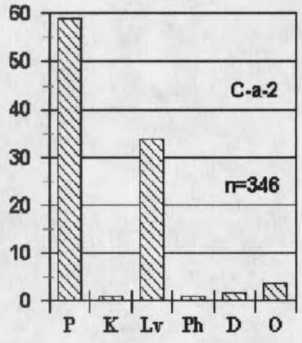
APPENDIX D: Table 3. Point-count data for Two Medicine Formation sandstones. Sample number refers to stratigraphic section and unit location. N is number of counts. F = total feldspar; Qm = monocrystalline quartz; Qm1= monocrystalline quartz, rounded; Qm2= monocrystalline quartz, angular; Qp = polycrystalline quartz; Lv, Lp, Ls = volcanic, pyroclastic, and sedimentary lithic fragments; Ca = calcite; Cl = chlorite; Ph = total micas; M = mafic grains; D= opaques; A = analcime; O = other.

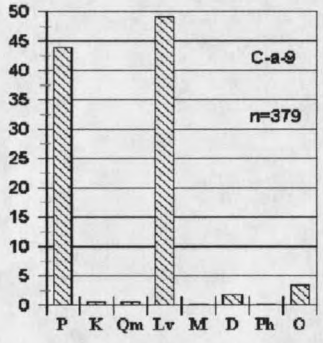
Sample #	n	Gr. Size	F	Qm	Qm1	Qm2	Qp	Lv	Lp	Ls	Ca	Cl	Ph	M	D	A	O
RE-Kte-2	329	fine	65	2	0	0	0	150	27	4	1	77	1	0	1	1	1
RE-Kte-11	360	v. fine	35	80	0	0	11	81	5	8	120	0	6	0	3	5	6
RE-Kte-24	375	coarse	19	27	0	0	7	30	260	4	0	0	0	9	6	0	13
E2-Kte-8	384	v. fine	16	0	17	64	18	0	79	8	157	0	7	0	5	0	13
E2-Kte-10	328	v. fine	38	66	0	0	4	13	52	4	138	0	3	0	2	2	6
A-1a-612d	452	fine	118	0	18	81	61	0	126	15	0	0	27	0	3	0	13
A-1b-613c	498	med	35	0	12	97	21	0	129	3	186	0	7	0	3	0	5
A-1b-613f	350	fine	7	13	0	0	0	10	124	8	137	26	0	19	6	0	0
A-1c-614c	323	v. co	98	6	0	0	5	18	151	12	0	10	3	7	6	0	7
A-1c-614g	302	med	86	0	0	8	4	8	151	0	0	0	0	18	20	0	7
A-1c-614j	252	coarse	34	0	0	12	0	0	164	6	0	0	0	17	6	0	3
A-1c-614t	299	v. fine	26	110	0	0	4	0	68	0	59	2	10	0	6	4	10
Kamv-9	289	v. co	2	0	0	0	70	127	1	3	5	10	0	58	3	0	10
Kamv-14	430	fine	39	129	0	0	13	65	148	0	0	4	6	12	6	8	2
Kamv-15	466	med	58	136	0	0	62	5	198	1	2	0	0	0	0	3	0
C-a-2	346	fine	207	0	0	0	0	117	0	0	0	0	0	3	6	0	13
C-a-9	379	fine	169	2	0	0	0	186	0	0	0	0	1	1	7	0	15
C-a-10	260	v. co	98	8	0	0	0	139	0	0	0	0	0	8	6	0	1
C-a-11	311	v. co	113	0	0	0	0	151	0	0	0	0	3	22	18	0	4
C-d-4	342	med	47	0	0	0	0	172	0	7	66	30	0	0	7	0	13
C-d-33	360	med	59	0	0	0	0	178	4	10	68	25	2	7	6	0	1
C-d-61	311	med	121	3	0	0	0	119	16	1	22	8	1	9	8	0	3
S-d-1	321	coarse	38	0	0	0	1	111	82	4	32	35	0	0	13	0	6
S-d-5	341	med	87	4	0	0	0	102	69	11	20	16	0	19	13	0	0
N-d-100	394	coarse	103	10	0	0	0	41	156	18	2	0	8	0	8	0	53
S-f-7	357	v. co	5	0	0	0	0	287	6	15	0	0	0	25	15	0	4
S-f-21	254	v. co	28	0	0	0	0	88	82	16	0	0	0	18	22	0	0
N-f-6	369	v. co	52	0	0	0	1	195	77	8	0	0	1	23	10	0	3

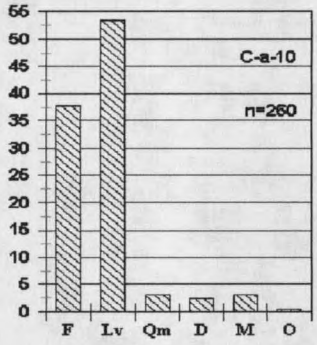
APPENDIX E

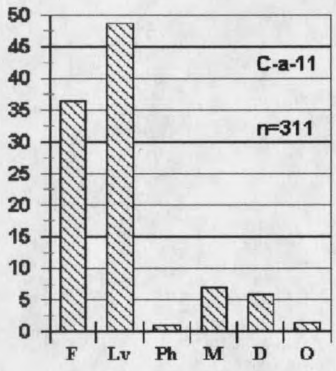
HISTOGRAM PLOTS OF POINT-COUNT DATA

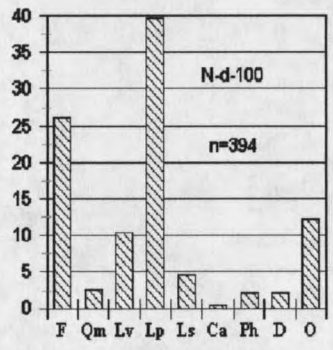
APPENDIX E: Histogram plots of relative percentages for sandstones of the Two Medicine Formation. Sample number refers to stratigraphic section and unit location. N is number of counts. F = total feldspar; Qm = monocrystalline quartz; Qm1= monocrystalline quartz, rounded; Qm2= monocrystalline quartz, angular; Qp = polycrystalline quartz; Lv, Lp, Ls = volcanic, pyroclastic, and sedimentary lithic fragments; Ca = calcite; Cl = chlorite; Ph = total micas; M = mafic grains; D= opaques; A = analcime; O = other.

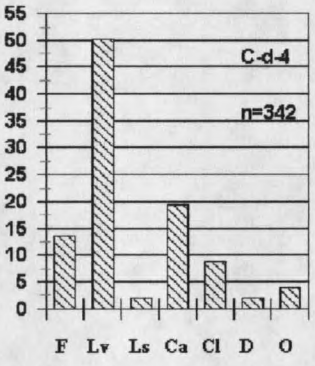


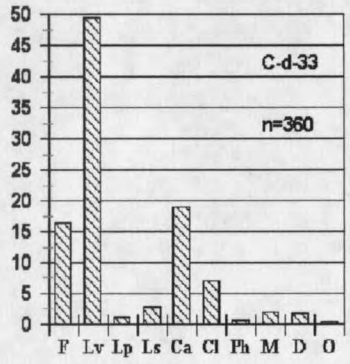


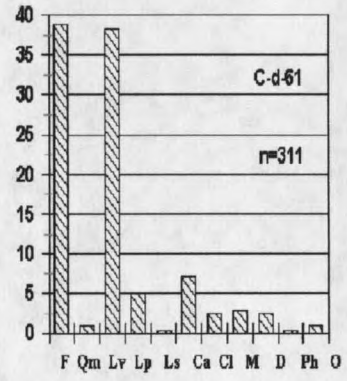


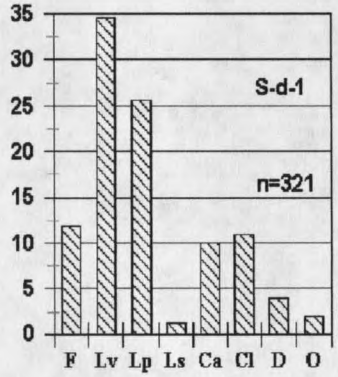




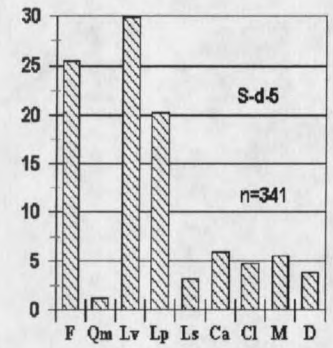


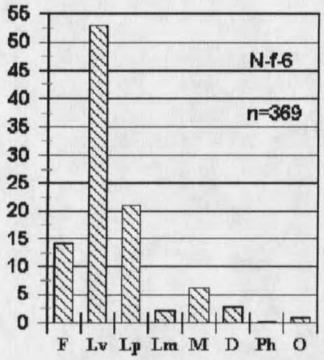


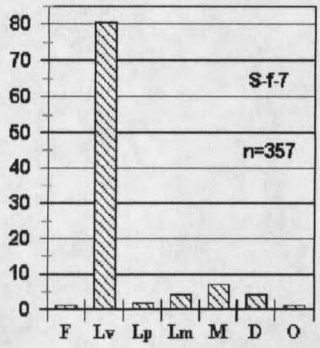


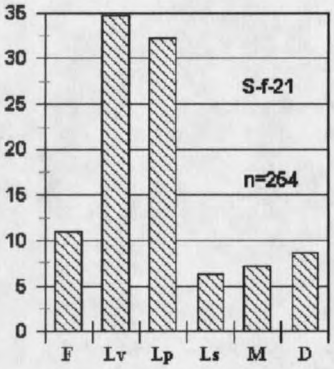


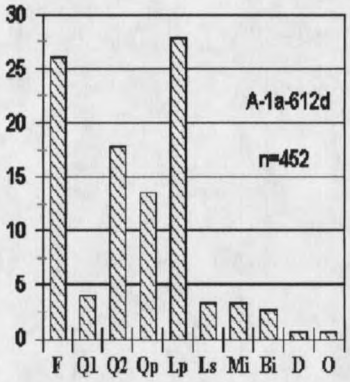
APPENDIX E: Continued:

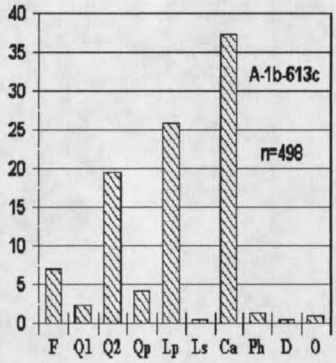


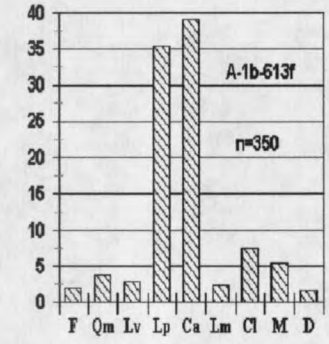


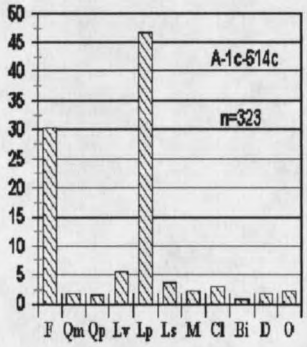


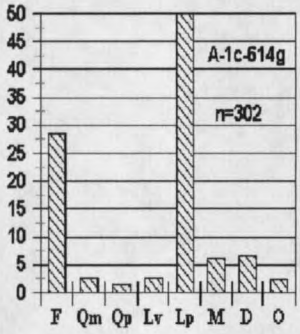


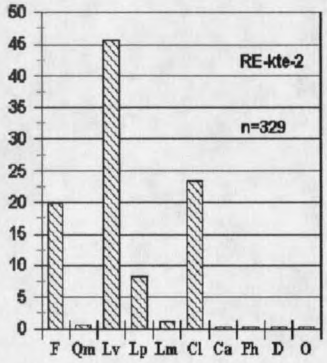


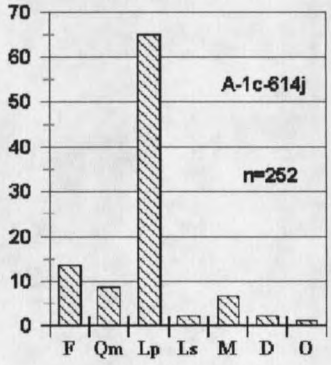


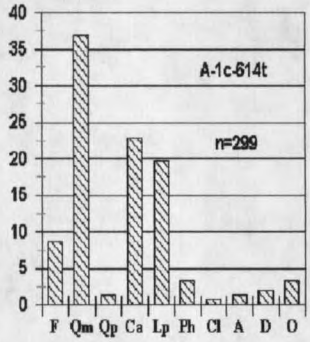




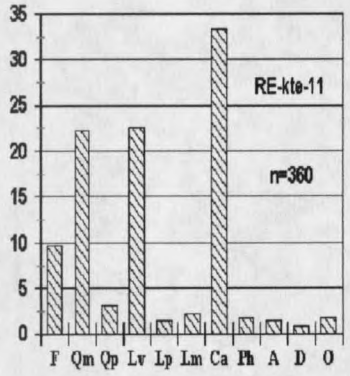


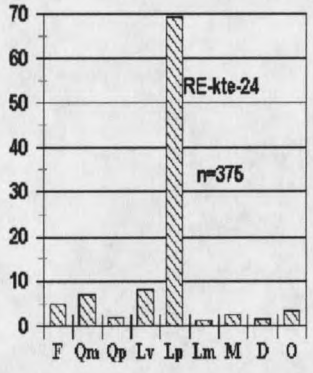


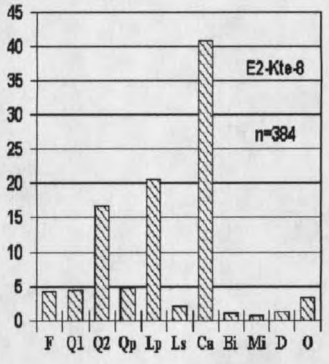


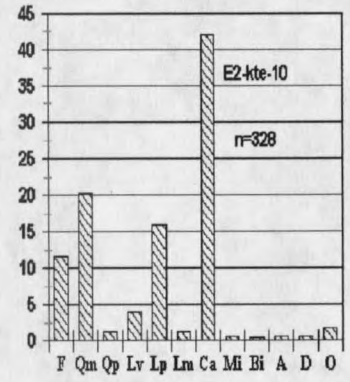


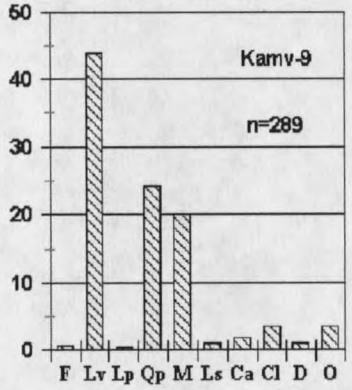
APPENDIX E: Continued:

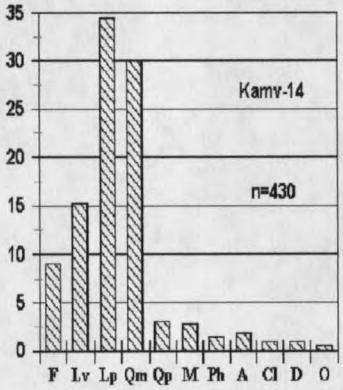


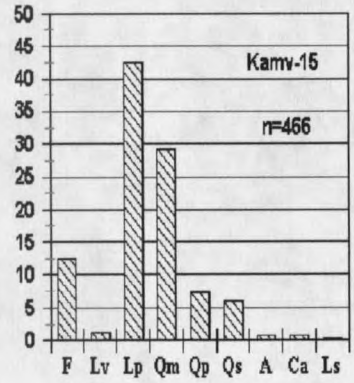












MONTANA STATE UNIVERSITY - BOZEMAN
3 1762 10421003 2